Materials Advances

REVIEW

View Article Online
View Journal | View Issue

Cite this: *Mater. Adv.*, 2023, 4, 3140

Recent progress in B_4C–SiC composite ceramics: processing, microstructure, and mechanical properties

Wei Zhang

Received 28th March 2023,
Accepted 27th May 2023

DOI: 10.1039/d3ma00143a

rsc.li/materials-advances

B_4C–SiC composite ceramics are a very promising alternative to pure B_4C ceramics and pure SiC ceramics. B_4C–SiC composite ceramics exhibit a combination of the desirable performance of B_4C and SiC. B_4C–SiC composite ceramics are a better candidate material for engineering applications as structural ceramic materials. The sintering performance, microstructure, and mechanical properties of B_4C–SiC composite ceramics are systematically elaborated in this review. Many factors can affect the sintering performance and microstructure of B_4C–SiC composite ceramics; also, the microstructure plays an important role in the mechanical properties of B_4C–SiC composite ceramics. The mechanical properties of B_4C–SiC composite ceramics are crucial for their applications. Finally, the future development trend of B_4C–SiC composite ceramics as structural ceramic materials is proposed.

1. Introduction

Both boron carbide (B_4C) and silicon carbide (SiC) have been recognized as important structural ceramic materials due to their outstanding properties, including high melting point, ultra-high hardness, high elastic modulus, good wear resistance, low density, excellent chemical stability, high thermal tolerance, *etc.*[1–5] Especially, B_4C has a high neutron capacity cross-sectional area and good thermoelectric properties, and SiC has high thermal conductivity, excellent thermal shock resistance, and good oxidation resistance; these properties allow B_4C and SiC to have unique applications, respectively. B_4C and SiC with excellent properties are widely used in the modern high-technology industry, such as mechanical and automotive engineering, high-temperature thermoelectric conversion, tribology, aviation, aerospace, military, chemical industry, nuclear energy, *etc.*[6,7] In particular, the materials with a combination of low density and high hardness are more desirable than the materials without these characteristics; thus, both B_4C and SiC are very suitable for use as lightweight structural materials and rotating tribo-components.[8,9] Therefore, compared with other ceramics (Al_2O_3 ceramics, ZrO_2 ceramics, Si_3N_4 ceramics, *etc.*), B_4C and SiC ceramics serve much better as vehicle armors and rotating rings in mechanical seals. It is noteworthy that B_4C is an acronym for boron carbide, rather than its actual chemical formula, because boron carbide exists over a range of chemical compositions $B_{12+x}C_{3-x}$ ($0.06 < x < 1.7$).[10–13]

Despite the numerous advantages of B_4C and SiC ceramics, both pure B_4C ceramics (monolithic B_4C ceramics) and pure SiC ceramics (monolithic SiC ceramics) are difficult to sinter to achieve high densification because of their high covalent bond ratios and oxide film contamination on the raw materials.[14,15] In the case of no external pressure, extremely high sintering temperatures are necessary to fabricate pure B_4C ceramics and pure SiC ceramics. The high sintering temperature, however,

Nagoya University, Graduate School of Engineering, Department of Chemical Systems Engineering, Nagoya 4648603, Japan. E-mail: cnzhangwei2008@126.com

Wei Zhang

Wei Zhang obtained his PhD degree from Nagoya University, Japan. He completed his Master's degree from Shenyang University of Technology, China. He is an elected fellow of the Vebleo Association. He has published more than 100 academic papers as the first author or corresponding author in journals of international/national repute, and he holds 15 patents to his credit. He won the National Scholarship for Outstanding Self-funded International Students from the China Scholarship Council – China's highest government award for international students, the ISSN International Science & Technology Awards "International Best Researcher Award", and the Asia's Science, Technology and Research Awards "Outstanding Researcher Award". His research interests include ceramics, refractories, heat-resistant coatings, mineral materials, and mechanism analysis of friction and wear.

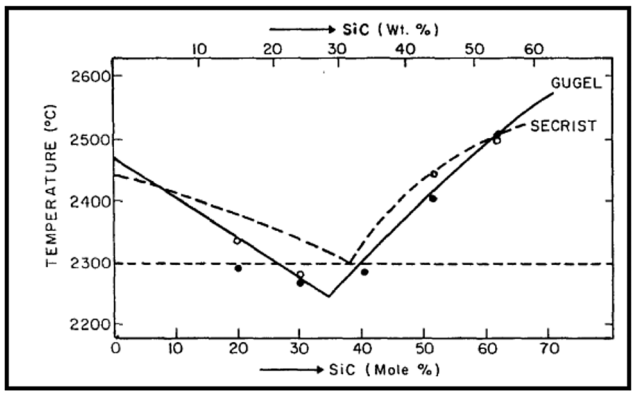

Fig. 1 Binary phase diagram of B_4C–SiC[19] (reprinted with permission, Copyright 1979, Elsevier).

will induce abnormal grain growth, deteriorating the mechanical properties of ceramics.[16] Currently, the production of pure B_4C ceramics and pure SiC ceramics with high relative density through a pressureless sintering method can be achieved only by adding sintering aids. A variety of additives are used as sintering aids to facilitate the densification of pure B_4C ceramics and pure SiC ceramics. In theory, according to the binary phase diagram of B_4C–SiC (Fig. 1),[17–19] B_4C and SiC can be used as the sintering aid for each other to improve each other's sinterability; thus, the sintering of B_4C–SiC composite ceramics is possible at lower temperatures than pure B_4C ceramics and pure SiC ceramics.

For B_4C ceramics, Thévenot[20,21] reported that the addition of SiC coupled with C can promote the densification of pressureless sintered B_4C ceramics. The addition of SiC can lead to segregation at grain boundaries of B_4C ceramics, thus limiting B_4C grain coarsening or facilitating diffusion in grain boundaries. Zorzi *et al.*[22] found that the addition of 4 wt% SiC alone can also promote the sintering of B_4C ceramics, which in turn increases the hardness of B_4C ceramics. For SiC ceramics, the simultaneous introduction of B, which can be introduced as elemental B, $LiBH_4$ or B_4C,[23,24] and C can promote the sintering of α-SiC ceramics and β-SiC ceramics.[23–28] On the one hand, both B and C upset an unfavorable equilibrium at grain boundary–pore surface intersections by reducing the grain boundary–surface energy ratio (B can reduce the grain boundary energy, and C can increase the interfacial energy), thereby inducing the driving force for diffusional mass transport necessary for solid-state sintering.[23,25] Furthermore, B segregated at the grain boundaries of SiC ceramics can impede surface and vapor-phase transport and grain growth at low temperatures, leading to increased densification due to improved grain boundary diffusivity at high temperatures.[29] On the other hand, carbon forms a uniform layer on the surface of SiC grains in the first stage of sintering, which occurs because of the high grain boundary and surface diffusion coefficient of C; as the temperature increases, C can react with SiO_2 existing on the surface of SiC grains, forming a secondary SiC phase and removing the oxide film contamination, which can increase the surface energy of SiC and limit the formation of the SiO_2 glass phase.[27,30,31] Meanwhile, C can prevent the evolution of gaseous products in chemical reactions or the thermal decomposition of SiC.[32,33] In order to enhance the densification of SiC ceramics by the addition of sole B_4C, Bind *et al.*[34] stated that B atoms can partly replace C atoms in the SiC lattice, forming a solid solution, which can improve the SiC volume diffusion. In contrast, Li *et al.*[35] noted that B atoms replace Si atoms, forming a solid solution in SiC ceramics, and the densification of SiC ceramics is promoted by the generation of Si and C vacancies in the SiC lattice.

Moreover, the fracture toughness of both pure B_4C ceramics and pure SiC ceramics is relatively low, especially B_4C ceramics, which is mainly attributed to their transgranular fracture mode.[36,37] Although the utilization of nano/submicron-sized B_4C and SiC powders as starting materials can improve the fracture toughness and sinterability of pure B_4C ceramics and pure SiC ceramics,[38,39] these nano/submicron-sized powders are limited to laboratory use because of low yield and high cost; thus, nano/submicron-sized B_4C and SiC powders are not suitable for the industrial preparation of B_4C ceramics and SiC ceramics. Both B_4C powders and SiC powders obtained through industrial manufacturing are micron-sized. Adding a second phase into B_4C ceramics and SiC ceramics can improve their fracture toughness to a certain extent; however, the addition of some second phases, such as Al, Al_2O_3, and ZrO_2, reduces the hardness of B_4C ceramics and SiC ceramics.[40,41] Both B_4C and SiC have high microhardness; theoretically, B_4C and SiC can be added to each other to improve each other's mechanical properties. B_4C shows higher hardness and lower density than SiC, and SiC exhibits higher fracture toughness than B_4C. Given that each component can act as a second phase to affect matrix performance, the production of B_4C–SiC composite ceramics is an effective approach to combine the advantages of B_4C and SiC.

In brief, a uniform distribution of B_4C and SiC in B_4C–SiC composite ceramics can prevent direct contact between B_4C–B_4C and SiC–SiC; thus, B_4C and SiC seem to act as grain growth inhibitors for each other in B_4C–SiC composite ceramics, which is conducive to densification. Also, B_4C and SiC have good physical and chemical compatibility with each other; the B_4C–SiC system can offer a combination of good sinterability and relatively high fracture toughness with high hardness and low density. B_4C–SiC composite ceramics can exhibit better mechanical properties and tribological performance as compared to pure B_4C and SiC ceramics;[42,43] thus, B_4C–SiC composite ceramics are a better candidate material for engineering applications as structural ceramic materials.

In recent years, B_4C–SiC composite ceramics have attracted more and more attention from scientific and commercial disciplines because B_4C–SiC composite ceramics provide some outstanding properties, such as mechanical properties, tribological properties, and thermoelectric properties,[44,45] for applications in harsh environments. So far, there have been some review articles on pure B_4C ceramics[46–49] and pure SiC ceramics;[50,51] however, the review articles on B_4C–SiC materials are very limited. The synthesis of B_4C–SiC composite powders and tribological properties of B_4C–SiC composite ceramics have been summarized in the previous

review papers;[52,53] therefore, the sintering performance, microstructure, and mechanical properties of B_4C–SiC composite ceramics are systematically elaborated in this review. It is of great importance to colligate this information for current ceramic research. Furthermore, the future development trend of B_4C–SiC composite ceramics as structural ceramic materials is also proposed.

2. Sintering method of B_4C–SiC composite ceramics

The general methods used to sinter B_4C–SiC composite ceramics include pressureless sintering, hot-press (HP) sintering, spark plasma sintering (SPS), and reaction-bonded sintering. B_4C–SiC ceramics are difficult to sinter due to the high covalent bond ratios of both B_4C and SiC. When B_4C–SiC ceramics are prepared by pressureless sintering, sintering aids are often added to promote sintering. Prior to pressureless sintering, the green body needs to be prepared from composite powders using different molding technologies, such as dry pressing, cold isostatic press (CIP), and slip casting. Hot-press sintering is used to produce B_4C–SiC composite ceramics under external pressure from composite powders without pre-molding. Spark plasma sintering is a technology that utilizes an extremely high heating rate and is assisted by a uniaxial pressure. B_4C–SiC ceramics can be prepared by spark plasma sintering in a very short processing time at relatively low sintering temperatures; thus, a fine microstructure will be obtained for B_4C–SiC ceramics due to the high heating rate and short dwell time. The preparation of B_4C–SiC composite ceramics by reaction-bonded sintering was first developed by Taylor in the 1970s,[54] and the preparation method is similar to that of SiC ceramics produced by reaction-bonded sintering, in which molten Si with appropriate fluidity infiltrates into a porous green/partially sintered body composed of SiC and free C at high temperatures.[55,56] The mechanism of reaction-bonded sintering for B_4C–SiC composite ceramics is the same as that for SiC ceramics. The porous green preforms have interconnected pores, which can provide a good channel for the penetration of molten Si; molten Si infiltrates into a green preform, which is composed of only B_4C, the mixture of B_4C and free C, or B_4C–SiC–C or B_4C–SiC powders,[57] driven by capillary force in a vacuum because the wetting angle of Si with both B_4C and C is 0° at 1430 °C.[58] Then, the molten Si infiltrated reacts with C either from free C or B_4C to form SiC,[59,60] the reaction of which leads to volume expansion occupying partial pores in the preform;[61] the remaining excess pores in the preform are filled with molten Si after the reaction, making the reaction-bonded B_4C–SiC ceramics dense.[62] The preparation of reaction-bonded B_4C–SiC ceramics is actually an *in situ* chemical reaction. In addition to the conventional process, the microwave-assisted processing method, which can shorten the processing time, is another strategy employed to prepare reaction-bonded B_4C–SiC ceramics.[63] Recently, a so-called ultra-high pressure (4 GPa) sintering method has been developed to successfully prepare additive-free B_4C–SiC ceramics at a low temperature (1500 °C).[64] It is noteworthy that the pressure applied during ultra-high pressure sintering is significantly higher than the pressures applied during HP and SPS, leading to the rapid densification of B_4C–SiC ceramics. This phenomenon results from the fact that the ultra-high pressure sintering allows the reduction of distance between the grains and endures the improvement of contact between individual grains resulting in plastic deformation.[65] Also, the ultra-high pressure has an influence on particle redistribution, agglomerate omission, and pore elimination.[66] The sintering performance, microstructure, and mechanical properties of the B_4C–SiC ceramics prepared through different sintering methods mentioned above will be described in detail later.

Each sintering method used to prepare B_4C–SiC ceramics has its own advantages and disadvantages. Pressureless sintering is suitable for large-scale production and products with complicated shapes or large sizes. Pressureless sintering has a much wider range of applications and is suitable for extensive industrialization. But the disadvantages of pressureless sintering to fabricate B_4C–SiC ceramics are that the sintering temperature is high and the sintering time is long; it is difficult to obtain high relative density and small grain size for B_4C–SiC ceramics. Hence, various sintering aids are often added to reduce the sintering temperature and ultra-fine powders are usually chosen as raw materials. For hot-press sintering and spark plasma sintering, highly dense B_4C–SiC ceramics without sintering aids can be prepared at relatively low temperatures *via* these routes, applying heat and pressure simultaneously. The sintering time of these routes is relatively short, especially SPS. The grain size of B_4C–SiC ceramics prepared *via* these routes, especially by SPS, is relatively small. Also, less costly coarser-grained initial powders can be densified into compacts of acceptable density *via* these routes. However, compared with pressureless sintering, these routes are more limiting in terms of the shape and size of products and more costly; thus, these technologies are not suitable for industrial applications. Moreover, the physical properties of B_4C–SiC ceramics produced *via* hot-press sintering and spark plasma sintering perpendicular and parallel to the uniaxial pressure direction show direction dependence. Reaction-bonded sintering is an energy-saving process due to much lower sintering temperatures and is favorable of producing large, complex-shaped products. In the case of B_4C–SiC ceramics prepared by reaction-bonded sintering, B_4C, SiC, and residual Si particles can interconnect into a uniform and strong three-dimensional network at low sintering temperatures without the need for applied pressure; near-net shaped products with zero shrinkage can be produced.[67] Also, fine reactive starting powders capable of being densified are not required, reducing the cost of raw materials. Therefore, the preparation of B_4C–SiC ceramics *via* reaction-bonded sintering is a low-cost method; this route is suitable for large-sized and complex-shaped products. Reaction-bonded B_4C–SiC ceramics have reached the industrial production stage; however, their characteristics of inhomogeneous microstructures and residual Si with low hardness and stiffness may limit the application of B_4C–SiC ceramics in terms of reliability and high-temperature

mechanical properties. Therefore, the B_4C–SiC products produced by reaction-bonded sintering lose the partial superior performance of B_4C–SiC ceramics.

3. Sintering performance and microstructure of B_4C–SiC composite ceramics

Although the sintering temperature of B_4C–SiC composite ceramics is lower than that of pure B_4C ceramics and pure SiC ceramics theoretically, B_4C–SiC ceramics are still difficult to sinter because both B_4C and SiC have strong bonding, high resistance to grain boundary sliding, low plasticity, and low superficial tension in the solid state. Many factors can affect the sintering performance and microstructure of B_4C–SiC ceramics, such as the ratio of B_4C to SiC, raw materials, preparation process, sintering aids, *etc.*, which will be summarized in detail in this part. High relative density can achieve some properties and applications of B_4C–SiC ceramics, such as good wear resistance in the tribo-component application and acceptable ballistic resistance in the armor application. Also, the microstructure plays an important role in the mechanical properties of B_4C–SiC ceramics.

3.1. Ratio of B_4C to SiC

Different ratios of B_4C to SiC will cause different impacts on the sintering performance and microstructure of B_4C–SiC ceramics. When the volume fraction of B_4C is more than that of SiC, SiC grains distribute in the B_4C matrix; otherwise, B_4C grains distribute in the SiC matrix. Meanwhile, the density of SiC (3.21 g cm^{-3}) is higher than that of B_4C (2.51 g cm^{-3}); thus, the density of B_4C–SiC ceramics increases with an increase in the ratio of SiC.

The high covalent bond ratio, which is responsible for intrinsically low diffusion mobility, is one of the factors inhibiting the sintering performance of ceramic materials. Theoretically, the densification of B_4C is more difficult than that of SiC because the covalent bond ratio in B_4C (94%) is higher than that in SiC (88%);[15] thus, the B_4C–SiC ceramics with more SiC content than B_4C content can achieve better sintering performance. This means that a higher sintering temperature may be required to achieve a higher relative density for the composite ceramic containing more B_4C.

For the sintering performance and microstructure of B_4C–SiC ceramics with different ratios of B_4C to SiC prepared by different sintering methods, some regular results have been found by the researchers. Magnani *et al.*[68] found that the pressureless sintered SiC-5 vol% B_4C ceramics show a higher relative density than pure SiC ceramics in the sintering temperature range of 1950–2200 °C. The presence of B_4C as a secondary phase can improve the sinterability of SiC powders. Furthermore, the addition of B_4C reduces the abnormal growth of SiC grains; thus, the SiC-5 vol% B_4C ceramics exhibit a finer microstructure than pure SiC ceramics. Cho *et al.*[69] mentioned that the relative density of the pressureless sintered SiC ceramics decreases with the addition of B_4C particles from 1 to 5 wt%. This phenomenon can be explained by the fact that the B_4C grains existing between SiC grains impede mass transport through surface diffusion; thus, the grain growth of SiC is slowed down with the increase in B_4C addition, resulting in the formation of large amounts of pores. Thévenot[20] reported that the relative density of the pressureless sintered B_4C–SiC ceramics (10/90 < B_4C wt%/SiC wt% < 96/4) increases from 93 to 99% with an increase in α-SiC content from 10 to 90 wt%. The B_4C–SiC ceramic with the highest SiC content exhibits the best sintering capability. When the SiC content is less than 10 wt%, the densification of B_4C–SiC ceramics is low despite higher sintering temperature, and the grains are coarser (<80 μm). Zhang *et al.*[70] also observed similar results for the relative density of pressureless sintered B_4C–SiC ceramics (3/97 < B_4C wt%/SiC wt% < 100/0). The relative density is higher and fewer pores are observed on the ceramic surfaces when the SiC content is more than the B_4C content in the B_4C–SiC ceramics (Fig. 2a–f). Yaşar and Haber[71] noted that the relative density of the spark plasma sintered B_4C–SiC ceramics decreases from 99.6 to 98.9% with the increase in B_4C content from 10 to 50 wt%. So *et al.*[72] studied the sintering performance and microstructure of the hot-press sintered B_4C–SiC ceramics with the volume ratios of B_4C to SiC of 35 : 65, 56 : 44, and 75 : 25. It was found that the densification mechanisms are different for B_4C–SiC ceramics with different ratios of B_4C to SiC. When the B_4C grains distribute in the SiC matrix (the volume fraction of SiC is more than that of B_4C), the partial phase transition of SiC from 6H to 4H accompanying the grain growth promotes densification. In contrast, when the SiC grains distribute in the B_4C matrix (the volume fraction of B_4C is more than that of SiC), the ceramics are densified through grain boundaries and volume diffusion, and there is no phase transition of SiC in the ceramics. The solubility of B_4C in α-SiC is approximately 0.5 wt% at a temperature between 2000 and 2100 °C,[73] which can decrease the surface energy at the phase boundary between B_4C and SiC and can increase the mass transfer, promoting the densification of SiC. However, the diffusion coefficient and densification rate will decrease when the B_4C content is above the solubility. The grain growth of SiC is inhibited, but the grain size of B_4C is increased with an increase in B_4C content, leading to the larger grain size of B_4C than that of SiC, which is attributed to the growth of B_4C grains by the diffusion of B and C, and the difference in grain size between B_4C and SiC is increased with an increase in B_4C content in the composite ceramics. Zhang *et al.*[74] found that the relative density of the gas-pressure sintered B_4C–SiC ceramics decreases from 94.2 to 88.9% with the increase in B_4C content from 5 to 20 wt% in the composite ceramics, and the surface morphology changes from an island-like distribution and better continuity to a plate-type structure (Fig. 2g–j). Matović *et al.*[64] mentioned that B_4C–SiC ceramics can achieve a high relative density (>96%) *via* ultra-high pressure sintering at a relatively low temperature combined with a short holding time; the composite ceramics with the equal-weighted contributions of B_4C and SiC achieve the maximal relative density, which is attributed to the best mixing of the initial raw materials and thus their best distribution in the composite powders.

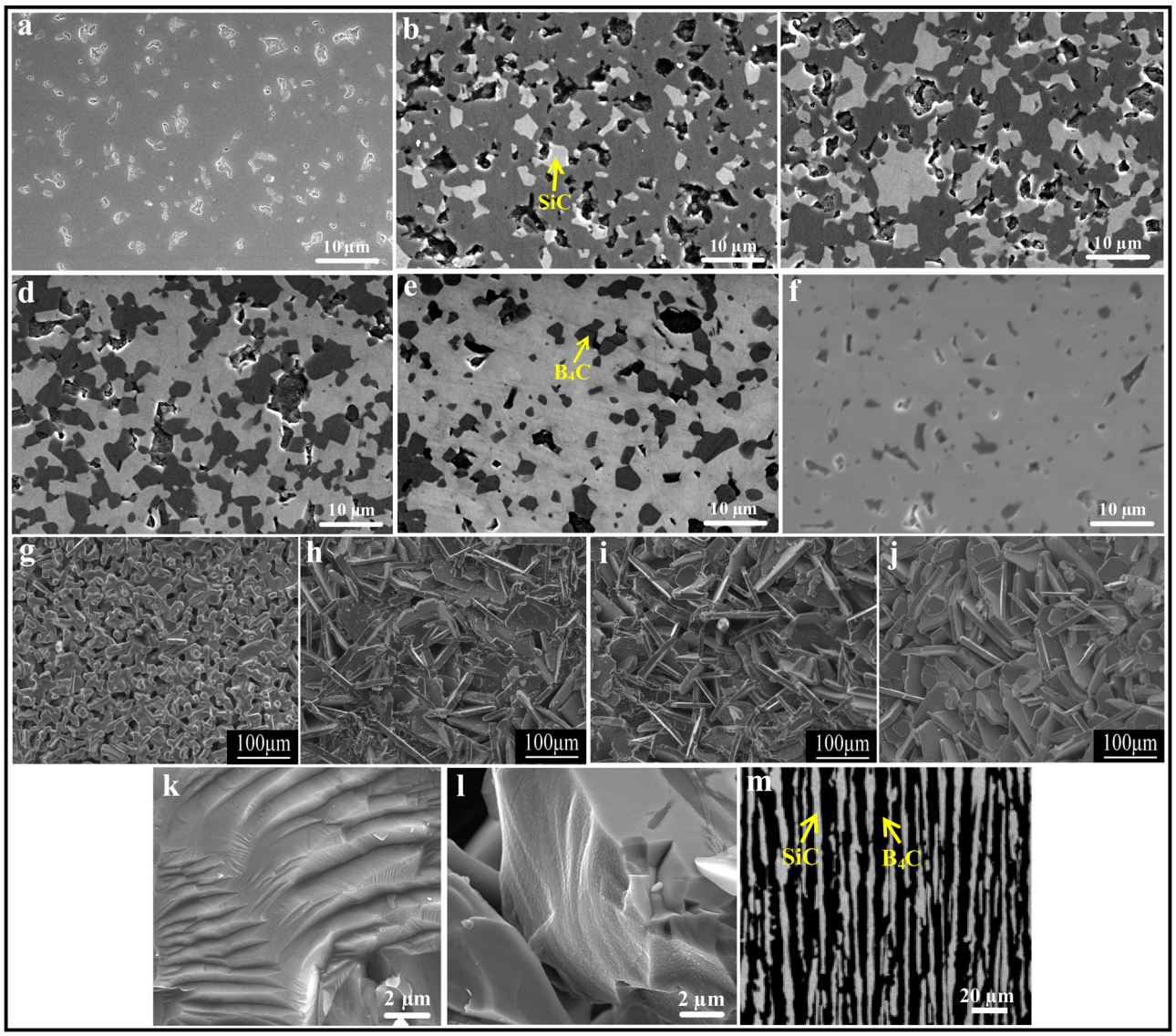

Fig. 2 Polished surfaces of the pressureless sintered B_4C–SiC ceramics with different ratios of B_4C to SiC: (a) B_4C, (b) B_4C-20 wt% SiC, (c) B_4C-40 wt% SiC, (d) B_4C-60 wt% SiC, (e) B_4C-80 wt% SiC, and (f) B_4C-97 wt% SiC[70] (reprinted with permission, Copyright 2020, Elsevier); microstructure of the gas-pressure sintered B_4C–SiC ceramics with different ratios of B_4C to SiC: (g) SiC-5 wt% B_4C, (h) SiC-10 wt% B_4C, (i) SiC-15 wt% B_4C, (j) SiC-20 wt% B_4C[74] (reprinted with permission, Copyright 2014, Trans Tech Publications); SEM images of B_4C–SiC ceramics revealing the cleavage surfaces: (k) B_4C-5 vol% SiC and (l) B_4C-7.5 vol% SiC[80] (reproduced with permission, Copyright 2017, Elsevier); (m) microstructure of eutectic B_4C–SiC ceramics showing lamellar texture[82] (reproduced with permission, Copyright 2002, The Japan Institute of Metals. This is an open access article distributed under the terms of the Creative Commons Attribution License).

For the reaction-bonded B_4C–SiC ceramics, different ratios of B_4C to SiC and microstructures can be obtained by adjusting the chemical composition and microstructure of their preforms. The preforms containing high C content can form B_4C–SiC ceramics rich in SiC after Si infiltration. Zhang *et al.*[75] reported that the content of generated SiC increases with an increase in the initial amount of nano-carbon black in the reaction-bonded B_4C–SiC ceramics. The density of reaction-bonded B_4C–SiC ceramics increases with the increase in the initial amount of carbon black (0–12 wt%), which is attributed to the gradually increased amount of SiC generated. Although the relative density of the B_4C–SiC ceramics slightly decreases with the increase in carbon black, B_4C–SiC ceramics with different amounts of carbon black are rather dense. Li *et al.*[76] also found that the amount of fine SiC grains formed increases with the increasing amount of the C source. In contrast, Hayun *et al.*[77] mentioned that the amount of SiC generated essentially depends on the porosity of the preform, and only depends on the C source to a slight extent.

Different from these regular results mentioned above, Tomohiro *et al.*[78] found that the relative density of the hot-press sintered B_4C–SiC ceramics is independent of the SiC content from 0 to 50 vol% when the sintering temperature is 2200 °C, and the relative density of composite ceramics is nearly fully dense.

However, when the sintering temperatures are 2000 and 2100 °C, the relative density of B_4C–SiC ceramics with an SiC addition of 10–20 vol% is at a maximum, the reason for which is not explained.

The microstructure of B_4C–SiC ceramics is also related to the ratio of B_4C to SiC. Compared with pure B_4C ceramics, the B_4C-20 wt% SiC ceramics achieve a more refined and denser microstructure due to the incorporation of SiC.[79] Moradkhani and Baharvandi[80] pointed out that the addition of SiC particles in the B_4C matrix leads to the formation of cleavage surfaces within grains (Fig. 2k and l); the greater the volume fraction of the SiC additive, the greater the density of cleavage surfaces. As for the microstructure of eutectic composites, it is mainly dependent on the volume fractions of phases.[81] The lamellar texture will appear when each phase is more than 30 vol%. Gunjishima *et al.*[82] observed lamellar texture in B_4C-40 vol% SiC ceramics prepared by the floating zone method (Fig. 2m), which is the eutectic composition of the B_4C–SiC binary system. Also, the spacing between lamellae is related to the solidification rate.

Some previous studies on the effect of the ratio of B_4C to SiC on the sintering performance and microstructure of B_4C–SiC ceramics are tabulated in Table 1.

3.2. Raw material

Raw materials are the basis for the preparation of B_4C–SiC ceramics. The characteristics of raw materials, such as particle size, oxide impurity, and species, can affect the sintering performance and microstructure of B_4C–SiC ceramics.

3.2.1. Particle size. Generally, raw materials with large sizes are not easy to sinter into dense blocks; inversely, raw materials with particle sizes in the submicron or even nanometer range are easier to sinter due to higher surface energy. Shi *et al.*[83] studied the sintering performance of hot-press sintered B_4C-20 vol% SiC ceramics using B_4C powders with a size of 10.22 μm and β-SiC powders with a size of 1.07 μm as raw materials. The porosity of the B_4C–SiC ceramics gradually decreases with an increase in sintering temperature from 1900 to 2100 °C; however, obvious pores can still be observed after sintering at 2100 °C. This indicates that it is difficult to obtain dense B_4C–SiC ceramics using B_4C powders with micron size as the raw material, although the increase of sintering temperature can reduce the porosity to a certain extent. Therefore, the utilization of raw materials with fine particle size is more conducive to promoting the sintering of B_4C–SiC ceramics. For the grain size of B_4C–SiC ceramics, Moradkhani and Baharvandi[80] found that the effect of the addition of SiC with nanoscale and microscale sizes on the grain size of the pressureless sintered B_4C–SiC ceramics is not very significant.

Using graded particles as raw materials is an effective strategy to improve the packing density of the green body. For the reaction-bonded B_4C–SiC ceramics, theoretically, high green density is conducive to reducing the fraction of residual Si in the final product. The lower the porosity, the lower the amount of residual Si present after the infiltration with Si. Therefore, it is reasonable to decrease the porosity of the green body as much as possible before the infiltration process. A multimodal particle size distribution results in maximal volume filling by the initial ceramic powers prior to infiltration, and thus reduces the fraction of residual Si after infiltration. Hayun *et al.*[84] used B_4C powders with different particle sizes (130, 70, 50, 13, and 1 μm) as raw materials to prepare the preform. Compared with the relative density (65%) of the preform composed of monosized fine B_4C particles (1 μm), the relative densities (70–75%) of the preforms composed of graded B_4C particles are higher. After Si infiltration, the space between coarse B_4C particles is uniformly filled with fine B_4C, newly formed SiC, and residual Si particles. Both the preforms composed of graded B_4C particles and the preform composed of monosized fine B_4C particles are fully infiltrated; however, the amount of residual Si in the final B_4C–SiC ceramics produced from the graded B_4C particles (8–10 vol%) is lower than that produced from the monosized fine B_4C particles (20 vol%). Li *et al.*[76] also proved that the relative density of the green body composed of graded B_4C powders with 8.671 μm and 323.7 nm can reach 75%, which is higher than that of the preform composed of monosized B_4C particles (59.9%). Meanwhile, compared with the green body with a similar relative density prepared by Hayun *et al.*,[84] the particle size of B_4C used by Li *et al.*[76] is much smaller, which contributes to decreasing open pore size of the preform and the consequent size of free Si. On the other hand, Song *et al.*[85] found that because there are coarse B_4C particles in the reaction-bonded B_4C–SiC preform composed of graded B_4C particles (14, 7, and 1.5 μm), the uniform distribution of the residual Si is prevented, leading to the formation of scattered fragments; thus, the use of fine B_4C particles makes it easier to form a uniform microstructure in the reaction-bonded B_4C–SiC ceramics. Therefore, using a multimodal powder mixture including coarse B_4C particles to prepare the green body is helpful for improving the relative density of the green body, which in turn contributes to reducing the amount of residual Si in the reaction-bonded B_4C–SiC ceramics; however, the use of coarse B_4C particles is not conducive to the formation of uniform microstructure in the reaction-bonded B_4C–SiC ceramics. Hereto, the size of coarse particles in the graded B_4C particles should be as small as possible under the premise of improving the relative density of the green body.

3.2.2. Oxide impurity. B_4C and SiC powders, as the main raw materials for preparing B_4C–SiC ceramics, have oxide layers on their surfaces.[14,86] These oxide film impurities (B_2O_3/H_3BO_3, SiO_2) on the raw materials can cause abnormal grain growth, increase porosity, and deteriorate sintering performance in the sintering process. In particular, the presence of these oxide impurities reduces the application potential of B_4C–SiC ceramics at high temperatures. Therefore, it is necessary to control surface oxide impurities on the raw materials. To remove these oxide impurities, there are two main approaches. One is adding C to remove these oxide layers according to the reactions between C and B_2O_3 and between C and SiO_2 in the sintering process.[70] The other is using acid etching to remove these oxide layers. HCl and HF are commonly used to wash B_4C and SiC to remove B_2O_3 and SiO_2, respectively.[71] It is worth noting that the

Table 1 Effect of the ratio of B_4C to SiC on the sintering performance and microstructure of B_4C–SiC ceramics

Ceramics	Raw material	Sintering method	Sintering temperature (°C)	Sintering aid	Relative density (%)	Phase composition	Average grain size (μm)
SiC[68]	α-SiC (0.6 μm)	Pressureless	2150	0.6 wt% B + 2 wt% carbon black	93.5	—	>8.0
SiC-5 vol% B_4C[68]	α-SiC (0.6 μm), B_4C (0.7–0.9 μm)	Pressureless	2150	1 wt% carbon black	96.0	—	SiC: 8.0, B_4C: 2.0
B_4C-10 wt% SiC[20]	B_4C (<5.0 μm), α-SiC	Pressureless	2200	2.5 wt% phenolic resin	93.0	—	0.5–3.0
B_4C-30 wt% SiC[20]	B_4C (<5.0 μm), α-SiC	Pressureless	2200	2.5 wt% phenolic resin	97.3	—	0.5–3.0
B_4C-70 wt% SiC[20]	B_4C (<5.0 μm), α-SiC	Pressureless	2200	2.5 wt% phenolic resin	97.6	—	0.5–3.0
B_4C-90 wt% SiC[20]	B_4C (<5.0 μm), α-SiC	Pressureless	2200	2.5 wt% phenolic resin	99.0	—	0.5–3.0
B_4C[70]	B_4C (0.8 μm)	Pressureless	2300	3 wt% carbon black	94.4	B_4C, C	3.0–4.0
B_4C-20 wt% SiC[70]	B_4C (0.8 μm), α-SiC (0.4 μm)	Pressureless	2300	3 wt% carbon black	93.8	B_4C, SiC, C	—
B_4C-40 wt% SiC[70]	B_4C (0.8 μm), α-SiC (0.4 μm)	Pressureless	2300	3 wt% carbon black	93.5	B_4C, SiC, C	B_4C: 2.0, SiC: 3.0
B_4C-60 wt% SiC[70]	B_4C (0.8 μm), α-SiC (0.4 μm)	Pressureless	2300	3 wt% carbon black	95.6	B_4C, SiC, C	—
B_4C-80 wt% SiC[70]	B_4C (0.8 μm), α-SiC (0.4 μm)	Pressureless	2300	3 wt% carbon black	96.5	B_4C, SiC, C	—
B_4C-97 wt% SiC[70]	B_4C (0.8 μm), α-SiC (0.4 μm)	Pressureless	2300	3 wt% carbon black	99.0	SiC, C	—
SiC-10 wt% B_4C[71]	B_4C, α-SiC	Spark plasma (50 MPa)	1950 (×5 min)	1.5 wt% C	99.6	B_4C, SiC, C	—
SiC-20 wt% B_4C[71]	B_4C, α-SiC	Spark plasma (50 MPa)	1950 (×5 min)	1.5 wt% C	99.2	B_4C, SiC, C	—
SiC-30 wt% B_4C[71]	B_4C, α-SiC	Spark plasma (50 MPa)	1950 (×5 min)	1.5 wt% C	98.8	B_4C, SiC, C	—
SiC-40 wt% B_4C[71]	B_4C, α-SiC	Spark plasma (50 MPa)	1950 (×5 min)	1.5 wt% C	98.8	B_4C, SiC, C	—
SiC-50 wt% B_4C[71]	B_4C, α-SiC	Spark plasma (50 MPa)	1950 (×5 min)	1.5 wt% C	98.9	B_4C, SiC, C	—
B_4C-65 vol% SiC[72]	B_4C (0.8 μm), α-SiC (0.5 μm)	Hot-press (40 MPa)	2000	No	100.0	B_4C, SiC	B_4C: 1.5, SiC: 1.3
B_4C-44 vol% SiC[72]	B_4C (0.8 μm), α-SiC (0.5 μm)	Hot-press (40 MPa)	2000	No	99.9	B_4C, SiC, C	B_4C: 1.6, SiC: 1.0
B_4C-25 vol% SiC[72]	B_4C (0.8 μm), α-SiC (0.5 μm)	Hot-press (40 MPa)	2000	No	99.8	B_4C, SiC, C	B_4C: 2.1, SiC: 1.1
B_4C-75 wt% SiC[64]	B_4C (2.5 μm), β-SiC (0.6 μm)	Ultra-high pressure (4 GPa)	1500 (×1 min)	No	96.4	B_4C, β-SiC	—
B_4C-50 wt% SiC[64]	B_4C (2.5 μm), β-SiC (0.6 μm)	Ultra-high pressure (4 GPa)	1500 (×1 min)	No	98.0	B_4C, β-SiC	—
B_4C-25 wt% SiC[64]	B_4C (2.5 μm), β-SiC (0.6 μm)	Ultra-high pressure (4 GPa)	1500 (×1 min)	No	96.9	B_4C, β-SiC	—
B_4C–SiC[75]	B_4C (4.08 μm), 0 wt% carbon black, Si (5–10 mm)	Reaction	1550	No	99.9	B_4C, SiC, Si, $B_{12}(B, C, Si)_3$	—
B_4C–SiC[75]	B_4C (4.08 μm), 6 wt% carbon black, Si (5–10 mm)	Reaction	1550	No	99.9	B_4C, SiC, Si, $B_{12}(B, C, Si)_3$	—
B_4C–SiC[75]	B_4C (4.08 μm), 8 wt% carbon black, Si (5–10 mm)	Reaction	1550	No	99.4	B_4C, SiC, Si, $B_{12}(B, C, Si)_3$	—
B_4C–SiC[75]	B_4C (4.08 μm), 10 wt% carbon black, Si (5–10 mm)	Reaction	1550	No	99.1	B_4C, SiC, Si, $B_{12}(B, C, Si)_3$	—
B_4C–SiC[75]	B_4C (4.08 μm), 12 wt% carbon black, Si (5–10 mm)	Reaction	1550	No	98.7	B_4C, SiC, Si, $B_{12}(B, C, Si)_3$	—

acid etching treatment cannot completely remove oxide film impurities; the content of oxide film contamination is reduced through this approach. After the pre-washing of raw materials, the relative density of the obtained B_4C–SiC ceramics can be slightly increased.[87]

3.2.3. Species. B_4C–SiC ceramics can be produced from different species of raw materials, which have different effects on the sintering performance and microstructure of B_4C–SiC ceramics. α-SiC and β-SiC are the two main species for SiC raw materials. Thévenot[20] found that B_4C–60 wt% SiC ceramics, when using β-SiC as the raw material, exhibit a poorer sintering behavior compared to those using α-SiC as the raw material. This phenomenon may be attributed to the partial transformation of β → α-SiC during the sintering process, resulting in the formation of plate-like (or acicular) grains with a length of 15 μm. Rocha and Melo[88,89] also proved that the relative density of the pressureless sintered B_4C–SiC ceramics with β-SiC as the raw material decreases from 81.3 to 67.5% with an increase in SiC content from 10 to 50 wt%. This conclusion is different from that with α-SiC as the raw material mentioned in Section 3.1. During the SiC phase transformation, equiaxed shaped β-SiC grains change to plate-like shaped α-SiC grains with a high aspect ratio, and the amount of these platelet-shaped SiC grains increases with an increase in SiC content in the ceramics. The platelet-shaped SiC grains can lead to early impingement of large grains, forming a skeleton that can arrest the densification of the ceramics. The higher the amount of platelet-shaped SiC grains, the lower the relative density the B_4C–SiC ceramics achieve.

Different from the mechanical method to physically mix B_4C and SiC powders, using organic precursors is another method to prepare B_4C–SiC ceramics. SiC can be generated from the pyrolysis of organic precursors. For example, polycarbosilane (PCS) can be converted to nanocrystalline SiC after pyrolysis at high temperatures (1000–1300 °C) with a conversion yield of 60–70 wt%.[90] Therefore, many researchers investigate the sintering performance and microstructure of the B_4C–SiC ceramics fabricated *via* the preceramic polymer (PCP) route. Thévenot[20] used PCS and Alnovol PN 320 as the precursors of SiC and C, respectively, mixing B_4C powders to prepare B_4C–SiC ceramics. The relative density of the green body is 60% after cold pressing, and the relative density of the resulting pressureless sintered B_4C–SiC ceramics is 95%. Du *et al.*[91] mentioned that the introduction of SiC in the form of PCS can promote the sinterability of B_4C–SiC ceramics. The SiC obtained from PCS after pyrolyzing at 850 °C is amorphous, but β-SiC crystals are formed after hot-press sintering at 1950 °C. On the one hand, the size distribution of SiC formed ranges from 80 nm to 1 μm. The fine SiC nanocrystals with high activity can bond B_4C grains together and fill spaces to generate a dense structure. On the other hand, a small amount of active carbon derived from the pyrolysis residue of PCS can remove oxide layers existing on B_4C raw materials, thus improving the sinterability of the B_4C–SiC ceramics. Hwang *et al.*[87] found that increasing the pyrolysis temperature of PCS cannot change the phase composition and content of the spark plasma sintered B_4C–SiC ceramics; however, it can change the ceramic microstructure, which in turn improves the relative density of the ceramics. This is because the increase in the pyrolysis temperature of PCS can reduce the gas evolution during the sintering process. Moreover, organic precursors not only provide a source of raw materials but are also used as polymer additives in a warm pressing process to increase the relative density of the B_4C–SiC green body. Lin and He[92] first used PCS as a precursor of SiC to prepare PCS-coated B_4C powders, and then the B_4C–SiC green bodies were produced from these powders by warm pressing at 300 °C. Because PCS can undergo plastic rheology at 300 °C, which can reduce the friction between B_4C particles as well as between B_4C particles and the die wall, thus, the powders can be rearranged smoothly under pressure. As a result, the relative density of the B_4C–15 wt% SiC green body (65%) produced through warm pressing (50 MPa) is higher than that of the B_4C–15 wt% SiC green body (54%) produced through cold isostatic pressing (800 MPa). The improvement in the relative density of the green body is helpful in increasing the densification of the final B_4C–SiC ceramics; therefore, the relative density of the B_4C–15 wt% SiC ceramics (97%) produced through warm pressing is higher than that of the B_4C-15 wt% SiC ceramics (91%) produced through cold isostatic pressing after pressureless sintering at 2000 °C. Meanwhile, β-SiC grains formed from PCS are uniformly distributed in the B_4C matrix.

The PCP route provides an approach for the improved microstructure control of B_4C–SiC ceramics, and it is an effective method to obtain fine-grained B_4C–SiC ceramic. For the microstructure of the B_4C–SiC ceramics prepared from the SiC generated by the pyrolysis of organic precursors, compared with the microstructure of the B_4C–SiC ceramics prepared by the conventional powder mixing, Lörcher *et al.*[93] found that B_4C–SiC ceramics show a preferable presence of SiC at the B_4C grain boundaries when the SiC phase is generated from the precursor of copolymerized polysilane containing dimethylsilylene and methylphenylsilylene groups; thus, SiC grains are more homogeneously distributed in the B_4C matrix. The SiC phase existing at the grain boundaries plays a role in inhibiting the growth of B_4C grains. Du *et al.*[91] noted that some SiC grains with nano or submicron size formed from PCS locate within B_4C grains (Fig. 3a) or at B_4C grain boundaries (Fig. 3b), forming intragranular and intergranular SiC structures. These nano-sized or submicron-sized SiC grains are favorable for forming a sub-boundary structure in B_4C–SiC ceramics under internal stress, which can refine B_4C grains and improve the mechanical properties of B_4C–SiC ceramics. Meanwhile, the formation of these fine SiC grains means that more barriers are placed in the way of grain boundaries, thereby pinning the migration of grain boundaries and inhibiting the growth of B_4C grains. In addition, the SiC grains formed from PCS show a layered structure (Fig. 3c), and dislocation defects appear in the SiC grains (Fig. 3b). The formation of the layered structure is caused by the pyrolysis of PCS and crystallization process. When SiC nuclei grow from an amorphous medium, the content of free C also increases, resulting in the formation of a heterogeneous material with an extremely divided microtexture: SiC nuclei are considered to be divided by a thin film of C arranged as a stack of few layers. Thus, the formation of the layered

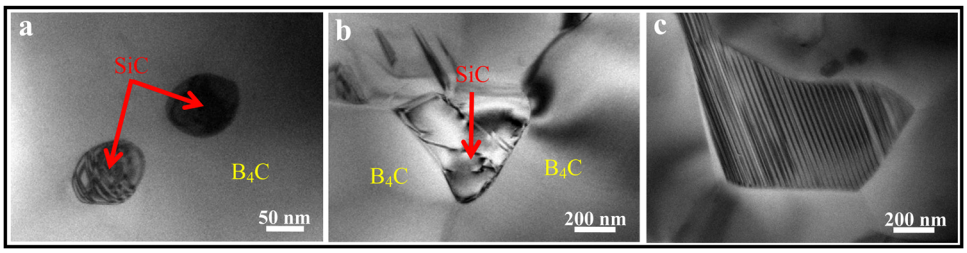

Fig. 3 TEM images of hot-press sintered B_4C–15 wt% SiC ceramics produced *via* the introduction of SiC in the form of PCS: (a) intragranular SiC structure, (b) intergranular SiC structure, and (c) SiC grains with a layered structure[91] (reproduced with permission, Copyright 2013, Elsevier).

structure within the SiC grains generated from PCS pyrolysis is due to the presence of disordered residual C between SiC layers. The microstructure characteristics of the layered structure and dislocation can affect the mechanical properties of B_4C–SiC ceramics produced by the introduction of SiC in the form of PCS, especially the fracture toughness, which will be discussed in Section 4.3.2. The use of PCS is a suitable approach to achieve a homogeneous structure in B_4C–SiC ceramics, which helps avoid the polluting milling process; however, the main drawback is that the β-SiC obtained from PCS pyrolysis will be transformed into α-SiC coarse grains during sintering.

Besides directly mixing commercial B_4C and SiC powders, B_4C–SiC ceramics can also be produced *in situ* through chemical reactions of two or more raw materials. Zhang *et al.*[94,95] first used B_4C, Si, and amorphous carbon powders to prepare B_4C–20 wt% SiC nanocomposite powders (50–150 nm) *in situ via* high-energy ball milling; then, B_4C–SiC ceramics were produced from these B_4C–SiC nanocomposite powders *via* hot-press sintering at 1950 °C or spark plasma sintering at 1800 °C. The relative densities of the resulting B_4C–SiC ceramics were in the range of 98.5% to 99.5%, and fine grains were obtained in the ceramics *via* this route. Sahin *et al.*[96] used B_4C, SiO_2, and carbon black as raw materials to produce B_4C–SiC ceramics *via* spark plasma sintering at 1750 °C, the formation of which is shown as follows:

$$B_4C + SiO_2 + 3C \rightarrow B_4C + SiC + 2CO \quad (1)$$

The relative density of the resulting B_4C–SiC ceramics decreased linearly from 97.7% to 88.3% with the increase in *in situ* formed SiC content from 5 to 20 vol%. This phenomenon is caused by the fact that the *in situ* formed SiC is oxidized by the intermediate product of B_2O_3 to SiO gas during the sintering process, resulting in the formation of residual pores in the B_4C–SiC ceramics; the formation of more SiC content *in situ* is accompanied by an increase in residual pores. This suggests that B_4C–SiC ceramics with a high SiC content are not easily densified through this route. In addition, Pánek[97] used B powders, Si platelets, and carbon black as raw materials to produce B_4C–SiC ceramics *in situ* (reaction (2)) by combustion hot-press sintering, which is based on the combination of the self-propagating high-temperature synthesis technique and hot-press sintering. The resulting B_4C–SiC ceramics can achieve an extremely low porosity (0.3%), and their purity is rather high.

$$4B + Si + 2C \rightarrow B_4C + SiC \quad (2)$$

Some previous studies on the effect of raw material on the sintering performance and microstructure of B_4C–SiC ceramics are tabulated in Table 2.

3.3. Preparation process

The sintering performance and microstructure of B_4C–SiC ceramics vary depending on the processing conditions and parameters. Various factors including powder mixing methods, preparation of the green body, and parameters during sintering affect the sintering performance and microstructure of B_4C–SiC ceramics.

3.3.1. Powder mixing method. In general, B_4C–SiC composite powders are prepared from multiple single-component powders by dry mixing or wet mixing. The difference between dry mixing and wet mixing is the presence of a liquid medium. Ethanol and water are commonly used as media for wet mixing to prepare B_4C–SiC composite powders. Yaşar and Haber[71] compared the effects of dry mixing and wet mixing methods of B_4C–SiC composite powders on the sintering performance and microstructure of spark plasma sintered B_4C–SiC ceramics. The B_4C–SiC ceramics produced from B_4C–SiC composite powders prepared by dry mixing cannot achieve a uniform microstructure; there are some large pockets of individual components (Fig. 4a), while the microstructure of the B_4C–SiC ceramics produced from B_4C–SiC composite powders prepared by wet mixing is uniform (Fig. 4b). Compared with the relative density of the B_4C–SiC ceramics produced from the B_4C–SiC composite powders prepared by dry mixing, the relative density of the B_4C–SiC ceramics produced from the B_4C–SiC composite powders prepared by wet mixing is higher. The agglomeration problem caused by dry mixing has a negative impact on the mechanical properties of B_4C–SiC ceramics.

Ball milling and high-energy ball milling are two common methods for mixing multiple single-component powders. Zhang *et al.*[98] first prepared B_4C–SiC composite powders by ball milling and high-energy ball milling, and then compared the sintering performance of B_4C–SiC ceramics produced from these B_4C–SiC composite powders synthesized by the two milling methods. Although the particle sizes of raw materials of B_4C and SiC used in the high-energy ball milling method are larger than those used in the ball milling method (Table 3), the resulting mean particle size (0.7 μm) after high-energy ball milling remains the same as that achieved through ball milling. In the B_4C–SiC ceramics produced from the B_4C–SiC composite powders

Table 2 Effect of raw material on the sintering performance and microstructure of B_4C–SiC ceramics

Ceramics	Raw material	Sintering method	Sintering temperature (°C)	Sintering aid	Relative density (%)	Phase composition	Average grain size (μm)
B_4C-20 vol% SiC[83]	B_4C (10.22 μm), β-SiC (1.07 μm)	Hot-press (20 MPa)	1900	No	73.7	B_4C, SiC	—
B_4C-20 vol% SiC[83]	B_4C (10.22 μm), β-SiC (1.07 μm)	Hot-press (20 MPa)	2000	No	77.8	B_4C, SiC	—
B_4C-20 vol% SiC[83]	B_4C (10.22 μm), β-SiC (1.07 μm)	Hot-press (20 MPa)	2100	No	87.0	B_4C, SiC	—
B_4C-5 vol% SiC[80]	B_4C (307 nm), SiC (80 nm)	Pressureless	2200	No	—	B_4C, SiC	16.1
B_4C-5 vol% SiC[80]	B_4C (307 nm), SiC (1.0 μm)	Pressureless	2200	No	—	B_4C, SiC	16.3
B_4C-7.5 vol% SiC[80]	B_4C (307 nm), SiC (80 nm)	Pressureless	2200	No	—	B_4C, SiC	15.8
B_4C-7.5 vol% SiC[80]	B_4C (307 nm), SiC (1.0 μm)	Pressureless	2200	No	—	B_4C, SiC	15.8
B_4C-10 vol% SiC[80]	B_4C (307 nm), SiC (80 nm)	Pressureless	2200	No	—	B_4C, SiC	15.6
B_4C-10 vol% SiC[80]	B_4C (307 nm), SiC (1.0 μm)	Pressureless	2200	No	—	B_4C, SiC	14.8
B_4C-60 wt% SiC[20]	B_4C (<5.0 μm), α-SiC	Pressureless	2200	2.5 wt% phenolic resin	97.5	B_4C, SiC, C	—
B_4C-60 wt% SiC[20]	B_4C (<5.0 μm), β-SiC	Pressureless	2200	2.5 wt% phenolic resin	95.7	B_4C, SiC, C	—
B_4C-10 wt% SiC[88]	B_4C, β-SiC	Pressureless	2000	No	81.3	B_4C, α-SiC, (β-SiC)	—
B_4C-30 wt% SiC[88]	B_4C, β-SiC	Pressureless	2000	No	74.0	B_4C, α-SiC, (β-SiC)	—
B_4C-50 wt% SiC[88]	B_4C, β-SiC	Pressureless	2000	No	67.5	B_4C, α-SiC, (β-SiC)	—
B_4C-5 wt% SiC[20]	B_4C, PCS	Pressureless	2175	Phenolic resin	95.0	B_4C, SiC	32.0
B_4C[91]	B_4C (3.5 μm)	Hot-press (30 MPa)	1950	No	91.7	B_4C	—
B_4C-15 wt% SiC[91]	B_4C (3.5 μm), PCS	Hot-press (30 MPa)	1950	No	96.1	B_4C, β-SiC	SiC < 1.0
B_4C-10 wt% SiC[87]	B_4C (0.3–0.6 μm, as-received), PCS (pyrolyzed at 800 °C)	Spark plasma (50 MPa)	1900 (×5 min)	No	96.2	B_4C, SiC, C	—
B_4C-10 wt% SiC[87]	B_4C (0.3–0.6 μm, washed off by HCl), PCS (pyrolyzed at 800 °C)	Spark plasma (50 MPa)	1900 (×5 min)	No	97.2	B_4C, SiC, C	—
B_4C-10 wt% SiC[87]	B_4C (0.3–0.6 μm, washed off by HCl), PCS (pyrolyzed at 1385 °C)	Spark plasma (50 MPa)	1900 (×5 min)	No	99.7	B_4C, SiC, C	—
B_4C-20 wt% SiC[87]	B_4C (0.3–0.6 μm, washed off by HCl), PCS (pyrolyzed at 1385 °C)	Spark plasma (50 MPa)	1900 (×5 min)	No	99.5	B_4C, SiC, C	—
B_4C-20 wt% SiC[94]	B_4C, SiC, mean particle size of 50–150 nm	Hot-press (30 MPa)	1950	No	98.6	B_4C, SiC	B_4C = 1.0–3.0, SiC < 2.0
B_4C-20 wt% SiC[95]	B_4C, SiC, mean particle size of 50–150 nm	Spark plasma (30 MPa)	1800 (×5 min)	No	99.2	B_4C, SiC	B_4C = 1.0, SiC < 1.0
B_4C-5 vol% SiC[96]	B_4C, SiO_2, carbon black	Spark plasma (40 MPa)	1750 (×5 min)	No	97.7	B_4C, SiC, C	—
B_4C-10 vol% SiC[96]	B_4C, SiO_2, carbon black	Spark plasma (40 MPa)	1750 (×5 min)	No	93.8	B_4C, SiC, C	—
B_4C-15 vol% SiC[96]	B_4C, SiO_2, carbon black	Spark plasma (40 MPa)	1750 (×5 min)	No	91.2	B_4C, SiC, C, SiO_2	—
B_4C-20 vol% SiC[96]	B_4C, SiO_2, carbon black	Spark plasma (40 MPa)	1750 (×5 min)	No	88.3	B_4C, SiC, C, SiO_2	—
B_4C-50 vol% SiC[97]	B powders (1.5 μm), Si platelets, carbon black	Combustion hot-press (30 MPa)	1900 (×20 min)	No	99.7	B_4C, SiC	—

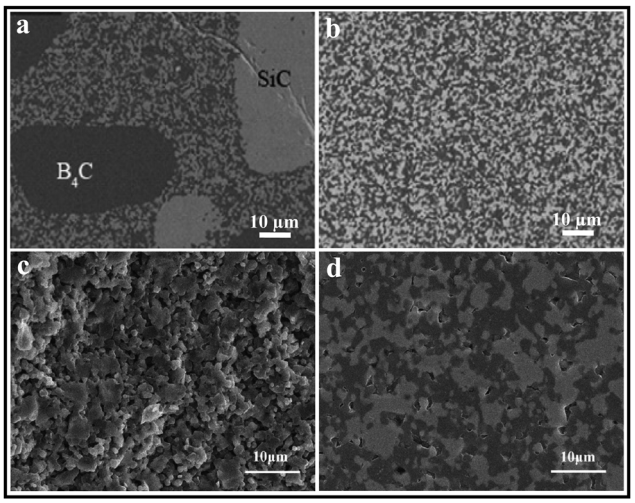

Fig. 4 Microstructure of spark plasma sintered SiC–40 wt% B_4C ceramics produced from the B_4C–SiC composite powders prepared by: (a) dry mixing and (b) wet mixing[71] (reproduced with permission, Copyright 2020, Elsevier). Fracture surfaces of hot-press sintered B_4C–50 wt% SiC ceramics using B_4C–SiC composite powders prepared by: (c) ball milling and (d) high-energy ball milling[98] (reprinted with permission, Copyright 2013, Elsevier).

synthesized *via* usual wet ball milling, there are a lot of pores and separate fine powders (Fig. 4c); the relative density of the ceramics is 85%. However, under the same sintering conditions, few pores and no separate fine powders exist in the B_4C–SiC ceramics produced from the B_4C–SiC composite powders synthesized *via* high-energy ball milling (Fig. 4d), whose relative density is up to 96%. With the same particle size and sintering conditions, using high-energy ball milling to prepare B_4C–SiC composite powders can decrease the sintering temperature and promote the sintering for the preparation of B_4C–SiC ceramics. High-energy ball milling can induce transformation of B_4C and SiC composite powders from an ordered to disordered structure during the milling process; then these composite powders with a disordered structure are transformed into B_4C–SiC ceramics with an ordered structure in the subsequent sintering process. The energy released during the transformation of disorder–order can serve as a sintering driving force. Therefore, using the composite powders prepared by high-energy ball milling can improve the sintering performance of B_4C–SiC ceramics.

Some previous studies on the effect of the powder mixing method on the sintering performance and microstructure of B_4C–SiC ceramics are tabulated in Table 3.

3.3.2. Preparation of the green body. For some preparation methods of B_4C–SiC ceramics, such as pressureless sintering and reaction-bonded sintering, multiple single-component powders need to be pre-compacted into the green body. At first, the mixed composite powders are loosely stacked in the mold; even after the compaction, there are still a large number of pores present in the green body. The improvement of the relative density of the green body can increase the relative density and mechanical properties of the resulting ceramics.

As mentioned in Section 3.2.1, the particle size and packing structure affect the relative density of the green body.

Table 3 Effect of the powder mixing method on the sintering performance and microstructure of B_4C–SiC ceramics

Ceramics	Raw material	Powder mixing method	Sintering method	Sintering temperature (°C)	Sintering aid	Relative density (%)	Phase composition	Average grain size (μm)
SiC-10 wt% B_4C[71]	B_4C, SiC	Dry mixing	Spark plasma (50 MPa)	1950 (×5 min)	1.5 wt% C	98.6	B_4C, SiC, C	—
SiC-10 wt% B_4C[71]	B_4C, SiC	Wet mixing (ethanol)	Spark plasma (50 MPa)	1950 (×5 min)	1.5 wt% C	99.6	B_4C, SiC, C	—
SiC-20 wt% B_4C[71]	B_4C, SiC	Dry mixing	Spark plasma (50 MPa)	1950 (×5 min)	1.5 wt% C	98.7	B_4C, SiC, C	—
SiC-20 wt% B_4C[71]	B_4C, SiC	Wet mixing (ethanol)	Spark plasma (50 MPa)	1950 (×5 min)	1.5 wt% C	99.2	B_4C, SiC, C	—
SiC-30 wt% B_4C[71]	B_4C, SiC	Dry mixing	Spark plasma (50 MPa)	1950 (×5 min)	1.5 wt% C	98.5	B_4C, SiC, C	—
SiC-30 wt% B_4C[71]	B_4C, SiC	Wet mixing (ethanol)	Spark plasma (50 MPa)	1950 (×5 min)	1.5 wt% C	98.8	B_4C, SiC, C	—
SiC-40 wt% B_4C[71]	B_4C, SiC	Dry mixing	Spark plasma (50 MPa)	1950 (×5 min)	1.5 wt% C	97.8	B_4C, SiC, C	—
SiC-40 wt% B_4C[71]	B_4C, SiC	Wet mixing (ethanol)	Spark plasma (50 MPa)	1950 (×5 min)	1.5 wt% C	98.8	B_4C, SiC, C	—
SiC-50 wt% B_4C[71]	B_4C, SiC	Dry mixing	Spark plasma (50 MPa)	1950 (×5 min)	1.5 wt% C	97.5	B_4C, SiC, C	—
SiC-50 wt% B_4C[71]	B_4C, SiC	Wet mixing (ethanol)	Spark plasma (50 MPa)	1950 (×5 min)	1.5 wt% C	98.9	B_4C, SiC, C	—
B_4C-50 wt% SiC[98]	B_4C (0.7 μm), SiC (0.8 μm)	Ball milling (ethanol)	Hot-press (30 MPa)	1950	No	85.0	B_4C, SiC	1.0
B_4C-50 wt% SiC[98]	B_4C (2.57 μm), SiC (3.11 μm), mean particle size of 0.7 μm after high-energy ball milling	High-energy ball milling (ethanol)	Hot-press (30 MPa)	1950	No	96.0	B_4C, SiC	<1.0

Furthermore, to achieve the maximal relative density of the green body without generating internal cracks, the compaction pressure during compaction should be taken into account.[99] A suitable compaction pressure is rather important to achieve the maximal relative density of the ceramic preform. Hayun *et al.*[84] found that the relative density of the green body composed of either graded B_4C particles or monosized fine B_4C particles increases with an increase in compaction pressure from 40 to 160 MPa. The relative density remains constant under a higher compaction pressure (180 MPa); however, excessive compaction pressure may result in the generation of internal cracks in the green body.

Warm pressing is one of the methods to increase the relative density of the green body. Adding a polymer into ceramic powders and pressing the green body above the softening temperature of the polymer can lead to the production of a green body with higher relative density by using the viscous flow of the polymer, thus improving the relative density and mechanical properties of the obtained ceramic. As mentioned in Section 3.2.3, the addition of PCS, which can be used as a precursor of SiC, can increase the relative density of the green body by warm pressing at 300 °C.

For the green body produced for the preparation of reaction-bonded B_4C–SiC ceramics, interconnected pores that can provide a penetration path for molten Si are necessary; thus, a necessary minimum porosity should be provided for capillary impregnation. Meanwhile, the high volume expansion caused by the siliconisation reaction easily blocks the capillary channels, inhibiting Si infiltration; thus, the pore size also needs to be considered. Both pore volume fraction and pore size control the impregnation efficiency and phase composition. On the one hand, increasing pore parameters can improve the impregnation efficiency of molten Si and increase the amount of SiC generated;[77] on the other hand, decreasing pore parameters contributes to limiting the fraction of residual non-reacted Si after infiltration.[84] Therefore, it is necessary to balance the two aspects to achieve an optimum relative density of the green body. In addition, the addition of C affects the porosity of the green body. Li *et al.*[76] found that carbon black can decrease the open pore size of the green body prepared by slip casting, but can increase the porosity of the green body, which is attributed to the particle agglomeration and consequently increased slip-casting slurry viscosity.

For the reaction-bonded B_4C–SiC ceramics, the properties of the green body decide the final properties of the ceramics. The forming technique for the green body affects the microstructures of the green body and the resulting B_4C–SiC ceramics. Conventionally, the green body composed of B_4C and carbon black is prepared by uniaxial compaction. However, the distribution of density and pores in the green body is not uniform *via* this route due to the inhomogeneous mold pressure, leading to the formation of some inhomogeneous carbon black agglomerates,[100] which in turn is not conducive to the homogenization of the microstructure of the obtained B_4C–SiC ceramics; many large-sized SiC zones and relatively large, uneven residual Si phases are formed in the obtained ceramics.[101] Xu *et al.*[102] found an alternative solution to prepare the green body with a uniform microstructure, *viz.*, gel-casting technique. A hierarchical porous B_4C–C green body with both mesopores and macropores is produced by the gel-casting method. The polymerization-induced phase separation and pyrolysis result in the formation of mesopores on the carbon matrix; the space occupied by solvent becomes macropores after evaporation. The hierarchical porous green body is suitable for the molten Si infiltration process and favors the reduction in the size of residual Si islands. Upon molten Si infiltration, such hierarchically porous structure in the C-bonded B_4C green body prepared by the gel-casting method can not only improve the uniformity of the microstructure but also generate a SiC-bonded B_4C scaffold structure in the resulting B_4C–SiC ceramics. In addition, the pore structure and porosity of the green body will control the content and size of the residual Si, which in turn affects the mechanical properties of the reaction-bonded B_4C–SiC ceramics. Therefore, the performance of reaction-bonded B_4C–SiC ceramics can be adjusted by controlling the pore characteristics of the green body. Ren *et al.*[103] found that adjusting the content of the catalyst Na_2CO_3 can help control the pore characteristics of the B_4C–C green body prepared by gel-casting, whose mechanism is that the degree of cross-linking within the gel is modified to control the phase separation process by adjusting the content of the catalyst. With an increase in catalyst content, the porosity and pore size of the green body decrease, and the pore structure of the green body changes from a single macroporous or mesoporous structure to a hierarchical macroporous–mesoporous structure, reducing the residual Si content in the B_4C–SiC ceramics.

3.3.3. Parameters during sintering

3.3.3.1. Sintering temperature. Sintering temperature is a crucial parameter for the preparation of B_4C–SiC ceramics in the sintering process. Generally, increasing the sintering temperature can accelerate the diffusion rate of atoms, which is beneficial for improving the densification of B_4C–SiC ceramics. Also, the grain size of B_4C–SiC ceramics increases with an increase in sintering temperature; however, excessive sintering temperature can cause grain coarsening and abnormal grain growth. For reaction-bonded sintering, increasing infiltration temperature can enhance the liquid–solid wettability and liquid Si fluidity,[104] thus improving its permeability in the preform; meanwhile, high temperature will accelerate the diffusion of C atoms in molten Si, accelerating the grain growth of SiC.[105,106]

For B_4C–SiC ceramics produced *via* pressureless sintering, Zhu *et al.*[107] studied the effect of sintering temperature in the range of 2100 to 2200 °C on the sintering performance and microstructure of B_4C–15 wt% SiC ceramics under the mechanism of solid-state sintering. The phase composition of the composite ceramics is B_4C, SiC, and graphite after sintering at different temperatures. The formation of graphite suggests that amorphous carbon black that is used as a sintering aid undergoes crystallization, whose degree increases with the increase in sintering temperature. The relative density of B_4C–SiC ceramics increases first and then decreases with increasing temperature from 2100 to 2200 °C; the grain size of the ceramics increases with an increase in sintering temperature. At 2100 °C, most of the

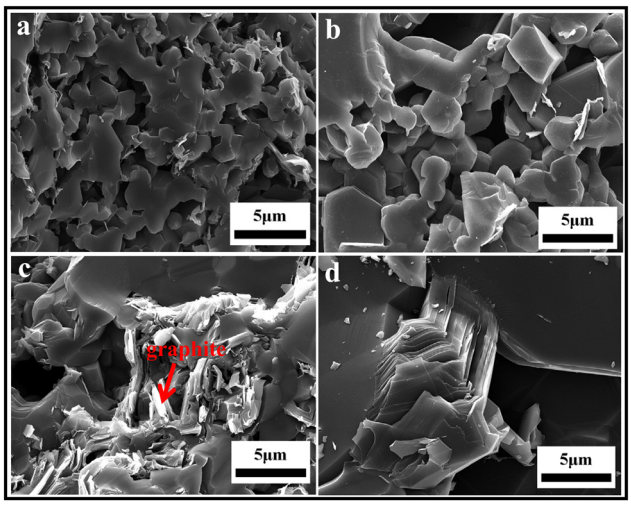

Fig. 5 Fracture surfaces of pressureless sintered B_4C–15 wt% SiC ceramics sintered at: (a) 2100 °C, (b) 2125 °C, (c) 2150 °C, and (d) 2175 °C[107] (reprinted with permission, Copyright 2019, Elsevier).

sintered necks do not grow, and there are a lot of pores in the matrix (Fig. 5a). With an increase in sintering temperature to 2150 °C, sintered necks grow gradually, and the number of pores is reduced (Fig. 5b and c). Meanwhile, some fine SiC grains uniformly distribute at the grain boundary, pinning the migrating grain boundaries and inhibiting the growth of B_4C grains. The lamellar graphite is located on the surface of B_4C grains. However, when the sintering temperature is further increased to more than 2150 °C, the movement of the grain boundary is so rapid that pores cannot be eliminated, resulting in the decreased relative density of B_4C–SiC ceramics. Also, the sizes of lamellar graphite and pore increase (Fig. 5d). Vandeperre and Teo[108] investigated the effect of sintering temperature in the range of 1950 to 2200 °C on the sintering performance of B_4C–SiC ceramics with different ratios of B_4C to SiC. The relative density of SiC-rich ceramics can reach up to 95% after sintering at 2050 °C. However, higher sintering temperatures are needed for B_4C-rich ceramics to achieve better sintering performance, and the relative density of B_4C-rich ceramics is 95% only after sintering at 2200 °C. This phenomenon may be caused by the greater proportion of covalent bonds in B_4C. Moradkhani and Baharvandi[80] found that the grain size of B_4C–10 wt% SiC ceramics slightly increases with the increase in sintering temperature from 2100 to 2200 °C. In addition, the excessive sintering temperature is also not beneficial for improving the densification of B_4C–SiC ceramics under the mechanism of liquid-phase sintering. Zhang *et al.*[109] observed that the relative density of SiC–10 wt% B_4C ceramics with the sintering aids of Al_2O_3 and La_2O_3 increases first and then decreases with the increase in sintering temperature from 1800 to 1935 °C. Higher sintering temperatures result in the volatilization of the liquid phase with a low melting point and the anisotropic growth of the SiC grains, decreasing the relative density.

For B_4C–SiC ceramics prepared by hot-press sintering, Zhang *et al.*[98] reported that the relative density of B_4C–50 wt% SiC ceramics increases linearly with an increase in sintering temperature in the range of 1800–1950 °C. At 1800 °C, the densification of B_4C–SiC ceramics begins, but most of the particles are not sintered. When the sintering temperature rises to 1950 °C, there are few pores in the ceramics and the relative density of B_4C–SiC ceramics is up to 96%. Chen *et al.*[110] found that the grains of B_4C–20 wt% SiC ceramics become smaller and the microstructure becomes denser with the increase in sintering temperature from 1800 to 1900 °C, which is attributed to the elimination of pores between grains due to the movement of grain boundaries with the increase in sintering temperature.

For spark plasma sintered B_4C–SiC ceramics, Wu *et al.*[111] observed that the relative density of the B_4C–20 vol% SiC ceramics increases with the increase in sintering temperature from 1900 to 2100 °C. When the sintering temperature is lower than 2000 °C, a large number of pores exist in the ceramics, but many sintered necks have been formed. When the sintering temperature is 2000 °C, the grown grains are tightly connected, and the pores almost completely disappear. When the sintering temperature is higher than 2000 °C, the microstructure of the ceramics no longer changes significantly. Moshtaghioun *et al.*[112] reported that the grain sizes of both B_4C and SiC in the B_4C–15 wt% SiC ceramics are independent of the sintering temperature in the range of 1650 to 1700 °C. Although the particle sizes of B_4C and SiC raw materials are the same, the B_4C grains are larger than the SiC grains in the resulting B_4C–SiC ceramics. This is because B_4C is the connected phase in the microstructure; as a result, the diffusion of B and C resulting in B_4C grain growth is easier.

The sintering temperature not only affects the porosity and grain size but also affects the crystallization of B_4C–SiC ceramics. Zhang *et al.*[94,95] noted that the structure of B_4C–SiC ceramics undergoes a disorder–order transformation from 1700 to 1900 °C *via* hot-press sintering or from 1600 to 1700 °C *via* spark plasma sintering when B_4C–SiC composite powders composed of B_4C with increased volume of lattice defects and amorphous SiC, which are prepared by high-energy ball milling, are used as raw materials. This indicates that increasing the sintering temperature within a certain range can increase the stacking order of the structure.

For B_4C–SiC ceramics fabricated by reaction-bonded sintering, because the melting temperature of Si is 1410 °C, there is little difference in phase composition between the sintered ceramics and the original powder mixture when the sintering temperature is lower than 1410 °C, indicating that no reaction occurs among B_4C, C, and Si.[113] When the sintering temperature is higher than 1410 °C, Si can melt and infiltrate into the top part of the green body to rapidly react with C to form β-SiC.[113] Although Si can infiltrate into the green body composed of B_4C and graphite, the resulting B_4C–SiC ceramics are still quite porous because the viscosity of molten Si at 1410 °C is relatively high, preventing the infiltration to the porous green body. This suggests that infiltration temperature affects the viscosity of molten Si, and a sufficient temperature is needed to ensure a good fluidity of molten Si. With the increase in sintering temperature to 1450 °C, the reaction between B_4C and Si is further promoted; thus, the obtained B_4C–SiC ceramics are very dense and nearly nonporous. Ordan'yan *et al.*[114]

also pointed out that the temperature of the impregnation process (1450–1800 °C) generally exceeds the melting temperature of Si, resulting from the need to decrease the viscosity of Si melt and enhance the wetting of B_4C and C to facilitate capillary impregnation. Therefore, 1410 °C is a critical temperature for Si infiltration and reaction bonding. Nesmelov and Perevislov[115] mentioned that the temperature interval of 1600–1800 °C is sufficient for Si viscosity to wet the total porous preform. Sun *et al.*[116] noted that the relative density of B_4C–SiC ceramics increases with the increase in sintering temperature from 1660 to 1780 °C. During the molten Si infiltration, C atoms on carbon particles are dissolved at the Si/C interface where a submicron SiC layer is formed; then this SiC layer rapidly cracks into crystalline particles because of the lattice mismatch between the carbon particles and SiC layer. After being dissolved in molten Si, the crystalline SiC particles precipitate on the initial SiC particles. Therefore, the dissolution rate of C atoms and the precipitation rate of crystalline SiC are the main factors affecting the reaction rate. A high sintering temperature is beneficial for increasing the solubility of C atoms and crystalline SiC, improving the reaction rate.

When the infiltration temperature is higher than 1410 °C, the sintering temperature will affect the phase amount of reaction-bonded B_4C–SiC ceramics. Zhang *et al.*[117] found that the amount of B_4C decreases, but the amounts of generated SiC phase and residual Si phase increase with the increase in infiltration temperature from 1450 to 1650 °C. On the one hand, the solubility of B and C in molten Si increases with an increase in infiltration temperature, leading to the increased amount of dissolved B_4C particles; on the other hand, the interface reaction between B_4C and molten Si (reaction (3)), which is negligible at 1450 °C but significant at 1650 °C, is gradually intensified with increasing infiltration temperature, causing further dissolution of B_4C particles in molten Si and increasing the amounts of generated SiC and precipitated $B_{12}(C, Si, B)_3$ on the original B_4C particles.

$$3B_4C(S) + Si(l) \rightarrow SiC(S) + B_{12}(C, Si, B)_3(S) \quad (3)$$

Moreover, the grain shape and grain size of reaction-bonded B_4C–SiC ceramics are also affected by the infiltration temperature.[118] When the sintering temperature is 1450 °C, the grain shape of B_4C basically maintains the original irregular shape of initial B_4C particles with flexuous edges due to the mild dissolution of B_4C grains in molten Si at temperatures below 1550 °C. When the sintering temperature is increased to 1650 °C, the shape of partial large B_4C grains evolves from an irregular shape to a faceted shape with sharp corners and straight edges; the small B_4C grains evolve into a spherical shape because the dissolution of B_4C grains in molten Si is intensified. The grain shape evolution of B_4C can be described by Ostwald ripening: the dissolution of the smaller grains and the precipitation of dissolved components on the grains that are larger than the critical ones.[119] The dissolved materials transfer and precipitate as $B_{12}(B, C, Si)_3$ on the defective concave surface of the large B_4C grains. Thus, the large B_4C grains exhibit the growth shape and the small grains show the dissolution shape. When the sintering temperature is further increased to 1750 °C, the grain shape of B_4C is mostly faceted. Zhang *et al.*[117] also observed that the B_4C particles with the precipitation of $B_{12}(C, Si, B)_3$ gradually develop a multifaced surface morphology with angular shapes and triangular prisms when the sintering temperature is between 1600 and 1650 °C. Meanwhile, the shape of the formed SiC is also affected by the sintering temperature.[117] The SiC morphology evolves from discontinuous, cloud-like SiC to continuous, integrated SiC zones with the increase in sintering temperature from 1450 to 1650 °C. With the increase in the amount of generated SiC, the original discontinuous SiC grains coalesce and connect to each other, forming continuous, integrated SiC zones. Also, the amount and size of these integrated SiC zones increase with an increase in sintering temperature. On the other side, the grain sizes of both B_4C with the precipitation of $B_{12}(C, Si, B)_3$ and generated SiC particles increase with an increase in infiltration temperature.[117] The increased grain size of B_4C with the precipitation of $B_{12}(C, Si, B)_3$ is attributed to the coalescence of neighboring B_4C particles. With the increase in infiltration temperature, there is a greater precipitation of the $B_{12}(C, Si, B)_3$ phase on the surfaces of original B_4C particles, increasing the chance for neighboring B_4C particles to coalesce. Most SiC grains are generated *via* the reaction between molten Si and carbon black, which is controlled by the dissolution–precipitation mechanism at the beginning,[105] and then by the diffusion of Si and C atoms in solid SiC when molten Si is not in contact with C.[106] With the increase in infiltration temperature, the dissolution of C in molten Si is promoted because of the higher solubility of C in molten Si, and the diffusion of Si and C atoms in solid SiC is accelerated; thus, the generated SiC grains grow and ripen at higher temperatures. Zhang *et al.*[118] pointed out that the growth behavior of B_4C grains depends on the sintering temperature and the grain shape. The grain size of B_4C increases with an increase in the sintering temperature. When the sintering temperature is below 1750 °C, the B_4C grains show a unimodal size distribution, suggesting normal grain growth; the grain growth of B_4C is primarily controlled by diffusion. However, when the sintering temperature is above 1750 °C, the B_4C grains exhibit a bimodal size distribution, indicating an abnormal grain growth; the grain growth of B_4C is controlled by coalescence-enhanced two-dimensional nucleation. Abnormal grain growth only occurs when the grain shape of B_4C is faceted.

Some previous studies on the effect of sintering temperature on the sintering performance and microstructure of B_4C–SiC ceramics are tabulated in Table 4.

3.3.3.2. Holding time. Holding time is another factor affecting the microstructure and phase composition of B_4C–SiC ceramics. Tomohiro *et al.*[78] reported that the grain size of the hot-press sintered B_4C–15 vol% SiC ceramics increases from 2–3 to 10 μm with the increase in holding time from 30 to 120 min when the sintering temperature is 2200 °C; however, the relative density of the ceramics is independent on the holding time. For reaction-bonded B_4C–SiC ceramics, when the sintering temperature is fixed at 1550 °C, increasing the holding time can enhance the transformation of B_4C grains from irregular shape to faceted

Table 4 Effect of sintering temperature on the sintering performance and microstructure of B_4C–SiC ceramics

Ceramics	Raw material	Sintering method	Sintering temperature (°C)	Sintering aid	Relative density (%)	Phase composition	Average grain size (μm)
B_4C-15 wt% SiC[107]	B_4C (0.8 μm), SiC (0.5 μm)	Pressureless	2100	2 wt% carbon black	91.6	B_4C, SiC, graphite	2.3
B_4C-15 wt% SiC[107]	B_4C (0.8 μm), SiC (0.5 μm)	Pressureless	2125	2 wt% carbon black	93.6	—	11.2
B_4C-15 wt% SiC[107]	B_4C (0.8 μm), SiC (0.5 μm)	Pressureless	2150	2 wt% carbon black	95.3	B_4C, SiC, graphite	13.6
B_4C-15 wt% SiC[107]	B_4C (0.8 μm), SiC (0.5 μm)	Pressureless	2175	2 wt% carbon black	93.1	—	17.2
B_4C-15 wt% SiC[107]	B_4C (0.8 μm), SiC (0.5 μm)	Pressureless	2200	2 wt% carbon black	—	—	27.9
B_4C-10 vol% SiC[80]	B_4C (307 nm), SiC (1.0 μm)	Pressureless	2100	No	—	B_4C, SiC	14.1
B_4C-10 vol% SiC[80]	B_4C (307 nm), SiC (1.0 μm)	Pressureless	2150	No	—	B_4C, SiC	14.3
B_4C-10 vol% SiC[80]	B_4C (307 nm), SiC (1.0 μm)	Pressureless	2200	No	—	B_4C, SiC	14.8
SiC-10 wt% B_4C[109]	α-SiC (1.0 μm), B_4C (0.5 μm)	Pressureless	1800	10 wt% (Al_2O_3 : La_2O_3 = 1 : 1, molar ratio)	90.2	SiC, B_4C, $LaAlO_3$	—
SiC-10 wt% B_4C[109]	α-SiC (1.0 μm), B_4C (0.5 μm)	Pressureless	1835	10 wt% (Al_2O_3 : La_2O_3 = 1 : 1, molar ratio)	91.8	SiC, B_4C, $LaAlO_3$	—
SiC-10 wt% B_4C[109]	α-SiC (1.0 μm), B_4C (0.5 μm)	Pressureless	1875	10 wt% (Al_2O_3 : La_2O_3 = 1 : 1, molar ratio)	94.0	SiC, B_4C, $LaAlO_3$	—
SiC-10 wt% B_4C[109]	α-SiC (1.0 μm), B_4C (0.5 μm)	Pressureless	1900	10 wt% (Al_2O_3 : La_2O_3 = 1 : 1, molar ratio)	96.8	SiC, B_4C, $LaAlO_3$	—
SiC-10 wt% B_4C[109]	α-SiC (1.0 μm), B_4C (0.5 μm)	Pressureless	1935	10 wt% (Al_2O_3 : La_2O_3 = 1 : 1, molar ratio)	95.3	SiC, B_4C, $LaAlO_3$	—
B_4C-50 wt% SiC[98]	B_4C, SiC, mean particle size of 0.7 μm	Hot-press (30 MPa)	1800	No	74.0	B_4C, SiC	—
B_4C-50 wt% SiC[98]	B_4C, SiC, mean particle size of 0.7 μm	Hot-press (30 MPa)	1850	No	79.2	B_4C, SiC	—
B_4C-50 wt% SiC[98]	B_4C, SiC, mean particle size of 0.7 μm	Hot-press (30 MPa)	1900	No	89.2	B_4C, SiC	—
B_4C-50 wt% SiC[98]	B_4C, SiC, mean particle size of 0.7 μm	Hot-press (30 MPa)	1950	No	96.4	B_4C, SiC	—
B_4C[110]	B_4C (0.8 μm)	Hot-press (30 MPa)	1800	10 wt% (Al_2O_3 + Y_2O_3)	97.2	B_4C	—
B_4C-20 wt% SiC[110]	B_4C (0.8 μm), SiC (0.45 μm)	Hot-press (30 MPa)	1800	10 wt% (Al_2O_3 + Y_2O_3)	94.0	B_4C, SiC	—
B_4C[110]	B_4C (0.8 μm)	Hot-press (30 MPa)	1900	10 wt% (Al_2O_3 + Y_2O_3)	98.6	B_4C	—
B_4C-20 wt% SiC[110]	B_4C (0.8 μm), SiC (0.45 μm)	Hot-press (30 MPa)	1900	10 wt% (Al_2O_3 + Y_2O_3)	98.5	B_4C, SiC	—
B_4C-20 vol% SiC[111]	B_4C (3.5 μm), SiC (0.5 μm)	Spark plasma (40 MPa)	1900 (×10 min)	No	90.1	B_4C, SiC	—
B_4C-20 vol% SiC[111]	B_4C (3.5 μm), SiC (0.5 μm)	Spark plasma (40 MPa)	1950 (×10 min)	No	91.0	B_4C, SiC	—
B_4C-20 vol% SiC[111]	B_4C (3.5 μm), SiC (0.5 μm)	Spark plasma (40 MPa)	2000 (×10 min)	No	96.3	B_4C, SiC	—
B_4C-20 vol% SiC[111]	B_4C (3.5 μm), SiC (0.5 μm)	Spark plasma (40 MPa)	2050 (×10 min)	No	96.6	B_4C, SiC	—
B_4C-20 vol% SiC[111]	B_4C (3.5 μm), SiC (0.5 μm)	Spark plasma (40 MPa)	2100 (×10 min)	No	96.8	B_4C, SiC	—
B_4C-15 wt% SiC[112]	B_4C (0.5 μm), β-SiC (0.5 μm)	Spark plasma (75 MPa)	1650 (×5 min)	No	96.6	B_4C, SiC	B_4C: 0.537, SiC: 0.05–0.25
B_4C-15 wt% SiC[112]	B_4C (0.5 μm), β-SiC (0.5 μm)	Spark plasma (75 MPa)	1700 (×3 min)	No	99.4	B_4C, SiC	B_4C: 0.537, SiC: 0.05–0.25
B_4C-20 wt% SiC[94]	B_4C, SiC, mean particle size of 50–150 nm	Hot-press (30 MPa)	1900	No	97.2	B_4C, SiC	—
B_4C-20 wt% SiC[94]	B_4C, SiC, mean particle size of 50–150 nm	Hot-press (30 MPa)	1950	No	98.6	B_4C, SiC	B_4C = 1.0–3.0, SiC < 2.0
B_4C-20 wt% SiC[95]	B_4C, SiC, mean particle size of 50–150 nm	Spark plasma (30 MPa)	1700 (×5 min)	No	96.7	B_4C, SiC	—
B_4C-20 wt% SiC[95]	B_4C, SiC, mean particle size of 50–150 nm	Spark plasma (30 MPa)	1750 (×5 min)	No	98.3	B_4C, SiC	—
B_4C-20 wt% SiC[95]	B_4C, SiC, mean particle size of 50–150 nm	Spark plasma (30 MPa)	1800 (×5 min)	No	99.2	B_4C, SiC	B_4C = 1.0, SiC < 1.0
B_4C–SiC[113]	B_4C (45 μm), graphite (10 μm), Si lump	Reaction	1380	No	—	B_4C, graphite	—
B_4C–SiC[113]	B_4C (45 μm), graphite (10 μm), Si lump	Reaction	1410	No	—	B_4C, SiC, graphite, $B_{12}(C,Si,B)_3$, $B_{10}C$, Si	—
B_4C–SiC[113]	B_4C (45 μm), graphite (10 μm), Si lump	Reaction	1450	No	—	B_4C, SiC, graphite, $B_{12}(C,Si,B)_3$, $B_{10}C$, Si	—
SiC-50 wt% B_4C[116]	B_4C (1.5 μm), α-SiC (7.0 μm), phenolic resin, carbon black, Si powder	Reaction	1660	No	92.7	—	—
SiC-50 wt% B_4C[116]	B_4C (1.5 μm), α-SiC (7.0 μm), phenolic resin, carbon black, Si powder	Reaction	1690	No	94.6	—	—

Table 4 (*continued*)

Ceramics	Raw material	Sintering method	Sintering temperature (°C)	Sintering aid	Relative density (%)	Phase composition	Average grain size (μm)
SiC-50 wt% B_4C[116]	B_4C (1.5 μm), α-SiC (7.0 μm), phenolic resin, carbon black, Si powder	Reaction	1720	No	97.2	—	—
SiC-50 wt% B_4C[116]	B_4C (1.5 μm), α-SiC (7.0 μm), phenolic resin, carbon black, Si powder	Reaction	1750	No	98.0	—	—
SiC-50 wt% B_4C[116]	B_4C (1.5 μm), α-SiC (7.0 μm), phenolic resin, carbon black, Si powder	Reaction	1780	No	98.2	—	—
B_4C–SiC[117]	B_4C (4.08 μm), carbon black, Si lump	Reaction	1450	No	99.8	B_4C, SiC, $B_{12}(C,Si,B)_3$, Si	B_4C: 2.9, SiC: 5.8
B_4C–SiC[117]	B_4C (4.08 μm), carbon black, Si lump	Reaction	1500	No	99.8	B_4C, SiC, $B_{12}(C,Si,B)_3$, Si	B_4C: 3.2, SiC: 5.8
B_4C–SiC[117]	B_4C (4.08 μm), carbon black, Si lump	Reaction	1550	No	99.9	B_4C, SiC, $B_{12}(C,Si,B)_3$, Si	B_4C: 3.3, SiC: 6.0
B_4C–SiC[117]	B_4C (4.08 μm), carbon black, Si lump	Reaction	1600	No	99.9	B_4C, SiC, $B_{12}(C,Si,B)_3$, Si	B_4C: 3.8, SiC: 6.5
B_4C–SiC[117]	B_4C (4.08 μm), carbon black, Si lump	Reaction	1650	No	99.8	B_4C, SiC, $B_{12}(C,Si,B)_3$, Si	B_4C: 4.6, SiC: 6.7

shape, and most of the B_4C grains evolve to the faceted shape after infiltration for 40 h.[118] Karandikar *et al.*[120] found that infiltration time has an effect on the phase composition of the reaction-bonded B_4C–SiC ceramics. When the infiltration temperature is 1530 °C, only the β-SiC phase is present at low infiltration time (60–120 min); however, some α-SiC is generated at a longer infiltration time (240–360 min), and the α-SiC content increases with the increase in infiltration time. Meanwhile, part of the B_4C phase is converted to the $B_{4-x}Si_xC$ phase when the infiltration time is within 60–120 min, while all the B_4C phase is converted to the $B_{4-x}Si_xC$ phase when the infiltration time is within 240–360 min. This indicates that the conversion of the B_4C phase to the $B_{4-x}Si_xC$ phase is a time-dependent phenomenon, whose mechanism is the diffusion of Si into the B_4C grain (lattice) or solution of the B_4C grain in molten Si and reprecipitation.

3.3.3.3. Sintering pressure. For some preparation methods, B_4C–SiC ceramics have to be sintered under a pressure, such as hot-press sintering and spark plasma sintering; pressure causes particle rearrangement, plastic flow, and grain boundary movement, promoting the sintering of B_4C–SiC ceramics. The sintering pressure will affect the sintering performance and microstructure of B_4C–SiC ceramics. According to Rahaman,[121] in the presence of sintering pressure, the densification rate of the ceramic can be described as follows:

$$\rho = \frac{1}{1}\frac{\mathrm{d}\rho}{\mathrm{d}t} = \frac{HD(\Phi P_a)^n}{G^m kT} \quad (4)$$

where ρ is the densification rate, H is a numerical constant, D is the diffusion coefficient of the rate-controlling species, Φ is the intensification factor, P_a is the applied pressure, G is the grain size, k is the Boltzman constant, and T is the absolute temperature. When other factors are constant, the densification rate is exponentially influenced by the sintering pressure. Chen *et al.*[122] found that the hot-press sintered B_4C-20 wt% SiC ceramics becomes denser and the grain size becomes smaller as the sintering pressure increases from 30 to 40 MPa (Fig. 6). During the sintering process, the growth of B_4C and SiC grains is inhibited due to the higher sintering pressure, leading to the formation of more refined grains.

Some previous studies on the effect of sintering pressure on the sintering performance and microstructure of B_4C–SiC ceramics are tabulated in Table 5.

3.4. Sintering aid

B_4C–SiC ceramics are difficult to sinter to obtain a sufficiently dense product, especially in the absence of externally applied pressure during sintering. Generally, a sintering temperature higher than 2000 °C is required to obtain a dense B_4C–SiC ceramics produced *via* hot-press sintering without sintering aids. Thus, to reduce the sintering temperature, one approach is to add sintering aids to promote the densification of B_4C–SiC ceramics; also, the use of some sintering aids can hinder grain growth. Various elements and compounds have been sought as suitable sintering aids for B_4C–SiC ceramics. The application of

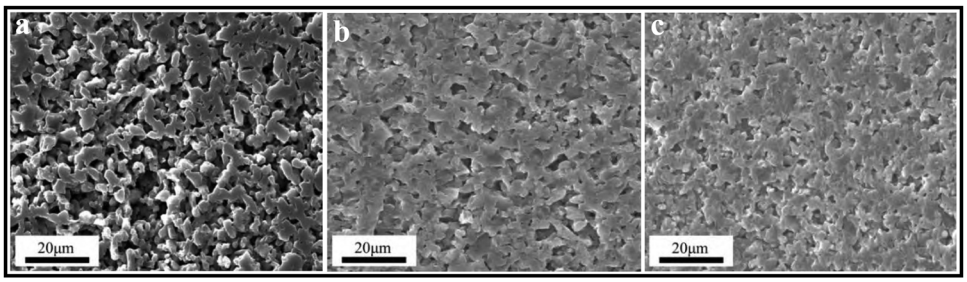

Fig. 6 Microstructure of hot-press sintered B_4C–20 wt% SiC ceramics sintered under different sintering pressures: (a) 30 MPa, (b) 35 MPa, and (c) 40 MPa.[122]

Table 5 Effect of sintering pressure on the sintering performance and microstructure of B_4C–SiC ceramics

Ceramics	Raw material	Sintering method	Sintering temperature (°C)	Sintering pressure (MPa)	Sintering aid	Relative density (%)	Phase composition	Average grain size (μm)
B_4C-20 wt% SiC[122]	B_4C (0.8 μm), SiC (0.45 μm)	Hot-press	1900	30	10 wt% (Al_2O_3 + Y_2O_3)	98.5	B_4C, SiC	—
B_4C-20 wt% SiC[122]	B_4C (0.8 μm), SiC (0.45 μm)	Hot-press	1900	35	10 wt% (Al_2O_3 + Y_2O_3)	98.6	B_4C, SiC	—
B_4C-20 wt% SiC[122]	B_4C (0.8 μm), SiC (0.45 μm)	Hot-press	1900	40	10 wt% (Al_2O_3 + Y_2O_3)	99.0	B_4C, SiC	—

sintering aids can affect the sintering performance and microstructure of B_4C–SiC ceramics. The sintering mechanisms of B_4C–SiC ceramics with the addition of sintering aids include solid-state sintering and liquid-phase sintering. Under the solid-state sintering mechanism, no liquid phase is generated; thus, B_4C–SiC ceramics have sufficient strength, especially at high temperatures. However, the sintering temperature for B_4C–SiC ceramics is relatively high. For liquid-phase sintering, liquid phases are formed at high temperatures. B_4C–SiC ceramics can be densified at relatively low temperatures; however, some amorphous secondary phases are generated at grain boundaries, causing grain coarsening, changing the crack propagation mode, and reducing the strength of B_4C–SiC ceramics.

3.4.1. C. Generally, oxide films (B_2O_3/H_3BO_3, SiO_2) are easily formed on the surfaces of B_4C and SiC raw powders during processing and storage. These oxide film impurities contribute to the evaporation-condensation process in the sintering process, resulting in the coarsening of grain rather than densification.[123] To prepare dense B_4C–SiC ceramics, it is necessary to eliminate these oxide film impurities. The addition of C into the B_4C–SiC system is an excellent method because C can remove surface oxides of B_4C and SiC raw powders by reacting with B_2O_3 and SiO_2, respectively, forming carbides and gas according to the following reactions,[124]

$$C + B_2O_3 \rightarrow B_4C + CO(CO_2)\uparrow \quad (5)$$

$$C + SiO_2 \rightarrow SiC + CO(CO_2)\uparrow \quad (6)$$

As a result, the surfaces of B_4C and SiC particles are purified, increasing the contact area of sintered particles; thus, the driving force for the densification of B_4C–SiC ceramics is improved. Furthermore, C does not generate a liquid phase in the system; thus, it is used as a sintering aid for solid-state sintering.[23] C can be added in the form of carbon black, phenolic resin, graphite, *etc.* In the case of preparing B_4C–SiC ceramics by pressureless sintering, if the B_4C–SiC composite powders contain a C precursor, the advantages of using such a precursor include: (1) it can serve as a binder and plasticizer for the subsequent cold-pressing process; and (2) it can distribute on the surface of composite powders uniformly and activate the sintering process.

Related studies have shown that C sintering aids can improve the densification of B_4C–SiC ceramics. Thévenot[20] found that the addition of C can promote the sintering of pressureless sintered B_4C–3.8 wt% SiC ceramics. When the amount of C precursor is 2.5 wt%, the relative density of B_4C–SiC ceramics can reach 95%. Most importantly, the obtained composite ceramics do not contain free carbon which is considered to impair the mechanical performance of B_4C–SiC ceramics. Furthermore, for B_4C–SiC ceramics with different ratios of B_4C to SiC, an increase in C precursor amount (2–9 wt%) does not change the final relative density (97–98%) of the composite ceramics, but increases the final free C content. Vandeperre and Teo[108] also demonstrated that 3 wt% C addition can allow pressureless sintered B_4C–SiC ceramics with different ratios of B_4C to SiC to achieve a high relative density. Moshtaghioun *et al.*[112] stated that the addition of graphite is beneficial for more intimate contact favoring the diffusion between the powders in B_4C–SiC ceramics during the first moment of spark plasma sintering. First, graphite is an effective process-control agent that can minimize the formation of agglomerates during the milling of brittle ceramics.[125] Second, graphite can lubricate the contacts during the compaction stage, improving the particle packing. As a result, graphite can further promote the densification of spark plasma sintered B_4C–SiC ceramics (Fig. 7a and b). The grain sizes of B_4C and SiC in the spark plasma sintered B_4C–SiC ceramics with graphite are slightly larger than those in the B_4C–SiC ceramics without graphite, the reason for which is not explained.[126]

3.4.2. Oxide. To promote the sintering of B_4C–SiC ceramics, some oxide sintering aids, such as Al_2O_3 and Y_2O_3, have been

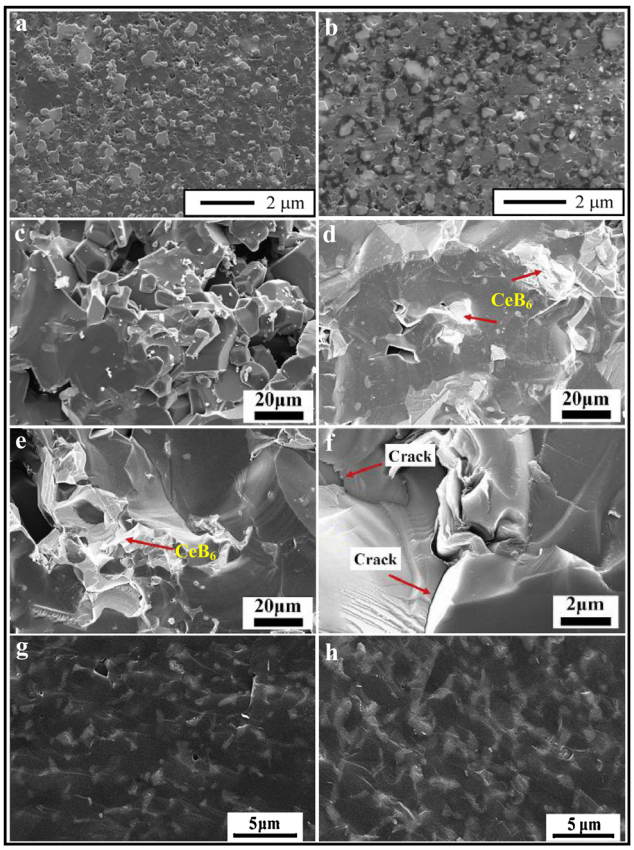

Fig. 7 Microstructure of B_4C–SiC ceramics with different sintering aids: (a) spark plasma sintered B_4C–15 wt% SiC ceramics without graphite and (b) spark plasma sintered B_4C–15 wt% SiC ceramics with 2 wt% graphite[112] (reprinted with permission, Copyright 2013, Elsevier); (c) pressureless sintered B_4C–15 wt% SiC ceramics without CeO_2, (d) pressureless sintered B_4C–15 wt% SiC ceramics with 5 wt% CeO_2, and (e) and (f) pressureless sintered B_4C–15 wt% SiC ceramics with 9 wt% CeO_2[129] (reprinted with permission, Copyright 2019, Elsevier); (g) hot-press sintered B_4C–15 wt% SiC ceramics without Si, and (h) hot-press sintered B_4C–15 wt% SiC ceramics with 8 wt% Si[91] (reprinted with permission, Copyright 2013, Elsevier).

extensively investigated. Oxide sintering aids are mainly used to achieve liquid-phase sintering.

Jamale and Kumar[127] found that the addition of Al_2O_3 can improve the densification of spark plasma sintered B_4C–10 wt% SiC ceramics due to the formation of liquid-phase Al_2SiO_5, and the relative density of the obtained ceramics is more than 99%. Sahin *et al.*[96] noted that three new phases (YBO_3, YB_4, and YB_2C_2) are formed after 5 wt% Y_2O_3 is added into the spark plasma sintered B_4C–SiC ceramics, and the formation of these liquid phases improves the densification of B_4C–SiC ceramics. Therefore, the relative densities of B_4C–SiC ceramics with the addition of 5 wt% Y_2O_3 are higher than those of B_4C–SiC ceramics without Y_2O_3. Rocha and Melo[88,89] reported that the addition of sintering aids of Al_2O_3–Y_2O_3 or AlN–Y_2O_3 can promote the sintering of the pressureless sintered B_4C–SiC ceramics. Compared with the sintering aids of Al_2O_3–Y_2O_3, the sintering aids of AlN–Y_2O_3 can better promote the densification of B_4C–SiC ceramics. B_4C–10 wt% SiC ceramics with AlN–Y_2O_3 exhibit the highest relative density. According to the observation of fracture surfaces of B_4C–SiC ceramics with sintering aids of AlN–Y_2O_3, platelet-shaped SiC grains are formed, which is attributed to the phase transformation from β-SiC to α-SiC at high temperatures. Regarding different sintering aids, on the one hand, it is possible that Al_2O_3 promotes the formation of a more elongated and interlocking structure;[128] thus, the use of sintering aids of Al_2O_3–Y_2O_3 leads to the formation of more platelet-shaped SiC grains in the B_4C–SiC ceramics, resulting in lower relative densities of B_4C–SiC ceramics with Al_2O_3–Y_2O_3 than those of B_4C–SiC ceramics with AlN–Y_2O_3. On the other hand, AlN can reduce the problem of volatilization of sintering aids at high temperatures. Zhang *et al.*[109] mentioned that the addition of Al_2O_3–La_2O_3 can promote the sintering of pressureless sintered SiC–10 wt% B_4C ceramics, which is attributed to the formation of the $LaAlO_3$ liquid phase through the reaction between Al_2O_3 and La_2O_3. Zhang *et al.*[74] noted that the densification of gas-pressure sintered B_4C–SiC ceramics can be improved using the Al_2O_3–Er_2O_3–SiO_2 sintering aid system. Al_2O_3 can react with Er_2O_3 and SiO, generating a eutectic point phase, which can reduce the sintering temperature and promote sintering.

Besides the sintering aid systems based on Al_2O_3 or Y_2O_3 systems, rare-earth oxide CeO_2 can also be used as a sintering aid for B_4C–SiC ceramics. Zhu *et al.*[129] studied the effect of CeO_2 addition on the sintering performance of pressureless sintered B_4C–15 wt% SiC ceramics. The phase compositions of the resulting B_4C–SiC ceramics with different CeO_2 contents are B_4C, SiC, and CeB_6. The formation of CeB_6 is according to the following reaction:

$$(3x + 1)B_4C + 2xCeO_2 \rightarrow 2xCeB_6 + 4xCO\uparrow + B_4C_{1-x} \quad (7)$$

The relative density of the ceramics first increases and then decreases with an increase in CeO_2 content from 0 to 9 wt% (Fig. 7c–f). B_4C–SiC ceramics achieve the highest relative density of 96.4% when the CeO_2 content is 5 wt%. The improvement in the sintering performance of B_4C–SiC ceramics by the addition of CeO_2 can be attributed to the following facts. First, the thermal conductivity of CeB_6 formed during sintering is 34.02 $W\,m^{-1}\,K^{-1}$, which is higher than that of B_4C (13.2 $W\,m^{-1}\,K^{-1}$); the formation of CeB_6 with a higher thermal conductivity can benefit the delivery of heat quantity, promoting the sintering of B_4C–SiC ceramics.[130] Second, according to reaction (7), B-rich transition zones, such as $B_{51.02}C_{1.82}$ and $B_{38.22}C_6$, are formed between CeB_6 and B_4C grains, causing local lattice distortion of the B_4C matrix. The lattice distortion can increase the chemical potential energy and consequently the sintering driving force. Furthermore, some vacancies are formed in some local areas, where C atoms combine with O atoms, forming CO gas that escapes from the ceramics, facilitating substance transport. However, when the CeO_2 content is more than 5 wt%, more CO gas is generated, and the gas cannot be timely discharged from inside the ceramics, resulting in a large number of residual pores (Fig. 7e). CeB_2 grains grow to form large grains, which introduce large residual stress between B_4C and CeB_6 as well as cracks because the irregular CeB_6 grains are subjected to uneven forces from the adjacent grains (Fig. 7f). The formation of a large number of pores and cracks results in a decrease in the relative density.

3.4.3. Si. In addition to C and oxide sintering aids, Si can also be used as a sintering aid for B_4C–SiC ceramics. On the one hand, the addition of an appropriate amount of Si can promote the sintering of the ceramics by forming a liquid phase; on the other hand, free C released from B_4C can react with molten Si to form SiC at high temperatures, increasing the SiC content.[131] Du *et al.*[91,132] reported that the addition of Si can not only improve the densification of the hot-press sintered B_4C–SiC ceramics produced with PCS as the precursor of SiC because of the formation of the liquid phase (Fig. 7g and h) but also react with C derived from pyrolysis residue of PCS and B_4C powders, increasing the SiC content. The dissolution of Si in B_4C can facilitate mass transfer in solid-state sintering of B_4C–SiC ceramics. The content of SiC increases with the increase in the content of added Si, leading to the refinement of B_4C grains. Compared with B_4C–SiC ceramics without Si additives, the grain size of B_4C is smaller in the B_4C–SiC ceramics with Si additives, which is attributed to the more efficient grain boundary pinning by the larger amount of SiC grains. Most SiC grains are located at B_4C grain boundaries; thus these SiC grains are dragged along as grain boundaries move. The more the SiC content, the more obvious the pinning effect is. This suggests that a larger SiC content is more helpful in inhibiting the growth of B_4C grains. Furthermore, the total area of the B_4C–SiC phase boundary increases with the increase in the Si additive; thus, the energy requirements for phase boundary diffusion and phase boundary mobility are increased. Therefore, the introduction of Si can refine B_4C grains. Although the addition of Si slightly increases the grain size of SiC, the average grain size of SiC is still less than 2 μm. Sahani and Chaira[131] mentioned that the improvement in the sintering performance of SiC–B_4C ceramics depends on the amount of Si added and the sintering method. When the SiC–B_4C ceramics are sintered by pressureless sintering, adding 2 or 5 wt% Si cannot improve the sintering performance of SiC–B_4C ceramics. Vandeperre and Teo[108] also demonstrated that the addition of 4 wt% Si cannot promote the sinterability for pressureless sintered B_4C–SiC ceramics. The mechanism that the low addition of Si cannot promote the sintering for B_4C–SiC ceramics needs to be further studied. However, the sintering performance of pressureless sintered SiC–B_4C ceramics is improved when the addition of Si is 10 or 20 wt%.[131] When the SiC–B_4C ceramics are sintered by spark plasma sintering, adding 2, 5, 10, or 20 wt% Si can improve the sintering performance of SiC–B_4C ceramics. The addition of Si is helpful for homogeneous microstructural distribution. When the amount of Si added is 10 wt%, the relative density of SiC–B_4C ceramics prepared by either pressureless sintering or spark plasma sintering is the highest.

Some previous studies on the effect of sintering aids on the sintering performance and microstructure of B_4C–SiC ceramics are tabulated in Table 6.

3.5. Microstructure characteristics of B_4C–SiC composite ceramics

B_4C–SiC composite ceramics have some unique microstructure characteristics different from those of pure B_4C or SiC ceramics. The microstructure of B_4C–SiC ceramics is controlled by many factors, which have been discussed in Sections 3.1 to 3.4. In this section, the microstructure characteristics of B_4C–SiC ceramics affected by the sintering mechanism and sintering method are described.

3.5.1. Phase boundary characteristics of B_4C–SiC ceramics prepared by solid-state sintering. Generally, the grain boundary is clean when the ceramics are produced by a solid-state sintering mechanism,[133] whereas the intergranular phase exists at the grain boundary when the sintering mechanism is liquid-phase sintering.[134,135]

For the phase boundary of B_4C–SiC ceramics, Matović *et al.*[64] found that there is no amorphous phase or secondary phase at the phase boundary of the ultra-high pressure sintered B_4C–SiC ceramics without sintering aids. Both Zhang *et al.*[136] and Zhu *et al.*[107] observed that the phase boundary between B_4C and SiC grains in the pressureless sintered B_4C–SiC ceramics with the sintering aid of carbon black is clean and clear (Fig. 8). Both B_4C and SiC grains reveal lattice fringes up to the phase boundary, and B_4C and SiC grains are in direct mutual contact. Such phase boundary characteristics indicate that the bonding between B_4C and SiC is very strong. The reason for this phenomenon is that the interplanar spacing between B_4C lattice planes and SiC lattice planes matches, leading to the direct connection between lattice planes of B_4C crystals and lattice planes of SiC crystals. This suggests that similar lattice parameters result in a good interfacial structure. Such a phase boundary is an advantage when the mechanical properties of the composite ceramics are concerned, especially at high temperatures. Good phase boundary strength between B_4C and SiC plays an important role in the crack growth and mechanical properties of B_4C–SiC ceramics, which will be discussed in Section 4.1.1.

3.5.2. Microstructure characteristics of B_4C–SiC ceramics prepared by reaction-bonded sintering. The preparation method of reaction-bonded sintering is different from other preparation methods to obtain B_4C–SiC ceramics; thus, the microstructure of reaction-bonded B_4C–SiC ceramics has its own characteristics.

3.5.2.1. Core–rim structure. When liquid and solid phases participate in the microstructure evolution, the core–rim structure is a common phenomenon in composites produced by powder metallurgy. Hayun *et al.*[137] observed the core–rim structure characteristic of the B_4C particles in the reaction-bonded B_4C–SiC ceramics for the first time. After the infiltration process of a green B_4C compact with molten Si, the resulting B_4C–SiC ceramics are composed of B_4C, $B_{12}(B, C, Si)_3$, β-SiC, and some residual Si. It is interesting to note that the microstructure of B_4C–SiC ceramics exhibit a core–rim structure of the B_4C particles, with B_4C cores being surrounded by a 3–7 μm thick $B_{12}(B, C, Si)_3$ envelope (Fig. 9a). Furthermore, the bonding between B_4C and $B_{12}(B, C, Si)_3$ is strong; no crack deflection occurs along the boundary between B_4C and $B_{12}(B, C, Si)_3$ (Fig. 9b).[138]

For the formation of the $B_{12}(B, C, Si)_3$ rim, different mechanisms are proposed. Hayun *et al.*[137] insisted that the original B_4C particles dissolve partially in molten Si during the infiltration process, and then the newly formed ternary $B_{12}(B, C, Si)_3$ carbide phase, which is treated as a solid solution of Si in B_4C, precipitates

Table 6 Effect of sintering aids on the sintering performance and microstructure of B_4C–SiC ceramics

Ceramics	Raw material	Sintering method	Sintering temperature (°C)	Sintering aid	Relative density (%)	Phase composition	Average grain size (μm)
B_4C-15 wt% SiC[126]	B_4C (0.5 μm), SiC (0.5 μm)	Spark plasma (75 MPa)	1700 (×3 min)	No	99.4	B_4C, SiC	B_4C: 0.53, SiC: 0.05–0.25
B_4C-15 wt% SiC[126]	B_4C (0.5 μm), SiC (0.5 μm)	Spark plasma (75 MPa)	1700 (×3 min)	2 wt% graphite	100.0	B_4C, SiC	B_4C: 0.61, SiC: 0.09–0.30
B_4C-10 wt% SiC[127]	B_4C, SiC	Spark plasma (40 MPa)	1800 (×10 min)	3 wt% Al_2O_3	99.5	B_4C, SiC, Al_2O_3, Al_2SiO_5	B_4C = 2.0–4.0, SiC = 1.0–2.0
B_4C-10 wt% SiC[127]	B_4C, SiC	Spark plasma (40 MPa)	1800 (×10 min)	6 wt% Al_2O_3	99.1	B_4C, SiC, Al_2O_3, Al_2SiO_5	B_4C = 2.0–4.0, SiC = 1.0–2.0
B_4C-5 vol% SiC[96]	B_4C, α-SiC	Spark plasma (40 MPa)	1750 (×5 min)	No	98.0	B_4C, SiC	—
B_4C-5 vol% SiC[96]	B_4C, α-SiC	Spark plasma (40 MPa)	1750 (×5 min)	5 wt% Y_2O_3	98.3	B_4C, SiC, YB_4, YB_2C_2	—
B_4C-10 vol% SiC[96]	B_4C, α-SiC	Spark plasma (40 MPa)	1750 (×5 min)	No	98.0	B_4C, SiC	—
B_4C-10 vol% SiC[96]	B_4C, α-SiC	Spark plasma (40 MPa)	1750 (×5 min)	5 wt% Y_2O_3	98.8	B_4C, SiC, YB_4, YB_2C_2, YBO_3	—
B_4C-15 vol% SiC[96]	B_4C, α-SiC	Spark plasma (40 MPa)	1750 (×5 min)	No	97.8	B_4C, SiC	—
B_4C-15 vol% SiC[96]	B_4C, α-SiC	Spark plasma (40 MPa)	1750 (×5 min)	5 wt% Y_2O_3	98.2	B_4C, SiC, YB_4, YB_2C_2	—
B_4C-10 wt% SiC[88]	B_4C, β-SiC	Pressureless	2000	No	81.3	B_4C, α-SiC, (β-SiC)	—
B_4C-10 wt% SiC[88]	B_4C, β-SiC	Pressureless	2000	10 vol% (Al_2O_3 : Y_2O_3 = 5 : 3, molar ratio)	91.5	—	—
B_4C-10 wt% SiC[88]	B_4C, β-SiC	Pressureless	2000	10 vol% (AlN : Y_2O_3 = 3 : 2, molar ratio)	93.4	—	—
B_4C-30 wt% SiC[88]	B_4C, β-SiC	Pressureless	2000	No	74.0	B_4C, α-SiC, (β-SiC)	—
B_4C-30 wt% SiC[88]	B_4C, β-SiC	Pressureless	2000	10 vol% (Al_2O_3 : Y_2O_3 = 5 : 3, molar ratio)	78.5	—	—
B_4C-30 wt% SiC[88]	B_4C, β-SiC	Pressureless	2000	10 vol% (AlN : Y_2O_3 = 3 : 2, molar ratio)	87.5	—	—
B_4C-50 wt% SiC[88]	B_4C, β-SiC	Pressureless	2000	No	67.5	B_4C, α-SiC, (β-SiC)	—
B_4C-50 wt% SiC[88]	B_4C, β-SiC	Pressureless	2000	10 vol% (Al_2O_3 : Y_2O_3 = 5 : 3, molar ratio)	69.8	B_4C, α-SiC	—
B_4C-50 wt% SiC[88]	B_4C, β-SiC	Pressureless	2000	10 vol% (AlN : Y_2O_3 = 3 : 2, molar ratio)	75.0	B_4C, α-SiC	—
SiC-10 wt% B_4C[109]	α-SiC (1.0 μm), B_4C (0.5 μm)	Pressureless	1900	10 wt% (Al_2O_3 : La_2O_3 = 1 : 1, molar ratio)	96.8	SiC, B_4C, $LaAlO_3$	—
SiC-5 wt% B_4C[74]	α-SiC (2.0 μm), B_4C (0.5 μm)	Gas-pressure (0.08 MPa)	1900	8 wt% (Al_2O_3 : Er_2O_3 : SiO_2 = 1 : 1 : 0.5, molar ratio)	94.2	SiC, B_4C	—
SiC-10 wt% B_4C[74]	α-SiC (2.0 μm), B_4C (0.5 μm)	Gas-pressure (0.08 MPa)	1900	8 wt% (Al_2O_3 : Er_2O_3 : SiO_2 = 1 : 1 : 0.5, molar ratio)	93.4	SiC, B_4C	—
SiC-15 wt% B_4C[74]	α-SiC (2.0 μm), B_4C (0.5 μm)	Gas-pressure (0.08 MPa)	1900	8 wt% (Al_2O_3 : Er_2O_3 : SiO_2 = 1 : 1 : 0.5, molar ratio)	91.7	SiC, B_4C	—
SiC-20 wt% B_4C[74]	α-SiC (2.0 μm), B_4C (0.5 μm)	Gas-pressure (0.08 MPa)	1900	8 wt% (Al_2O_3 : Er_2O_3 : SiO_2 = 1 : 1 : 0.5, molar ratio)	88.9	SiC, B_4C	—
B_4C-15 wt% SiC[129]	B_4C (0.8 μm), SiC (0.5 μm)	Pressureless	2150	No	85.8	B_4C, SiC	—
B_4C-15 wt% SiC[129]	B_4C (0.8 μm), SiC (0.5 μm)	Pressureless	2150	1 wt% CeO_2	91.2	B_4C, SiC, CeB_6	—
B_4C-15 wt% SiC[129]	B_4C (0.8 μm), SiC (0.5 μm)	Pressureless	2150	3 wt% CeO_2	92.6	B_4C, SiC, CeB_6	—
B_4C-15 wt% SiC[129]	B_4C (0.8 μm), SiC (0.5 μm)	Pressureless	2150	5 wt% CeO_2	96.4	B_4C, SiC, CeB_6	—
B_4C-15 wt% SiC[129]	B_4C (0.8 μm), SiC (0.5 μm)	Pressureless	2150	7 wt% CeO_2	94.6	B_4C, SiC, CeB_6	—
B_4C-15 wt% SiC[129]	B_4C (0.8 μm), SiC (0.5 μm)	Pressureless	2150	9 wt% CeO_2	93.4	B_4C, SiC, CeB_6	—
B_4C[91]	B_4C (3.5 μm)	Hot-press (30 MPa)	1950	No	91.7	B_4C	—
B_4C-15 wt% SiC[91]	B_4C (3.5 μm), PCS	Hot-press (30 MPa)	1950	No	96.1	B_4C, SiC	SiC < 1.0
B_4C-15 wt% SiC[91]	B_4C (3.5 μm), PCS	Hot-press (30 MPa)	1950	8 wt% Si	99.1	B_4C, SiC	B_4C < 5.0, SiC < 2.0
B_4C-60 wt% SiC[131]	B_4C, SiC	Pressureless	1950	No	89.0	B_4C, SiC	—
B_4C-60 wt% SiC[131]	B_4C, SiC	Pressureless	1950	2 wt% Si	88.0	B_4C, SiC, Si	—
B_4C-60 wt% SiC[131]	B_4C, SiC	Pressureless	1950	5 wt% Si	89.0	B_4C, SiC, Si	—
B_4C-60 wt% SiC[131]	B_4C, SiC	Pressureless	1950	10 wt% Si	92.0	B_4C, SiC, Si	—

Table 6 (*continued*)

Ceramics	Raw material	Sintering method	Sintering temperature (°C)	Sintering aid	Relative density (%)	Phase composition	Average grain size (μm)
B_4C-60 wt% SiC[131]	B_4C, SiC	Pressureless	1950	20 wt% Si	90.0	B_4C, SiC, Si	—
B_4C-60 wt% SiC[131]	B_4C, SiC	Spark plasma (50 MPa)	1600 (×5 min)	No	94.0	B_4C, SiC	—
B_4C-60 wt% SiC[131]	B_4C, SiC	Spark plasma (50 MPa)	1350 (×5 min)	2 wt% Si	94.6	—	—
B_4C-60 wt% SiC[131]	B_4C, SiC	Spark plasma (50 MPa)	1350 (×5 min)	5 wt% Si	96.3	B_4C, SiC, Si, B_4Si	—
B_4C-60 wt% SiC[131]	B_4C, SiC	Spark plasma (50 MPa)	1350 (×5 min)	10 wt% Si	98.0	B_4C, SiC, Si, B_4Si	—
B_4C-60 wt% SiC[131]	B_4C, SiC	Spark plasma (50 MPa)	1350 (×5 min)	20 wt% Si	97.0	B_4C, SiC, Si, B_4Si	—

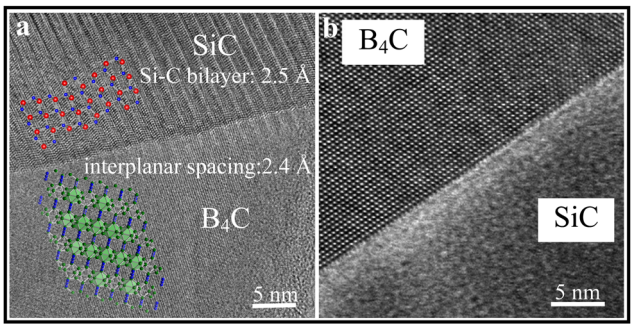

Fig. 8 HRTEM images of B_4C–SiC ceramics prepared by solid-state sintering revealing the phase boundary characteristics between B_4C and SiC: (a) B_4C–40 wt% SiC ceramics with 3 wt% carbon black[136] (reprinted with permission, Copyright 2019, Elsevier) and (b) B_4C–15 wt% SiC ceramics with 2 wt% carbon black[107] (reproduced with permission, Copyright 2019, Elsevier).

on the surface of original B_4C particles when the solubility of B and C in molten Si becomes saturated, forming rim regions. This indicates that the formation of the $B_{12}(B, C, Si)_3$ rim is the dissolution–precipitation process. This newly formed ternary phase $B_{12}(B, C, Si)_3$ at the boundaries of neighboring B_4C particles through dissolution–reprecipitation mechanism is also supported by Zhang *et al.*[117] in the reaction-bonded B_4C–SiC ceramics. In contrast, Jannotti *et al.*[139] proposed a different view that the $B_{12}(B, C, Si)_3$ phase is a Si-doped B_4C phase. The Si substitutes for the C atoms on the ends of the linear chain and inserts into the icosahedrons in the B_4C lattice, and C atoms react with liquid Si, generating SiC. Wang *et al.*[140] mentioned that the $B_{12}(B, C, Si)_3$ rim surrounding B_4C is generated by Si inward diffusion in B_4C from a liquid. Sun *et al.*[141] put forward that there are two types of $B_{12}(B, C, Si)_3$ phases in the reaction-bonded B_4C–SiC ceramics. One is $B_{12}(B, C, Si)_3$ with high Si content, derived from the reaction between Si and decomposed B_4C (Si, B, and a part of C react to generate $B_{12}(B, C, Si)_3$, and the remaining C diffuses into the liquid Si, generating plate-like SiC; the other is $B_{12}(B, C, Si)_3$ with low Si content, resulting from the diffusion of Si into B_4C (solid solution process).

The core–rim structure of B_4C is formed in the B_4C–SiC ceramics produced *via* a conventional reaction-bonded sintering route; however, Thuault *et al.*[63] found that there is no core–rim structure of B_4C in the reaction-bonded B_4C–SiC ceramics prepared by the microwave assisted processing method in an Ar–H_2 atmosphere. The compositions of the obtained composite ceramics are B_4C, β-SiC, and Si; there is no $B_{12}(B, C, Si)_3$ phase. The reason why the core-rim structure is not formed is that the rapid heating generated by microwaves and the infiltration process under an Ar–H_2 gas flow at atmospheric pressure prevents the secondary reaction among Si, C, and B.

In addition, when the preform containing α-SiC is used to prepare reaction-bonded B_4C–SiC ceramics, besides the core–rim structure of B_4C surrounded by the $B_{12}(B, C, Si)_3$ rim, the core–rim structure of primary α-SiC surrounded by the secondary β-SiC rim is also observed (Fig. 9c).[85,140] C first dissolves in molten Si and then diffuses to the vicinity of the original α-SiC

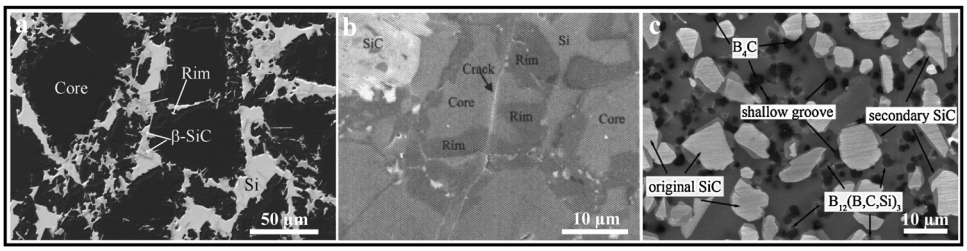

Fig. 9 SEM images of reaction-bonded B_4C–SiC ceramics exhibiting: (a) core–rim structure of B_4C particles[137] (reproduced with permission, Copyright 2009, Elsevier), (b) crack propagation path passing through the core–rim structure of B_4C[138] (reproduced with permission, Copyright 2010, John Wiley and Sons), and (c) core–rim structure of SiC particles[85] (reproduced with permission, Copyright 2016, Elsevier).

grains, forming supersaturated liquid Si[C]. Compared with the homogeneous nucleation in a liquid phase, the supersaturated liquid Si[C] is more prone to heterogeneously crystallize to form β-SiC attached to the original α-SiC grains because of the relatively lower energy. The initial α-SiC grains are interconnected by the newly formed β-SiC rim structure to generate a cluster of SiC grains. Because the β-SiC grows fast at a much lower temperature than that of the initial α-SiC, many faults (twinning and lattice distortion) generate inside the β-SiC grains. Song *et al.*[85] considered that the dissolution process is exothermic, allowing the local temperature to increase at the dissolution sites. When the C gradually dissolves in molten Si, the C activity gradient within Si will cause a rapid diffusion of C away from the dissolution sites. The C diffuses to locally cooler sites (the initial SiC particles) until a supersaturation occurs in the molten Si and then the C precipitates as an epitaxial SiC rim. β-SiC cannot nucleate on B_4C with rim, which is attributed to the lattice mismatch between β-SiC and $B_{12}(B, C, Si)_3$.

3.5.2.2. Morphology of SiC. Reaction-bonded B_4C–SiC ceramics can be produced with or without free C in the preform. The C used to form SiC *in situ* can come from free C or/and C originally present in B_4C. When the free C is present in the preform, the siliconization chemical reaction (**8**) predominates.

$$Si + C \rightarrow SiC \quad (8)$$

The reaction (**3**) also occurs in parallel in the region where the free carbon concentration is locally reduced. However, when only B_4C is used as the C source, the formation of SiC is completely based on the reaction (**3**). Different C sources give rise to different morphologies of SiC grains *in situ* generated. Hayun *et al.*[137] noted that the β-SiC particles have a plate-like shape (Fig. 10a) when B_4C acts as the sole source of C (without free C addition), while β-SiC particles show a polygonal shape (Fig. 10b) and only a small fraction of SiC displays a plate-like shape in the presence of 5 wt% free C, which is added by infiltration with an aqueous sugar solution. In the absence of free C, the gradual diffusion of C from B_4C favors the plate-like shape of the obtained secondary SiC. In fact, the polygonal β-SiC particles are built by mutually bonded plate-like particles; thus, a key factor that determines the morphology of the β-SiC particles is the available amount of C. Two C sources are available for β-SiC formation in the presence of free C, resulting in the formation of polygonal SiC particles. SiC particles precipitate at the melt/graphite interface after the dissolution of free C in the melt. Liquid Si continues to react with B_4C after the consumption of free C and some additional plate-like SiC particles are formed. Although the addition of C controls the morphology of the formed SiC particles, it is very interesting to note that the relative amounts of the SiC formed are similar for the B_4C–SiC ceramics produced with and without free C addition for a certain initial porosity of the preforms.[142] This indicates the following two points: (1) porosity of the preform is a key factor determining the amount of SiC formed. As the initial porosity of the preform increases from 20 to 40 vol%, the amount of SiC formed slightly increases from 8 to 12 vol%; and (2) B_4C–SiC ceramics can be produced by molten Si infiltration even in the absence of free C (external C source). Although secondary SiC particles with a plate-like morphology were observed by Hayun *et al.*[137] in the B_4C–SiC ceramics produced from the preform composed of sole B_4C without free C addition, Aroati *et al.*[143] found that no plate-like SiC particles are formed

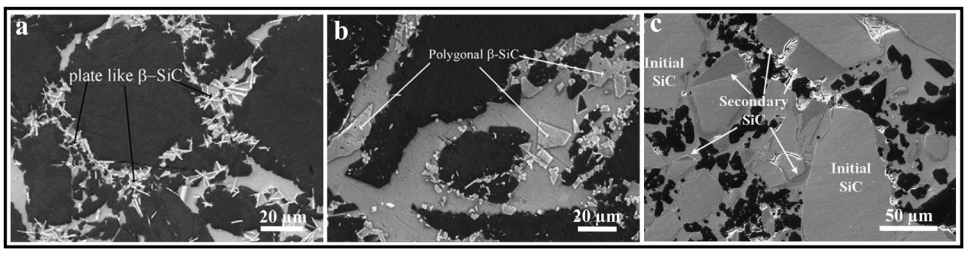

Fig. 10 Morphology of SiC grains in reaction-bonded B_4C–SiC ceramics produced from the preforms with different compositions: (a) B_4C without free C addition, (b) B_4C with 5 wt% free C addition[137] (reproduced with permission, Copyright 2009, Elsevier), and (c) the mixture of B_4C and SiC without free C addition[143] (reproduced with permission, Copyright 2010, Elsevier).

in the B_4C–SiC ceramics produced from the preform composed of a mixture of SiC and B_4C without free C addition (Fig. 10c). This is because there are SiC particles in the preform, so heterogeneous nucleation of secondary SiC occurs on the surface of these initial SiC particles.

3.5.2.3. Particle size. The particle sizes of B_4C and SiC in reaction-bonded B_4C–SiC ceramics are also related to C sources and contents. Gao *et al.*[144] reported that B_4C–SiC ceramics can be produced without the addition of C *via* reaction-bonded sintering; however, the particle sizes of B_4C and SiC are not uniform in the case of without adding C, which is attributed to the difficulty of B_4C sintering. The addition of C in the range of 5 to 10 vol% can make the particle sizes of B_4C and SiC smaller and make their particle size distributions more uniform. However, large-sized particles, which come from the aggregation of SiC formed, and Si spots are generated in the B_4C–SiC ceramics when the addition of C is more than 10 vol%. This indicates that the addition of excessive C will lead to the increase in the particle size of B_4C–SiC ceramics and less uniform phase distribution. Li *et al.*[76] also found that compared with no C addition, the grain sizes of SiC and Si are smaller in the case of carbon black addition, which may result from the decreased pore size in the preform as the content of carbon black increases.

The particle size of B_4C is affected by two competing factors; one is the dissolution and reaction of B_4C with liquid Si, consuming the B_4C particles and decreasing the particle size and the other is the precipitation of $B_{12}(C, Si, B)_3$, forming the coarsened B_4C particles and increasing the particle size. Meanwhile, the formed $B_{12}(C, Si, B)_3$ promotes the generation of a sintering neck between neighboring B_4C grains. The distance between neighboring B_4C grains is decreased with further expansion of the sintering neck, allowing the neighboring B_4C grains to grow together and increasing the particle size of B_4C. Therefore, the formation of $B_{12}(C, Si, B)_3$ results in the loss of B_4C, which reduces the hardness of B_4C–SiC ceramics, the aggregation and bonding of neighboring B_4C grains, and the consequent increase in particle size. In order to protect the B_4C grains from dissolution and reaction in liquid Si, several methods can be used to limit the formation of a large number of $B_{12}(B, C, Si)_3$ phases.

First, the pre-production of C-coated B_4C particles. Zhang *et al.*[101] first used the phenolic resin as an external C source to prepare C (10 wt%)-coated B_4C particles by pyrolysis and carbonization, during which the phenolic resin uniformly attached to the B_4C particles is transformed into an amorphous C layer or C nanoparticles, which were then used to fabricate the reaction-bonded B_4C–SiC ceramics. As a result, the C layer acts a barrier between B_4C grains and molten Si, and the molten Si preferentially reacts with the C layer. The C-coating can effectively protect the B_4C grains from reacting with molten Si, reducing the dissolution and reaction loss of B_4C. Compared with the reaction-bonded B_4C–SiC ceramics prepared from a mixture of B_4C and carbon black powders (an external C source), which is formed only by the mechanical mixing of the two, the content of B_4C in the B_4C–SiC ceramics prepared from the C-coated B_4C particles is higher and the B_4C grains can maintain the initial irregular shape. In contrast, the B_4C grains in the B_4C–SiC ceramics prepared from uncoated B_4C particles change from irregular shape to faceted shape. It is reported that the B_4C grains will grow rapidly after they are transformed into the faceted shape;[118] thus, the grain size of B_4C in the B_4C–SiC ceramics prepared from the C-coated B_4C particles is smaller than the ones in the B_4C–SiC ceramics prepared from the mixture of uncoated B_4C and carbon black. On the other hand, *in situ* formed nano-SiC grains wrap the B_4C grains forming a nano-SiC grain-coating layer in the B_4C–SiC ceramics prepared from the C-coated B_4C particles; the neighboring B_4C grains can be bonded together with these nano-SiC grains, generating a continuous ceramic skeleton. In contrast, for the B_4C–SiC ceramics prepared from a mixture of uncoated B_4C and carbon black, most of the formed SiC grains with a size of 1 μm are isolated in free Si, and many large-sized SiC zones of 50 μm are formed, which is attributed to the nonuniform dispersion of the nano-carbon black. Although the pre-production of C-coated B_4C particles is relatively complex for the production of B_4C–SiC ceramics, this method can achieve not only a uniform distribution of B_4C and SiC but also a continuous ceramic skeleton composed of nano-SiC grain-coated and -bonded B_4C grains.

Second, the introduction of free B into the preform; free B dissolves in molten Si and decreases the Si activity towards B_4C.[115] This method increases the possibility that a mixture of boron silicides with varying stoichiometry will be present in the resulting ceramics, lowering the additive cracking resistance.[115]

Third, a decrease in the siliconization temperature to approximately 1450–1550 °C, at which the predominant process is reaction (**8**); an improvement in the sintering temperature to 1600 °C leads to an appreciable acceleration of reaction (**3**).[115] This method may increase the viscosity of molten Si and decrease the relative density, leading to the formation of residual C and deteriorated mechanical properties.

Actually, although these methods can protect the B_4C grains and limit the formation of $B_{12}(B, C, Si)_3$, their effects on the microstructure and other properties of B_4C–SiC ceramics should also be considered.

3.5.2.4. Residue and morphology. B_4C–SiC ceramics produced by reaction-bonded sintering often contain undesirable residual phases. If the ceramics have a Si deficit or are poorly homogenized, there will be some incompletely siliconized regions containing C in the resulting B_4C–SiC ceramics. Similarly, residual C also forms in cases where the porosity of the preform lies below the threshold for molten Si to flow through the porous preform, the sintering temperature is too low for molten Si to reach the required viscosity, or the holding time is too short. In contrast, residual Si will form in the case of a C deficit or excessive porosity. These residues affect the mechanical properties of B_4C–SiC ceramics, which will be discussed in Section 4.2.2.

The source of free C can not only come from carbon black, but also from carbon fibers. Two different sources of free C affect the morphology of residual Si. Song *et al.*[85] used carbon fibers as a carbon source to produce reaction-bonded B_4C–SiC

ceramics. The porous self-supporting interpenetrating network structure of carbon fibers is helpful for Si infiltration. During the Si infiltration, homogeneously and randomly distributed carbon fibers completely react with the molten Si, whose dominant mechanism is diffusion, and the residual Si particles occupy the original positions of carbon fibers, forming fiber-like extensions. This microstructure is different from that of the reaction-bonded B_4C–SiC ceramics using carbon black as the C source. The residual Si with fiber-like extensions is a revamped form of residual Si, and the residual Si is spread out throughout the matrix, reducing the dimensions of the Si islands. With the increase in carbon fiber content, the amount of newly formed β-SiC is increased and the amount of residual Si is reduced. Meanwhile, the formation of β-SiC during the siliconisation reaction between the carbon fibers and molten Si causes a large volume expansion, which is favorable for decreasing the space of residual Si.

4. Mechanical properties of B_4C–SiC composite ceramics

The mechanical properties of B_4C–SiC ceramics are crucial for their applications. Hardness, fracture toughness, and bending strength are important mechanical properties of B_4C–SiC ceramics. Higher hardness will make B_4C–SiC ceramics a very interesting material for applications where high wear resistance is required, and higher bending strength will make B_4C–SiC ceramics an interesting material from the structural application point of view. For example, due to excellent mechanical and physical properties, *i.e.*, high hardness, high bending strength, relatively high fracture toughness, and low density, B_4C–SiC ceramics are one of the most potential candidates for novel bulletproof materials. To obtain desirable mechanical properties for polycrystalline B_4C–SiC ceramics, various aspects have been investigated. The research works focus on the effect of the microstructure, phase composition, raw materials, preparation process, and sintering aids on the mechanical properties of B_4C–SiC ceramics, which will be discussed in detail in this part.

4.1. Microstructure

The good mechanical properties of B_4C–SiC ceramics are related to the control of the microstructure, which mainly includes the grain characteristics, grain boundary characteristics, pores, and flaws. In general, when the composition of the material is determined, the hardness is controlled by its relative density and grain size. To improve the hardness of B_4C–SiC ceramics, their grain size should be as low as possible, and their relative density should be as high as possible. The bending strength of B_4C–SiC ceramics is determined by the flaw size, and the bending strength increases with decreased flaw size. Generally, the flaws generated at the interface propagate to a maximum of up to one grain size.[145] Pores, as a major flaw, are also detrimental to the bending strength of B_4C–SiC ceramics. On the one hand, pores can reduce the cross-sectional areas across which a load is applied; on the other hand, pores act as stress concentrators. Therefore, reducing the porosity is beneficial for improving the hardness and bending strength of B_4C–SiC ceramics. There are many methods to reduce the porosity to improve the mechanical properties of B_4C–SiC ceramics, such as refinement of raw materials, improvement of sintering temperature, and addition of sintering aids, *etc.*, which will be described later. The fracture toughness of B_4C–SiC ceramics is closely related to the crack propagation mode, which is decided through various factors, such as the phase boundary characteristics between B_4C and SiC grains (bonding strength of the interface), residual stress development, and grain morphology. In addition, dislocations, as a kind of crystal defect, can change the course of the crack when a crack runs into dislocations; also, complicated dislocation lines can be regarded as a second refinement on matrix grains.

4.1.1. Phase boundary characteristics between B_4C and SiC. For composite materials, the characteristics of the two-phase interface play a crucial role in the mechanical properties. For B_4C–SiC ceramics, the phase boundary characteristics decide the interfacial bonding between B_4C and SiC. Cracks always propagate along the weak joint in the stress field. If the interfacial bonding between B_4C and SiC is weak, cracks will extend along the phase boundary, causing an intergranular crack. In contrast, if the interfacial bonding is stronger than the cohesion strength of individual B_4C and SiC grains, a transgranular crack will be the predominant fracture mode. Intergranular fracture contributes to increasing fracture toughness, while transgranular fracture plays a positive role in strength. As reported in the liquid-phase sintered SiC ceramics, the aluminosilicate interphase provides a tortuous path for cracks and facilitates crack branching; the comparatively weak intergranular interphase is the preferential path for crack propagation, improving the fracture toughness.[146] Generally, the phase boundary of solid-state sintered B_4C–SiC ceramics is clean (Fig. 8); conversely, some secondary phase or amorphous layer exists between B_4C and SiC grains after liquid-phase sintering.

The clean phase boundary makes the bond between B_4C and SiC grains very strong. Zhang *et al.*[98] and Yaşar and Haber[71] found that cracks cross the B_4C and SiC grains, rather than propagating along the phase boundary, when cracks propagate in the hot-press sintered B_4C–50 wt% SiC ceramics without any sintering aid (Fig. 11a) and spark plasma sintered 10–50 wt% B_4C–SiC ceramics with a sintering aid of 1.5 wt% C, respectively. This indicates that interface cohesion between B_4C and SiC is powerful, and no crack deflection happens at the clean phase boundary. Normally, intergranular fracture plays a positive role in toughness. Although transgranular fracture is the predominant fracture mode of solid-state sintered B_4C–SiC ceramics, the fracture toughness of B_4C–SiC ceramics is higher than that of pure B_4C ceramics,[98] which solves the problem that the widespread application of pure B_4C ceramics is restricted due to their low fracture toughness. The powerful interfacial bonding between B_4C and SiC plays a key role in fracture toughness. For B_4C–SiC ceramics with transgranular cracks, the usual toughening mechanisms of crack propagation, such as crack bridging, deflection, and branching, are not applicable.

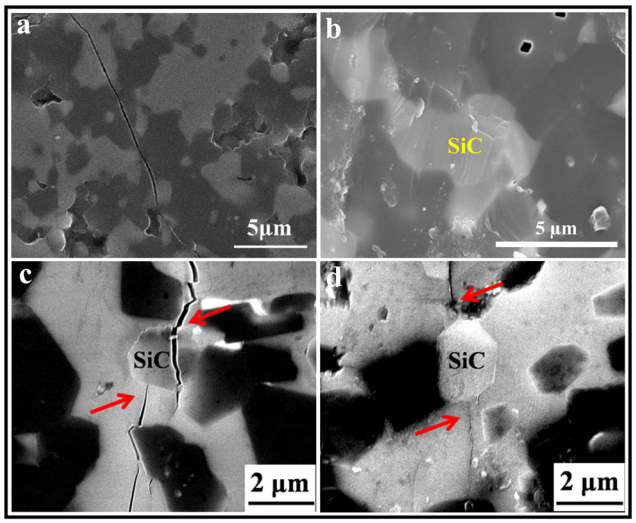

Fig. 11 (a) Cracks in hot-press sintered B_4C–50 wt% SiC ceramics showing a transgranular mode[98] (reprinted with permission, Copyright 2013, Elsevier), (b) fracture surface of spark plasma sintered B_4C–20 vol% SiC ceramics exhibiting rougher SiC grains than B_4C grains,[111] and indentation crack propagation in reaction-bonded B_4C–SiC ceramics revealing: (c) crack branching and (d) crack bridging[117] (reprinted with permission, Copyright 2014, John Wiley and Sons).

With regard to the increased fracture toughness of B_4C–SiC ceramics, different mechanisms have been proposed by the researchers. The classical thermal expansion mismatch theory in toughening states that the fracture toughness is determined by the residual stress that can control the interaction between the composite microstructure and crack propagation;[147] the residual stress is caused because of the mismatch of thermal expansion coefficients between matrix and the second phase or inclusions. The release of residual stress plays an effective role in the improvement of fracture toughness. For B_4C–SiC ceramics, the residual stress is generated by a difference in the thermal expansion coefficients of B_4C and SiC. Zhang *et al.*[98] stated that the difference in thermal expansion coefficients of B_4C (5.73×10^{-6} °C^{-1}) and SiC (4.50×10^{-6} °C^{-1}) is not obvious, leading to the minimal residual thermal stress at their interface, which is inadequate to cause crack deflection or intergranular fracture. Hwang *et al.*[87] calculated the theoretical residual stress between the B_4C matrix and SiC particulate and verified experimentally by the Raman mapping that the compressive residual stress developed in the B_4C matrix around SiC particulates is small, whose value is between 27–64 MPa for ΔT (temperature range over which stress is not relieved by a diffusive process) = 800–1900 °C. This means that the contribution of residual thermal stress to the toughening of B_4C–SiC ceramics is quite limited; thereby, the microstructure is responsible for the marked increase in fracture toughness. Small residual stress explains why cracks cross the B_4C and SiC grains, rather than crack deflection at the B_4C–SiC interface. Zhang *et al.*[98] claimed that the increased fracture toughness is attributed to the crack impeding mechanism rather than the crack deflection mechanism, and the SiC content is a more important factor than the residual stress. The fracture toughness of SiC is higher than that of B_4C, and cracks consume more energy when crossing SiC grains. This hypothesis was demonstrated by the observation of Wu *et al.*[111] that the SiC grains are rougher than B_4C grains on the fracture surface of the spark plasma sintered B_4C–20 vol% SiC ceramics (Fig. 11b). Therefore, the fracture toughness of B_4C–SiC ceramics is higher than that of pure B_4C ceramics. However, Moradkhani and Baharvandi[80] argued that the increased fracture toughness is related to residual stress. They observed that the fracture toughness of pressureless solid-state sintered B_4C–SiC ceramics increases with the addition of SiC from 2.5 to 10 vol%, and the fracture mode of B_4C–SiC ceramics changes from intergranular fracture to transgranular fracture with the increase in SiC content, which is ascribed to the formation of compressive residual stress around the reinforcing SiC particles and tensile stress in the matrix B_4C phase due to the unequal thermal expansion coefficients between B_4C and SiC. First, the compressive stress is transferred to the phase boundary between B_4C and SiC. When cracks move toward the phase boundary, the existing compressive stress at the phase boundary will divert the cracks toward the grain interior, consuming the energy of the crack. The compressive stress can increase the fracture toughness for B_4C–SiC ceramics by preventing crack nucleation and growth. Second, the release of residual stress will lead to the formation of dislocations around the reinforcing SiC particles and microcracks within grains. The generation of dislocations can make it difficult for cracks to propagate; the emergence of microcracks can increase the fracture toughness by microcrack toughening mechanism.

For the reaction-bonded B_4C–SiC ceramics produced *via* liquid-phase sintering, the crack propagation mode is different from that of B_4C–SiC ceramics with a clean phase boundary prepared by solid-state sintering. Crack bridging and crack branching, both of which are considered to enhance the fracture toughness of materials, are observed in the reaction-bonded B_4C–SiC ceramics (Fig. 11c and d).[117] SiC particles cause crack branching and also play a bridging role. Both crack branching and crack bridging can consume more energy and thus increase the resistance to crack propagation for B_4C–SiC ceramics.

4.1.2. Grain morphology. Grain morphology affects the mechanical properties of B_4C–SiC ceramics. The grain morphology of B_4C–SiC ceramics is mainly influenced by the raw material size, raw material specie, and parameters during sintering.

Moradkhani and Baharvandi[80] observed cleavage surfaces within grains (Fig. 2k and l) in the pressureless sintered B_4C–SiC ceramics. These cleavage surfaces can act as a crack path diverter, the generation of which is beneficial for improving the fracture toughness of B_4C–SiC ceramics.

As mentioned in Section 3.5.2, the grain morphology in the reaction-bonded B_4C–SiC ceramics is complex, which depends primarily on the C source, the addition of SiC, and the processing method. In the case of the conventional reaction-bonded sintering route, B_4C grains show a core–rim structure characteristic. There is a debate on the effect of the $B_{12}(B, C, Si)_3$ phase in the form of rims generated on B_4C cores on the mechanical properties of B_4C–SiC ceramics. Hayun *et al.*[84,138] claimed that

Young's modulus and hardness of the $B_{12}(B, C, Si)_3$ phase are slightly higher than those of B_4C. Jannotti *et al.*[139] reported that the $B_{12}(B, C, Si)_3$ phase can yield improved mechanical properties for B_4C–SiC ceramics. However, Song *et al.*[60,85] argued that the $B_{12}(B, C, Si)_3$ phase has high brittleness, which can be proved by the obvious grooves formed on the surface, resulting from the peeling off of the $B_{12}(B, C, Si)_3$ phase during polishing. Therefore, the generation of a large number of $B_{12}(B, C, Si)_3$ phases may increase the brittleness of B_4C–SiC ceramics, which is not conducive to improving the fracture toughness of the ceramics.[115] The contribution of the B_4C grains with a core–rim structure to the mechanical properties of B_4C–SiC ceramics needs to be further elucidated. Furthermore, from the view of grain size, coarse B_4C grains become the crack source during the fracture process; thus large-sized B_4C grains are unfavorable to improving the bending strength of B_4C–SiC ceramics.[99] On the other hand, when the reaction-bonded B_4C–SiC ceramics are prepared by a microwave-assisted processing method, no core–rim structure of B_4C is observed.[63] The hardness (22 GPa) of B_4C–SiC ceramics prepared by the microwave-assisted processing method is comparable to that prepared by the conventional reaction-bonded process, but Young's modulus (309 GPa) is lower than that obtained using the conventional process.

The C source (free C addition or C originating from B_4C) directly affects the morphology of SiC grains formed *in situ* (Section 3.5.2.2), which in turn controls the mechanical properties of reaction-bonded B_4C–SiC ceramics.[148] Compared with the SiC with polygonal morphology, the SiC with plate-like morphology can provide higher bending strength, fracture toughness, and compressive strength for B_4C–SiC ceramics. The volume fraction of SiC formed is not dependent on the C source. The SiC grains with a polygonal morphology are coarser than those with plate-like morphology; thus, the density of plate-like SiC grains is higher than that of polygonal SiC grains. Therefore, the number of inter-particle boundaries which have to be crossed by a propagating crack is large in the B_4C–SiC ceramics with plate-like SiC grains, leading to increased fracture toughness. Dariel and Frage[99] also mentioned that the morphology of SiC grains has a strong effect on the bending strength and fracture toughness of B_4C–SiC ceramics. The B_4C–SiC ceramics with plate-like shaped SiC possess higher bending strength and fracture toughness than the B_4C–SiC ceramics with polygonal SiC. This phenomenon is attributed to the strengthening and toughening effects of SiC particles with a plate-like shape. The SiC particles with a plate-like shape have a high aspect ratio, and SiC grains with a plate-like morphology likely cause crack deflection compared to those with a polygonal morphology. These plate-like shaped SiC particles can affect crack propagation through the B_4C–SiC ceramics *via* a large number of boundaries that are crossed by cracks, which can cause larger crack energy losses. Although the plate-like morphology of SiC grains can improve the fracture toughness and bending strength of B_4C–SiC ceramics, it does not affect the hardness and stiffness of B_4C–SiC ceramics.

4.2. Phase composition

The mechanical properties of B_4C–SiC ceramics depend on the relative amount of phases present. For example, the intrinsic hardness of the individual phase affects the hardness of B_4C–SiC ceramics. For B_4C–SiC ceramics prepared by solid-state sintering using B_4C and SiC as raw materials, an unexpected phase does not form during sintering. However, there are some unexpected residual phases in the B_4C–SiC ceramics prepared by reaction-bonded sintering, and these residual phases can affect the mechanical properties of B_4C–SiC ceramics.

4.2.1. Ratio of B_4C to SiC. The mechanical properties of B_4C–SiC ceramics are influenced by the ratio of B_4C to SiC. The intrinsic hardness of B_4C is higher than that of SiC; thus, according to the rule of mixture, B_4C–SiC ceramics with higher ratios of B_4C to SiC possess a higher hardness theoretically on the condition that the samples have the same relative density, and *vice versa*. On the other hand, the ratio of B_4C to SiC affects the sintering performance and microstructure of the ceramics (Section 3.1). B_4C–SiC ceramics with higher ratios of B_4C to SiC are prone to have more pores, and pores play a detrimental role in the mechanical properties; refined grains and dense microstructure, both of which are beneficial in improving the mechanical properties of B_4C–SiC ceramics, can be obtained by adjusting the ratio of B_4C to SiC. Therefore, the ratio of B_4C to SiC affects the mechanical properties of B_4C–SiC ceramics by regulating the microstructure and following the rule of mixtures, and it is necessary to balance the ratio of B_4C to SiC in order to obtain B_4C–SiC ceramics with excellent mechanical properties.

For B_4C–SiC ceramics produced by pressureless sintering, Magnani *et al.*[68] reported that the fracture toughness of SiC–5 vol% B_4C ceramics is similar to that of pure SiC ceramics; however, the hardness and bending strength of SiC–5 vol% B_4C ceramics are higher than those of pure SiC ceramics. Higher mechanical properties of SiC–5 vol% B_4C ceramics are attributed to the finer microstructure and less strength-controlling flaws like porosity as compared to pure SiC ceramics. Cho *et al.*[69] mentioned that the hardness reduces but the fracture toughness increases when the content of B_4C increases from 1 to 5 wt% in the SiC–B_4C ceramics. The reduced hardness is attributed to the increased porosity of the ceramics, while the increased fracture toughness is caused by the toughening mechanisms of crack bridging, crack deflection, and crack branching, resulting from the presence of increased B_4C at the grain boundary. Zhang *et al.*[70] studied the mechanical properties of B_4C–SiC ceramics with the change of the ratio of B_4C to SiC ($3/97 < B_4C$ wt%/SiC wt% $< 100/0$). The fracture toughness of B_4C–SiC ceramics does not show an obvious difference with a difference in the ratio of B_4C to SiC under the same sintering conditions. The fracture toughness of B_4C–SiC ceramics varies between 3.1 and 3.7 MPa $m^{1/2}$, and the fracture toughness of B_4C–SiC ceramics is slightly lower than that of pure B_4C ceramics. The hardness of B_4C–SiC ceramics varies between 27 and 33 GPa, and the hardness of B_4C–SiC ceramics is higher than that of pure B_4C ceramics. SiC–40 wt% B_4C ceramics exhibit the highest hardness. When B_4C content is more than 40 wt%, excessive porosity caused by the worse sintering performance of B_4C leads to the decreased hardness for B_4C–SiC ceramics, despite the higher hardness of B_4C than SiC. Vandeperre and Teo[108] found that

the nanohardness of B_4C–SiC ceramics (5/95 < B_4C wt%/SiC wt% < 100/0) increases linearly from 29.3 to 33.3 GPa as the B_4C content increases. The measured nanohardness values of the B_4C–SiC ceramics are close to the average theoretical hardness of B_4C and SiC because the indents made are relatively small compared to the scale of the microstructure. Furthermore, Young's modulus of B_4C–SiC ceramics hardly varies with the increase in B_4C content (356–375 GPa), which is consistent with the similar Young's modulus values of single crystal SiC (450 GPa[149]) and single crystal B_4C (467 GPa[150]). The measured Young's modulus values are lower than the theoretical values, attributed to the residual porosity in the ceramics.

For B_4C–SiC ceramics prepared *via* hot-press sintering, So *et al.*[72] noted that the hardness of B_4C–SiC ceramics slightly increases with the increase in B_4C content from 30 to 70 wt%; the fracture toughness decreases with the increase in B_4C content, which is attributed to the decrease in the content of SiC with relatively high toughness. When the B_4C content is 50 wt%, the ceramics achieve the highest bending strength, which is attributed to the smallest grain size, as mentioned in Section 3.1. Chen *et al.*[79] observed that the bending strength and fracture toughness of B_4C–SiC ceramics increase with the increase in SiC content from 0 to 20 wt%, but the hardness of the ceramics slightly decreases. Tomohiro *et al.*[78] reported that the hardness of B_4C–SiC ceramics decreases with the increase in SiC addition from 0 to 50 vol%, resulting from the lower hardness of SiC compared to B_4C. However, both the bending strength and fracture toughness of the ceramics are maximum when the SiC content is 20 vol%. Crack deflection, bridging, and branching by SiC grains are the main toughening mechanisms for the B_4C–SiC ceramics. Meanwhile, the microcrack caused by the difference in thermal expansion coefficients between B_4C and SiC is also responsible for the increased fracture toughness. When the SiC content is more than 20 vol%, the grain size of SiC gradually increases from 2–3 μm to 5–6 μm; also, SiC grains agglomerate, leading to inhomogeneous dispersion of SiC grains in the ceramics. Thus, the bending strength and fracture toughness of the ceramics decrease. Keçeli *et al.*[151] found that the bending strength and hardness of SiC–B_4C ceramics increase with the increase in B_4C content from 0 to 15 wt%, which is attributed to the finer microstructure of the ceramics with the increased B_4C content.

For spark plasma sintered B_4C–SiC ceramics, Moshtaghioun *et al.*[112] found that the fracture toughness of B_4C–15 wt% SiC ceramics is higher than that of pure B_4C ceramics, which is attributed to the smaller grain sizes of B_4C and SiC in the B_4C–SiC ceramics than the grain size of B_4C in pure B_4C ceramics. Meanwhile, the addition of SiC changes the fracture mode of the ceramics from transgranular fracture to a mixture of transgranular and intergranular fracture. Crack bridging by the SiC grains is the main toughening mechanism. However, the hardness of B_4C–15 wt% SiC ceramics is slightly lower than that of pure B_4C ceramics because SiC is softer than B_4C. Sahin *et al.*[96] observed that the hardness of B_4C–SiC ceramics decreases from 34.4 to 31.1 GPa with the increase in SiC content from 5 to 15 vol%. Yaşar and Haber[71] found that with the content of B_4C in the composite ceramics increasing from 10 to 50 wt%, the hardness of SiC–B_4C ceramics increases, but the fracture toughness, Poisson's ratio, and elastic modulus decrease.

For B_4C–SiC ceramics fabricated by reaction-bonded sintering, Lee *et al.*[152] reported that the hardness of SiC–B_4C ceramics increases from 15.4 to 30.0 GPa as the B_4C content in the preform increases from 0 to 50 wt%. The increased hardness of SiC–B_4C ceramics with an increase in B_4C content is attributed to two aspects. First, B_4C has higher hardness. Second, B_4C provides more C due to partial decomposition during the reaction bonding because a locally exothermic reaction with Si and C will cause the temperature to exceed the heating temperature, reducing the residual Si content in the matrix by the reaction of C and Si. Han *et al.*[153] found that the reaction-bonded SiC–B_4C ceramics exhibit higher hardness, bending strength, and fracture toughness compared to the reaction-bonded SiC ceramics; the mechanical properties of the reaction-bonded SiC–B_4C ceramics linearly increase with an increase in B_4C content from 5 to 30 wt%. Lin and Fang[154] researched the mechanical properties of SiC–B_4C ceramics when the content of B_4C in the green body varies between 20 and 40 wt%. It was also found that the hardness of SiC–B_4C ceramics gradually increases with the increase in B_4C content. Furthermore, the fracture toughness and bending strength first increase and then decrease with the increase in B_4C content, both of which show the maximum values when the B_4C content is 30 wt%. The decreased fracture toughness and bending strength are attributed to the higher porosity when the B_4C content is more than 30 wt%, which is caused by the sintering difficulty of B_4C. Sun *et al.*[116] also noted that the hardness of B_4C–SiC ceramics increases with the increase in B_4C content from 10 to 70 wt%; however, both the bending strength and the fracture toughness increase first and then decrease. The decreased bending strength is ascribed to the destruction of the continuous phase. The SiC phase in the ceramics is continuous, but the B_4C phase is not bonded, existing in the form of a dispersion phase. Therefore, the SiC phase contacting each other in the form of a bridge is decreased with the increase in the non-bonded B_4C phase, reducing the bending strength.

In addition, Matović *et al.*[64] reported that despite the highest relative density achieved for the ultra-high pressure sintered B_4C–SiC ceramics with the equal-weighted contributions of B_4C and SiC, the highest hardness is obtained for the B_4C–SiC ceramics with the highest B_4C content when the B_4C content ranges from 25 to 75 wt%.

Some previous studies on the effect of the ratio of B_4C to SiC on the mechanical properties of B_4C–SiC ceramics are tabulated in Table 7.

4.2.2. Residual phase. For B_4C–SiC ceramics produced by reaction-bonded sintering, there is some residual phase in the resulting ceramics, eventually in the presence of a C or Si excess. The addition of excessive C in the green body will lead to insufficient Si to completely react with C, forming residual C. In contrast, residual Si is formed when free C added is insufficient or Si is excessive. In the case of introducing free C, the

Table 7 Effect of the ratio of B_4C to SiC on the mechanical properties of B_4C–SiC ceramics

Ceramics	Raw material	Sintering method	Sintering temperature (°C)	Sintering aid	Relative density (%)	Hardness (GPa)	Fracture toughness (MPa $m^{1/2}$)	Bending strength (MPa)	Young's modulus (GPa)
SiC[68]	α-SiC (0.6 μm)	Pressureless	2150	0.6 wt% B + 2 wt% carbon black	93.5	27.5	4.25	333	—
SiC-5 vol% B_4C[68]	α-SiC (0.6 μm), B_4C (0.7–0.9 μm)	Pressureless	2150	1 wt% carbon black	96.0	30.2	4.19	422	—
B_4C[70]	B_4C (0.8 μm)	Pressureless	2300	3 wt% carbon black	94.4	26.9	3.70	240	—
B_4C-20 wt% SiC[70]	B_4C (0.8 μm), α-SiC (0.4 μm)	Pressureless	2300	3 wt% carbon black	93.8	29.7	3.22	—	—
B_4C-40 wt% SiC[70]	B_4C (0.8 μm), α-SiC (0.4 μm)	Pressureless	2300	3 wt% carbon black	93.5	30.4	3.19	390	—
B_4C-60 wt% SiC[70]	B_4C (0.8 μm), α-SiC (0.4 μm)	Pressureless	2300	3 wt% carbon black	95.6	33.1	3.33	—	—
B_4C-80 wt% SiC[70]	B_4C (0.8 μm), α-SiC (0.4 μm)	Pressureless	2300	3 wt% carbon black	96.5	29.2	3.13	—	—
B_4C-97 wt% SiC[70]	B_4C (0.8 μm), α-SiC (0.4 μm)	Pressureless	2300	3 wt% carbon black	99.0	28.3	3.18	—	—
B_4C-70 wt% SiC[72]	B_4C (0.8 μm), α-SiC (0.5 μm)	Hot-press (40 MPa)	2000	No	100.0	30.3	3.60	590	—
B_4C-50 wt% SiC[72]	B_4C (0.8 μm), α-SiC (0.5 μm)	Hot-press (40 MPa)	2000	No	99.9	30.5	3.02	645	—
B_4C-30 wt% SiC[72]	B_4C (0.8 μm), α-SiC (0.5 μm)	Hot-press (40 MPa)	2000	No	99.8	30.8	2.82	560	—
B_4C[79]	B_4C (0.8 μm)	Hot-press (40 MPa)	1900	6 wt% Al_2O_3 + 4 wt% Y_2O_3	98.2	38.7	6.44	394	—
B_4C-10 wt% SiC[79]	B_4C (0.8 μm), SiC (0.45 μm)	Hot-press (40 MPa)	1900	6 wt% Al_2O_3 + 4 wt% Y_2O_3	98.7	34.9	6.78	407	—
B_4C-20 wt% SiC[79]	B_4C (0.8 μm), SiC (0.45 μm)	Hot-press (40 MPa)	1900	6 wt% Al_2O_3 + 4 wt% Y_2O_3	99.0	32.6	7.21	448	—
B_4C[78]	B_4C (0.72 μm)	Hot-press (30 MPa)	2200	No	99.9	28.9	3.90	620	—
B_4C-10 vol% SiC[78]	B_4C (0.72 μm), β-SiC (0.3 μm)	Hot-press (30 MPa)	2200	No	99.9	26.5	4.50	628	—
B_4C-15 vol% SiC[78]	B_4C (0.72 μm), β-SiC (0.3 μm)	Hot-press (30 MPa)	2200	No	99.9	25.9	4.71	674	—
B_4C-20 vol% SiC[78]	B_4C (0.72 μm), β-SiC (0.3 μm)	Hot-press (30 MPa)	2200	No	99.9	25.4	4.90	740	—
B_4C-30 vol% SiC[78]	B_4C (0.72 μm), β-SiC (0.3 μm)	Hot-press (30 MPa)	2200	No	99.9	25.4	4.60	645	—
B_4C-50 vol% SiC[78]	B_4C (0.72 μm), β-SiC (0.3 μm)	Hot-press (30 MPa)	2200	No	99.9	25.2	4.59	628	—
SiC[151]	SiC (0.11 μm)	Hot-press (50 MPa)	2100	No	77.0	—	—	65	—
SiC-5 wt% B_4C[151]	SiC (0.11 μm), B_4C (2.54 μm)	Hot-press (50 MPa)	2100	No	77.0	—	—	115	—
SiC-10 wt% B_4C[151]	SiC (0.11 μm), B_4C (2.54 μm)	Hot-press (50 MPa)	2100	No	79.0	—	—	123	—
SiC-15 wt% B_4C[151]	SiC (0.11 μm), B_4C (2.54 μm)	Hot-press (50 MPa)	2100	No	80.0	—	—	130	—
B_4C[112]	B_4C (0.5 μm)	Spark plasma (75 MPa)	1700 (×3 min)	No	100.0	39.3	3.50	—	—
B_4C-15 wt% SiC[112]	B_4C (0.5 μm), β-SiC (0.5 μm)	Spark plasma (75 MPa)	1700 (×3 min)	No	99.4	36.2	5.70	—	—
B_4C-5 vol% SiC[96]	B_4C, α-SiC	Spark plasma (40 MPa)	1750 (×5 min)	No	98.0	34.4	—	—	—
B_4C-10 vol% SiC[96]	B_4C, α-SiC	Spark plasma (40 MPa)	1750 (×5 min)	No	98.0	33.4	—	—	—
B_4C-15 vol% SiC[96]	B_4C, α-SiC	Spark plasma (40 MPa)	1750 (×5 min)	No	97.8	31.1	—	—	—
SiC-10 wt% B_4C[71]	B_4C, α-SiC	Spark plasma (50 MPa)	1950 (×5 min)	1.5 wt% C	99.6	26.1	2.89	—	415
SiC-20 wt% B_4C[71]	B_4C, α-SiC	Spark plasma (50 MPa)	1950 (×5 min)	1.5 wt% C	99.2	28.8	2.79	—	409
SiC-30 wt% B_4C[71]	B_4C, α-SiC	Spark plasma (50 MPa)	1950 (×5 min)	1.5 wt% C	98.8	29.5	2.74	—	402
SiC-40 wt% B_4C[71]	B_4C, α-SiC	Spark plasma (50 MPa)	1950 (×5 min)	1.5 wt% C	98.8	30.0	2.66	—	392
SiC-50 wt% B_4C[71]	B_4C, α-SiC	Spark plasma (50 MPa)	1950 (×5 min)	1.5 wt% C	98.9	30.3	2.64	—	388
SiC[152]	α-SiC (44 μm, 3 μm), carbon black, Si powder (1 mm)	Reaction	1650	No	—	15.4	—	—	—
SiC-50 wt% B_4C[152]	α-SiC (44 μm, 3 μm), B_4C (15 μm), carbon black, Si powder (1 mm)	Reaction	1650	No	—	30.0	—	—	—
SiC[153]	α-SiC (44 μm, 3 μm), carbon black, Si powder (1 mm)	Reaction	1650	No	—	15.0	—	108	—
SiC-5 wt% B_4C[153]	α-SiC (44 μm, 3 μm), B_4C (15 μm), carbon black, Si powder (1 mm)	Reaction	1650	No	—	18.5	—	129	—
SiC-10 wt% B_4C[153]	α-SiC (44 μm, 3 μm), B_4C (15 μm), carbon black, Si powder (1 mm)	Reaction	1650	No	—	20.9	—	143	—
SiC-20 wt% B_4C[153]	α-SiC (44 μm, 3 μm), B_4C (15 μm), carbon black, Si powder (1 mm)	Reaction	1650	No	—	24.4	—	200	—
SiC-30 wt% B_4C[153]	α-SiC (44 μm, 3 μm), B_4C (15 μm), carbon black, Si powder (1 mm)	Reaction	1650	No	—	27.5	—	289	—
SiC-20 wt% B_4C[154]	B_4C (5 μm), SiC (11 μm), carbon black (10 μm), Si	Reaction	1600	No	99.9	31.0	3.60	458	—
SiC-30 wt% B_4C[154]		Reaction	1600	No	99.8	32.0	3.80	475	—

Table 7 (*continued*)

Ceramics	Raw material	Sintering method	Sintering temperature (°C)	Sintering aid	Relative density (%)	Hardness (GPa)	Fracture toughness (MPa $m^{1/2}$)	Bending strength (MPa)	Young's modulus (GPa)
SiC-40 wt% B_4C[154]	B_4C (5 μm), SiC (11 μm), carbon black (10 μm), Si	Reaction	1600	No	99.7	32.5	3.10	400	—
SiC-10 wt% B_4C[116]	B_4C (5 μm), SiC (11 μm), carbon black (10 μm), Si	Reaction	1750	No	—	28.4	4.15	423	—
SiC-20 wt% B_4C[116]	B_4C (1.5 μm), α-SiC (7 μm), phenolic resin, carbon black, Si powder	Reaction	1750	No	—	—	4.71	458	—
SiC-30 wt% B_4C[116]	B_4C (1.5 μm), α-SiC (7 μm), phenolic resin, carbon black, Si powder	Reaction	1750	No	—	30.2	5.07	487	—
SiC-50 wt% B_4C[116]	B_4C (1.5 μm), α-SiC (7 μm), phenolic resin, carbon black, Si powder	Reaction	1750	No	—	34.0	4.50	430	—
SiC-70 wt% B_4C[116]	B_4C (1.5 μm), α-SiC (7 μm), phenolic resin, carbon black, Si powder	Reaction	1750	No	—	35.5	3.85	394	—
B_4C-75 wt% SiC[64]	B_4C (2.5 μm), β-SiC (0.6 μm)	Ultra-high pressure (4 GPa)	1500 (×1 min)	No	96.4	23.1	—	—	—
B_4C-50 wt% SiC[64]	B_4C (2.5 μm), β-SiC (0.6 μm)	Ultra-high pressure (4 GPa)	1500 (×1 min)	No	98.0	27.0	—	—	—
B_4C-25 wt% SiC[64]	B_4C (2.5 μm), β-SiC (0.6 μm)	Ultra-high pressure (4 GPa)	1500 (×1 min)	No	96.9	31.2	—	—	—

presence of residual Si means the complete consumption of C initially added to the green body, and the quantity of infiltrated Si is enough to react with the introduced free C. The amount of Si introduced is related to the original porosity present in the preform before infiltration; thus, the amount of residual Si mainly depends on the amount of C and initial porosity of the preform.

The content and distribution of residual Si play an important role in the mechanical properties of B_4C–SiC ceramics. First, Si is a brittle phase with lower hardness (7 GPa) and strength than B_4C and SiC. Second, the thermal stress is developed by the thermal expansion coefficient mismatch between the matrix and Si at weak interfacial sites during cooling.[155] Third, the bonding strength of the interface in the ceramics is reduced due to the existence of residual Si, which does not help in improving the bending strength of B_4C–SiC ceramics. Fourth, large-sized Si pools that are crack sources will be generated from residual Si, which can reduce the strength of B_4C–SiC ceramics. Hayun *et al.*[156] found that the mechanical properties of B_4C–SiC ceramics depend on the amount of residual Si. The B_4C preforms without the addition of free C achieve 30 and 20 vol% porosity after pre-infiltration sintering at 2000 and 2100 °C, respectively. For the B_4C preform with 20 vol% porosity, the amount of residual Si in the resulting ceramics is 7 vol%. For the B_4C preform with 30 vol% porosity, the amount of residual Si in the resulting ceramics is 13 vol%. The B_4C–SiC ceramics with less residual Si amount has higher hardness and Young's modulus, which is attributed to the increased fraction of the ceramic phases within the ceramics. Chhillar *et al.*[157] reported that the hardness, bending strength, and Young's modulus of the B_4C–SiC ceramics decrease with the increase in residual Si content, but its fracture toughness increases as the residual Si content increases. The decreased hardness and Young's modulus are attributed to the relatively low hardness and stiffness of residual Si, respectively; the decreased bending strength is caused by the larger critical flaw size in the ceramics with greater Si content; the increased fracture toughness results from ductile-like failure of the Si phase, and more tortuous fracture paths and more Si phase deformation occur in the ceramics with more Si content. Hayun *et al.*[148] pointed out that the amount of residual Si affects not only the static mechanical properties but also the dynamic mechanical properties. The stress at the Hugoniot elastic limit of the B_4C–SiC ceramics monotonically reduces with the increasing amount of residual Si. In addition, as armor materials, the compressive strength of ceramics is also an important parameter. Patel *et al.*[158] reported that the reaction-bonded B_4C–SiC ceramics fail in a typical brittle failure under compressive load, and the compressive strength of the reaction-bonded B_4C–SiC ceramics increases with the increase in the strain rate, the trend of which is similar to that of hot-pressed B_4C ceramics. However, the compressive strength of the reaction-bonded B_4C–SiC ceramics (700 MPa) is lower than those of hot-pressed B_4C ceramics (3.52 GPa) and hot-pressed SiC ceramics (5.46 GPa),[159] which is attributed to 20 vol% residual Si. The weak residual Si interface between the B_4C grains is the main reason for the low compressive strength of the reaction-bonded B_4C–SiC ceramics.

Besides the amount of residual Si, the size of residual Si also affects the mechanical properties of B_4C–SiC ceramics. When the Si region is small (<5 μm), the Si phase is under a state of residual compressive stress due to thermal mismatch between Si and the matrix during the cooling, which can improve the fracture toughness because of increased resistance to crack propagation in the Si phase.[100] In contrast, when the Si region is large (>5 μm) and irregularly shaped, the Si phase attains a state of tensile stress, promoting easy transgranular cracking with the Si region as the size of residual Si increases beyond a critical level.[100] Li *et al.*[76] reported that the hardness of B_4C–SiC ceramics increases with a decrease in residual Si size.

Although B_4C–SiC ceramics can be produced by reaction-bonded sintering, due to the inhomogeneous structure and presence of abundant residual Si, the reliability and mechanical properties of products, especially at high temperatures, are inferior. For example, soft spots left by residual Si can detract from the overall ballistic efficiency of B_4C–SiC ceramics. The products lose the partial superior properties of B_4C–SiC ceramics. Therefore, it is meaningful to decrease the amount of residual Si in the reaction-bonded B_4C–SiC ceramics. Several approaches have been attempted, such as the use of a powder mixture with an appropriate multimodal particle size distribution to decrease the initial porosity of the green body (Section 3.2.1),[76,84] infiltration of the partially sintered preform to increase the relative density of the preform,[142,156] the addition of elements that react with Si to form stable silicides,[160] and addition of elements (Ti and Fe) or compounds (TiC) that react with B_4C and release an additional amount of free C.[161–163]

As to the effect of residual C, Lin and Fang[154] reported that the residual C in the B_4C–SiC ceramics produced *via* the addition of free C can worsen the mechanical properties of B_4C–SiC ceramics even more seriously than residual Si. The mechanical properties of reaction-bonded B_4C–SiC ceramics first increase and then decrease with the increase in carbon black addition from 10 to 30 wt%.

In order to improve the mechanical properties of B_4C–SiC ceramics, the amount of residual phase needs to be reduced as much as possible. Some previous studies on the effect of the residual phase on the mechanical properties of reaction-bonded B_4C–SiC ceramics are tabulated in Table 8.

4.3. Raw material

As mentioned in Section 3.2, the characteristics of raw materials affect the sintering performance and microstructure of B_4C–SiC ceramics, which in turn can affect the mechanical properties of B_4C–SiC ceramics. The particle size and species of raw materials have a great influence on the mechanical properties of B_4C–SiC ceramics.

4.3.1. Particle size. For the B_4C–SiC ceramics produced by reaction-bonded sintering, the particle size of initial B_4C powders significantly affects the mechanical properties of B_4C–SiC ceramics.[164] Various findings have been put forward. Hayun *et al.*[84] reported that using B_4C powders with a suitable particle size distribution as raw materials can improve the relative density of the green body and reduce the amount of residual Si; thus, the mechanical properties of the obtained B_4C–SiC ceramics are increased. Dariel and Frage[99] mentioned that coarse B_4C grains are unfavorable for improving the bending strength of B_4C–SiC ceramics, while the effect of initial size of the B_4C particles on fracture toughness is minor. Zhai *et al.*[165] found that the hardness, fracture toughness, and bending strength of B_4C–SiC ceramics increase first and then decrease with the increase in particle size of B_4C (1, 2.5, 8, 15, 17, and 34 μm). When the particle size of B_4C is 17 μm, the mechanical properties of B_4C–SiC ceramics reach the maximum, which is attributed to the closed packing effect of the green body. Barick *et al.*[166] noted that the smaller the particle size of B_4C powders in the range of 18.7–63.4 μm, the greater the fracture toughness and bending strength of B_4C–SiC ceramics will be. For the fracture toughness of reaction-bonded SiC ceramics, Chakrabarti *et al.*[167] stated that the number of grains for crack propagation that will pass through is dependent on the average grain size and intergranular Si thickness. Similarly, the ratio of grain size to Si thickness decreases with the increase in particle size of B_4C powders in the reaction-bonded B_4C–SiC ceramics, which indicates that the crack propagates a longer distance for the B_4C–SiC ceramics with smaller particle size. Furthermore, the interfacial debonding mechanism dominates over transgranular fracture as the grain size decreases, and the debonding at B_4C–Si and SiC–Si interfaces can further improve fracture toughness for B_4C–SiC ceramics as compared to transgranular fracture. Therefore, the B_4C–SiC ceramics produced from the

Table 8 Effect of the residual phase on the mechanical properties of reaction-bonded B_4C–SiC ceramics

Ceramics	Raw material	Sintering temperature (°C)	Relative density (%)	Residual phase	Content of residual phase	Hardness (GPa)	Fracture toughness (MPa $m^{1/2}$)	Bending strength (MPa)	Young's modulus (GPa)
B_4C-13 vol% SiC[156]	B_4C, Si	1480	—	Si	7 vol%	22.5	5.5	390	410
B_4C-17 vol% SiC[156]	B_4C, Si	1480	—	Si	13 vol%	20.3	7.9	415	370
B_4C–SiC[157]	B_4C, resin, Si	—	—	Si	5 vol%	19.5	4.4	324	432
B_4C–SiC[157]	B_4C, resin, Si	—	—	Si	10 vol%	16.7	4.8	280	406
B_4C–SiC[157]	B_4C, resin, Si	—	—	Si	14 vol%	15.3	5.0	276	380
B_4C-70 wt% SiC[154]	B_4C (5 μm), SiC (11 μm), 10 wt% carbon black (10 μm), Si	1600	99.9	Si	—	30.0	3.4	415	—
B_4C-60 wt% SiC[154]	B_4C (5 μm), SiC (11 μm), 20 wt% carbon black (10 μm), Si	1600	99.9	Si	—	31.0	3.6	458	—
B_4C-50 wt% SiC[154]	B_4C (5 μm), SiC (11 μm), 30 wt% carbon black (10 μm), Si	1600	99.8	C	—	28.5	2.1	370	—

B_4C powders with smaller particle sizes exhibit higher fracture toughness. As to bending strength, residual thermal stress formed due to thermal expansion mismatch between the matrix and Si during cooling can generate flaws or cracks in weak interfacial zones. On the one hand, the probability of the formation of flaws with larger sizes is higher for the B_4C–SiC ceramics with larger grain size owing to the larger scale of the interfacial area between B_4C and Si grains; on the other hand, these flaws can propagate maximum up to one-grain size. Thereby, the B_4C–SiC ceramics with a larger grain size have flaws with a larger size. According to the Griffith equation:

$$\sigma_f = (2\gamma Y/\Pi C)^{1/2} \quad (9)$$

where σ_f is the bending strength (MPa), γ is the fracture surface energy (J m^{-2}), Y is Young's modulus (GPa), and C is half of the crack length (μm);[168] the larger the flaw size, the lower the bending strength is. As a result, the B_4C–SiC ceramics produced from B_4C powders with larger particle sizes show lower bending strength. However, the hardness of B_4C–SiC ceramics decreases with the decrease in particle size of B_4C powders. This is because the reaction-bonded B_4C–SiC ceramics with fine particle size have a larger interface boundary area, which is a weak zone. The larger the interface boundary area, the larger the volume fraction of the weak interfacial zone is. Therefore, the B_4C–SiC ceramics produced from B_4C powders with a smaller particle size exhibit lower hardness.[166] Furthermore, the smaller size of B_4C grains is beneficial for increasing the compressive strength of the reaction-bonded B_4C–SiC ceramics.[148] Based on these findings, adjusting the size of raw materials is one of the effective means to control the mechanical properties of B_4C–SiC ceramics.

Some previous studies on the effect of particle size of raw materials on the mechanical properties of reaction-bonded B_4C–SiC ceramics are tabulated in Table 9.

4.3.2. Species. As mentioned in Section 3.2.3, the species of raw materials control the microstructure of the obtained B_4C–SiC ceramics, which in turn gives rise to different mechanical properties of B_4C–SiC ceramics.

When β-SiC is used as the raw material, the microstructure of the resulting B_4C–SiC ceramics is different from that of B_4C–SiC ceramics prepared using α-SiC as the raw material; due to the partial transformation of β → α-SiC during sintering, platelet-shaped SiC grains are formed. Excessive platelet-shaped SiC grains in B_4C–SiC ceramics are not favorable for improving the densification of the ceramics; however, these platelet-shaped SiC grains can act as a factor for enhancing the fracture toughness of B_4C–SiC ceramics, which plays an equally important role in obtaining lightweight ballistic material.

In addition to directly mixing commercial B_4C and SiC raw powders to fabricate B_4C–SiC ceramics, other raw materials can also be used to prepare B_4C–SiC ceramics.

PCS is widely used as the precursor of SiC. The generation of fine SiC grains from PCS can reduce the size and density of structural defects that deteriorate the mechanical properties of B_4C–SiC ceramics by filling the pores and voids. Also, these fine SiC grains affect the crack propagation; when a crack

Table 9 Effect of particle size of raw materials on the mechanical properties of reaction-bonded B_4C–SiC ceramics

Ceramics	Raw material	Particle size of B_4C (μm)	Relative density of green body (%)	Sintering temperature (°C)	Relative density (%)	Hardness (GPa)	Fracture toughness (MPa $m^{1/2}$)	Bending strength (MPa)	Young's modulus (GPa)
B_4C–SiC[84]	B_4C, Si	66 vol%130.0 + 15 vol%13.0 + 19 vol%1.0	74.2	1450	99.9	22.6	—	318	400
B_4C–SiC[165]	B_4C, α-SiC (9 μm), carbon black (0.56 μm), phenolic resin, Si powder (50 μm)	1.0	—	1560	—	18.6	3.03	274	—
B_4C–SiC[165]	B_4C, α-SiC (9 μm), carbon black (0.56 μm), phenolic resin, Si powder (50 μm)	2.5	—	1560	—	18.9	3.56	289	—
B_4C–SiC[165]	B_4C, α-SiC (9 μm), carbon black (0.56 μm), phenolic resin, Si powder (50 μm)	8.0	—	1560	—	21.5	3.84	319	—
B_4C–SiC[165]	B_4C, α-SiC (9 μm), carbon black (0.56 μm), phenolic resin, Si powder (50 μm)	15.0	—	1560	—	24.6	4.20	346	—
B_4C–SiC[165]	B_4C, α-SiC (9 μm), carbon black (0.56 μm), phenolic resin, Si powder (50 μm)	17.0	—	1560	—	28.2	4.49	376	—
B_4C–SiC[165]	B_4C, α-SiC (9 μm), carbon black (0.56 μm), phenolic resin, Si powder (50 μm)	34.0	—	1560	—	24.3	3.89	340	—
B_4C–SiC[166]	B_4C, phenolic resin, carbon black	18.7	55.9	1550	—	12.4	5.76	403	—
B_4C–SiC[166]	B_4C, phenolic resin, carbon black	33.7	58.9	1550	—	13.6	5.00	359	—
B_4C–SiC[166]	B_4C, phenolic resin, carbon black	63.4	62.7	1550	—	16.4	3.40	265	—

encounters these fine SiC grains, either it has to break them or bypass them to continue the propagation, both of which consume the crack propagation energy. On the other hand, the thermal decomposition of PCS yields not only SiC but also free C. The C impurity has an effect on the hardness, strength, and oxidation resistance of B_4C–SiC ceramics. Therefore, different from the direct use of SiC powders, the use of PCS will have a certain impact on the mechanical properties of B_4C–SiC ceramics. Du *et al.*[91] used B_4C and PCS as raw materials to prepare B_4C–SiC ceramics by hot-press sintering. The hardness and fracture toughness of B_4C–15 wt% SiC ceramics are higher than those of pure B_4C ceramics. The improvement in hardness is attributed to the reduction of residual porosity in B_4C–SiC ceramics. The enhancement of fracture toughness is ascribed to two aspects. First, the layered structure and dislocation defects are generated in SiC grains (Fig. 3). Dislocation has a passivated effect on the crack tip. When cracks propagate to the dislocation zone, dislocation can absorb partial crack propagation energy by self-deformation and pin the crack, which is similar to microcrack toughening. Thereby, the layered structure and dislocation can consume much crack propagation energy, forming effective barriers for crack propagation. Second, SiC grains formed from the pyrolysis of PCS have a particle size in the range of nanometers to micrometers. Although transgranular fracture is still the main fracture mode of B_4C–SiC ceramics, SiC grains of micron size cause crack bridging and nano-sized SiC grains within B_4C grains induce crack deflection, both of which increase the fracture toughness of B_4C–SiC ceramics. Crack deflection is related to the tensile residual stress field induced by nano or quasi-nano SiC grains in the B_4C matrix. B_4C and SiC have similar thermal expansion coefficients; however, the thermal expansion properties of SiC may be changed greatly because of the nanometer size effect as SiC grain size reduces to nanoscale or quasi-nanoscale. As a result, a thermal residual stress field around nano or quasi-nano SiC grains is induced by the mismatch in the thermal expansion coefficients between the B_4C matrix and SiC grains during cooling. Hwang *et al.*[87] also observed the layered microstructure (or planar defects) and/or subgrains in the PCS pyrolyzed SiC grains. This microstructure can further improve the fracture toughness of the spark plasma sintered B_4C–SiC ceramics because cracks frequently deflect within SiC grains generated from PCS pyrolysis (Fig. 12a), which results from either the grain boundary between subgrains or the layered structure of grains (Fig. 12b). As a result, the toughening mechanism of SiC grains generated from PCS pyrolysis for the B_4C–SiC ceramics is a combination of crack deflection within SiC grains and crack impeding by SiC grains. It is noteworthy that the fracture toughness (indentation K_{IC}) of spark plasma sintered B_4C–SiC ceramics (2.7 MPa $m^{1/2}$) prepared from the pyrolysis of PCS is lower than the fracture toughness reported for the spark plasma sintered B_4C–SiC ceramics (5.7 MPa $m^{1/2}$) produced from SiC powders (Table 7), which is attributed to the residual C from the conversion of PCS to SiC, the difference in grain size, or other unknown factors; however, it is not recommended to compare the values of fracture toughness between different ceramic systems due to the complex crack tip arrest environment.[169] Furthermore, the hardness of spark plasma sintered B_4C–SiC ceramics decreases with the increased content of SiC formed by PCS pyrolysis. Besides the rule of mixtures that the hardness of SiC is lower than that of B_4C, the amount of residual C generated accompanied by the pyrolysis of PCS to form SiC also gradually increases, which can also lead to the reduction of hardness. Meanwhile, the hardness of spark plasma sintered B_4C–SiC ceramics ($\sim$29 GPa) prepared from the pyrolysis of PCS is lower than the hardness reported for the spark plasma sintered B_4C–SiC ceramics (31–36 GPa) produced from SiC powders (Table 7), resulting from the residual C accompanied by the PCS conversion to SiC. The introduction of an appropriate amount of Si can convert residual C into SiC, thus increasing the hardness of B_4C–SiC ceramics.[91] In addition, Zhou *et al.*[170] utilized PCS as a SiC precursor to prepare reaction-bonded B_4C–SiC ceramics from the green body composed of graded B_4C powders and PCS. Compared with the reaction-bonded B_4C–SiC ceramics produced from the green body composed of B_4C without the addition of PCS, the reaction-bonded B_4C–SiC ceramics prepared from the green body composed of B_4C with the addition of 5–10 wt% PCS exhibit higher bending strength, which is attributed to their lower porosity. The formed β-SiC and C particles by PCS pyrolysis can segment the large pores in the preform, decreasing the median pore diameter, which can increase the capillary force and is beneficial for the infiltration process. However, the excessive addition of PCS will reduce the bending strength of reaction-bonded B_4C–SiC ceramics because Si accumulation areas are generated in the ceramics, leading to the formation of residual stress in weak interfacial zones and flaws with large sizes. The layered structure of SiC derived from PCS pyrolysis is also observed in the reaction-bonded B_4C–SiC ceramics.[117]

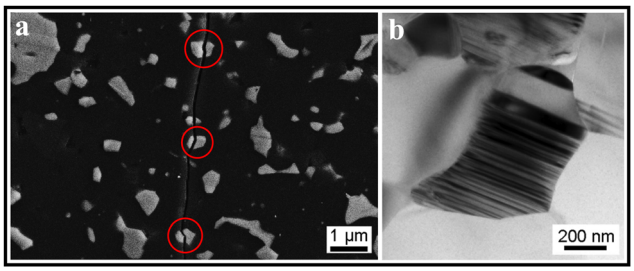

Fig. 12 (a) Cracks in spark plasma sintered B_4C–SiC ceramics whose SiC is generated from PCS pyrolysis showing frequent deflection and (b) SiC grain generated from PCS pyrolysis in the B_4C–SiC ceramics showing a layered structure (or planar defects)[87] (reprinted with permission, Copyright 2018, Elsevier).

Moreover, SiC can be formed *in situ* through some chemical reactions of two raw materials, which can cause a different effect on the mechanical properties of B_4C–SiC ceramics. Zhang *et al.*[94,95] used B_4C, Si, and amorphous carbon powders to produce B_4C–SiC ceramics *via* high-energy ball milling by hot-press sintering or spark plasma sintering. It was found that the hardness and fracture toughness of the obtained B_4C–SiC ceramics are higher than those of B_4C–SiC ceramics produced from B_4C and PCS as raw materials[91] or produced directly from B_4C and SiC powders *via* high-energy ball milling.[98] For the B_4C–SiC ceramics made from B_4C, Si, and amorphous carbon

via hot-press sintering, a number of nano-sized SiC and B_4C grains (100–200 nm) exist within the B_4C grains (1–3 μm). During high-energy ball milling, some smaller SiC and B_4C particles are embedded into the larger B_4C particles. Thereby, these smaller SiC and B_4C particles are trapped into the larger B_4C particles during sintering because of the fast diffusion speed, which is attributed to the disordered structure of B_4C–SiC composite powders formed during high-energy ball milling. This intragranular structure, which can generate intracrystalline boundaries and stress, is helpful in improving the mechanical properties of B_4C–SiC ceramics, especially the fracture toughness. The transgranular fracture is still the main fracture mode; however, when cracks cross the B_4C grains and reach intragranular particles within B_4C grains, the cracks are deflected along the intracrystalline boundary, rather than crossing the intragranular particles, which is ascribed to the small-size and high-strength intragranular crystals that can consume crack extension energy. Therefore, the intragranular grains (including B_4C and SiC grains) induce crack deflection; the intragranular structure changes the fracture mode from the single transgranular fracture to a combination of transgranular fracture and intergranular fracture, improving the fracture toughness of B_4C–SiC ceramics. Furthermore, the hardness and fracture toughness of B_4C–SiC ceramics produced from B_4C, Si, and amorphous carbon powders *via* spark plasma sintering are slightly higher than those of B_4C–SiC ceramics produced from the same raw materials *via* hot-press sintering, which is attributed to the smaller grain size resulting from the lower sintering temperature and shorter holding time as well as to the sufficient utilization of high sintering activity of B_4C and SiC composite powders produced *via* high-energy ball milling resulting from the fast heating rate by the spark plasma sintering, which can lead to the production of abundant energy from the disorder–order transformation of SiC and B_4C to induce densification. Wei *et al.*[171,172] used Si powders (D_{50} = 1 μm) and B_4C containing free C (0.9%) powders (D_{50} = 1.5 μm) as raw materials to produce B_4C–SiC ceramics. At high temperatures, free C can react with Si, synthesizing SiC *in situ*. Only B_4C and SiC phases are detected in the resulting B_4C–SiC ceramics, which indicates that no free Si exists in the ceramics after adding different contents of Si powders (4–12 wt%). The residual Si after reaction with free C is fully solid soluted into the B_4C lattice, resulting in increased lattice parameters of B_4C. The Si powders can melt above 1400 °C; thus the existence of a liquid phase promotes the sintering and improves the densification, reducing the number and size of pores acting as the origin of fracture. Therefore, the bending strength of B_4C–SiC ceramics is higher than that of pure B_4C ceramics without adding Si powders. The formation of SiC in B_4C ceramics, on the one hand, is beneficial for increasing the relative density of the ceramics, and on the other hand, changes the fracture mode of the ceramics from transgranular fracture to a combination of transgranular fracture and intergranular fracture, resulting in the increased fracture toughness compared to pure B_4C ceramics. However, the addition of excessive Si powders (12 wt%) will cause a certain degree of decrease in the strength and toughness of B_4C–SiC ceramics because the excessive SiC particles formed *in situ* aggregate, leading to a much bigger grain size. Sahin *et al.*[96] used B_4C, SiO_2, and carbon black as raw materials to produce B_4C–SiC ceramics *via* spark plasma sintering according to reaction (1). The formation of SiC using SiO_2 and carbon black as raw materials is accompanied by the generation of gas; thus, the hardness of the resulting B_4C–SiC ceramics decreases with the increase in *in situ* formed SiC content from 5 to 20 vol%, which is attributed to the gradually decreased relative density.

SiC whiskers (SiC_w) with high strength and high elastic modulus are considered to be an excellent toughening phase; different researchers studied the effect of SiC addition in the form of whiskers (SiC_w) on the mechanical properties of B_4C–SiC ceramics. To improve the mechanical properties of reaction-bonded B_4C–SiC ceramics, Wang *et al.*[173] added SiC in the form of a whisker into the green body composed of B_4C and C. The stacking density of the mixed powders in the preform decreases with the increase in SiC_w addition from 0 to 24 wt%, resulting in the gradually decreased relative density of the preform. The fracture roughness of the reaction-bonded B_4C–SiC ceramics increases with the increase in SiC_w content from 0 to 24 wt%; the main toughening mechanism is the pulling out of SiC_w from the matrix, which is an energy-consuming process. However, the hardness and bending strength of the reaction-bonded B_4C–SiC ceramics decrease with the increase in SiC_w content from 0 to 24 wt%. The reduced hardness is attributed to the decreased proportion of B_4C in the ceramics; the decreased bending strength is ascribed to the dissolution of SiC_w and transformation to SiC particles during molten Si infiltration, the formation of microcracks within the ceramics resulting from the mismatch of thermal expansion coefficients between B_4C and SiC_w, and the weakening of interface bonding strength between B_4C and SiC_w due to the increased defects such as the porosity and the non-uniformity distribution of SiC_w. Tamari *et al.*[174] studied the effect of SiC whisker content in the range of 10 to 30 vol% on the mechanical properties of hot-press sintered B_4C–SiC_w ceramics. There was no pulling-out of the SiC whiskers and no crack deflection during fracture, which is opposite to what Wang *et al.*[173] found; thus, the fracture toughness of B_4C–SiC_w ceramics increases slightly with the increase in SiC whisker content. In contrast, the bending strength of B_4C–SiC_w ceramics decreases with the increase in SiC whisker content. The hardness and elastic modulus are independent of SiC whisker content.

Some previous studies on the effect of species of raw material on the mechanical properties of B_4C–SiC ceramics are tabulated in Table 10.

4.3.3. Use of C/SiC in the reaction-bonded B_4C–SiC ceramics. The addition of free C in the preform will help control the morphology of SiC grains formed (Section 3.5.2.2) and SiC phase volume fraction, which in turn will affect the mechanical properties of reaction-bonded B_4C–SiC ceramics. Furthermore, the use of C can affect the sintering performance and microstructure of reaction-bonded B_4C–SiC ceramics; thus, the mechanical properties of B_4C–SiC ceramics can be enhanced by adjusting the initial free C content. Gao *et al.*,[144] Zhang *et al.*,[75] and Lin *et al.*[175] reported that the addition of 5–10 vol% carbon powders, 8–10 wt%

Table 10 Effect of species of raw material on the mechanical properties of B_4C–SiC ceramics

Ceramics	Raw material	Sintering method	Sintering temperature (°C)	Sintering aid	Relative density (%)	Hardness (GPa)	Fracture toughness (MPa $m^{1/2}$)	Bending strength (MPa)	Young's modulus (GPa)
B_4C[91]	B_4C (3.5 μm)	Hot-press (30 MPa)	1950	No	91.7	24.1	3.34	—	—
B_4C-15 wt% SiC[91]	B_4C (3.5 μm), PCS	Hot-press (30 MPa)	1950	No	96.1	26.6	4.98	—	—
B_4C-15 wt% SiC[91]	B_4C (3.5 μm), PCS	Hot-press (30 MPa)	1950	8 wt% Si	99.1	33.5	5.57	—	—
B_4C[87]	B_4C (0.3–0.6 μm)	Spark plasma (50 MPa)	1900 (×5 min)	No	—	29.7	2.00	—	409
B_4C-10 wt% SiC[87]	B_4C (0.3–0.6 μm), PCS	Spark plasma (50 MPa)	1900 (×5 min)	No	99.7	29.1	2.36	—	416
B_4C-20 wt% SiC[87]	B_4C (0.3–0.6 μm), PCS	Spark plasma (50 MPa)	1900 (×5 min)	No	99.5	28.5	2.68	—	408
B_4C–SiC[170]	B_4C (139.0 μm, 2.01 μm), Si powder	Reaction	1500	No	99.1	15.1	4.26	260	348
B_4C–SiC[170]	B_4C (139.0 μm, 2.01 μm), 5 wt% PCS, Si powder	Reaction	1500	No	99.8	17.3	4.35	319	402
B_4C–SiC[170]	B_4C (139.0 μm, 2.01 μm), 10 wt% PCS, Si powder	Reaction	1500	No	99.8	17.2	—	281	393
B_4C–SiC[170]	B_4C (139.0 μm, 2.01 μm), 15 wt% PCS, Si powder	Reaction	1500	No	99.6	16.9	—	242	403
B_4C-20 wt% SiC[94]	B_4C (3 μm), Si (−200 mesh), amorphous carbon (1 μm)	Hot-press (30 MPa)	1900	No	97.2	30.1	6.10	—	—
B_4C-20 wt% SiC[94]	B_4C (3 μm), Si (−200 mesh), amorphous carbon (1 μm)	Hot-press (30 MPa)	1950	No	98.6	34.3	6.00	—	—
B_4C-20 wt% SiC[95]	B_4C (3 μm), Si (−200 mesh), amorphous carbon (1 μm)	Spark plasma (30 MPa)	1700 (×5 min)	No	96.7	28.8	5.75	—	—
B_4C-20 wt% SiC[95]	B_4C (3 μm), Si (−200 mesh), amorphous carbon (1 μm)	Spark plasma (30 MPa)	1750 (×5 min)	No	98.3	33.4	6.50	—	—
B_4C-20 wt% SiC[95]	B_4C (3 μm), Si (−200 mesh), amorphous carbon (1 μm)	Spark plasma (30 MPa)	1800 (×5 min)	No	99.2	35.8	6.80	—	—
B_4C-50 wt% SiC[98]	B_4C, SiC, mean particle size of 0.7 μm	Hot-press (30 MPa)	1900	No	96.4	24.0	4.60	430	—
B_4C[171]	B_4C (1 μm)	Hot-press (60 MPa)	1850	No	—	—	4.25	175	—
B_4C–SiC[171]	B_4C (1 μm), Si (1.5 μm)	Hot-press (60 MPa)	1850	4 wt% Si	—	—	4.37	283	—
B_4C–SiC[171]	B_4C (1 μm), Si (1.5 μm)	Hot-press (60 MPa)	1850	8 wt% Si	—	—	5.04	354	—
B_4C–SiC[171]	B_4C (1 μm), Si (1.5 μm)	Hot-press (60 MPa)	1850	12 wt% Si	—	—	4.76	302	—
B_4C-5 vol% SiC[96]	B_4C, SiO_2 (1 μm), carbon black	Spark plasma (40 MPa)	1750 (×5 min)	No	97.7	35.0	—	—	—
B_4C-10 vol% SiC[96]	B_4C, SiO_2 (1 μm), carbon black	Spark plasma (40 MPa)	1750 (×5 min)	No	93.8	34.5	—	—	—
B_4C-15 vol% SiC[96]	B_4C, SiO_2 (1 μm), carbon black	Spark plasma (40 MPa)	1750 (×5 min)	No	91.2	33.1	—	—	—
B_4C-20 vol% SiC[96]	B_4C, SiO_2 (1 μm), carbon black	Spark plasma (40 MPa)	1750 (×5 min)	No	88.3	32.1	—	—	—
B_4C–SiC[173]	B_4C (125 μm : 12.8 μm = 2 : 1), carbon black, Si	Reaction	1500	No	—	31.2	4.49	322	—
B_4C–SiC[173]	B_4C (125 μm : 12.8 μm = 2 : 1), carbon black, 6 vol% SiC whisker, Si	Reaction	1500	No	—	31.0	4.64	285	—
B_4C–SiC[173]	B_4C (125 μm : 12.8 μm = 2 : 1), carbon black, 12 vol% SiC whisker, Si	Reaction	1500	No	—	30.4	4.67	265	—
B_4C–SiC[173]	B_4C (125 μm : 12.8 μm = 2 : 1), carbon black, 18 vol% SiC whisker, Si	Reaction	1500	No	—	28.9	4.73	254	—
B_4C–SiC[173]	B_4C (125 μm : 12.8 μm = 2 : 1), carbon black, 24 vol% SiC whisker, Si	Reaction	1500	No	—	27.6	4.88	243	—
B_4C–SiC[174]	B_4C (0.24 μm), 10 vol% SiC whisker (diameter = 1.1 μm, length = 45 μm)	Hot-press (30 MPa)	2100	No	>99%	30.0	3.89	877	439
B_4C–SiC[174]	B_4C (0.24 μm), 20 vol% SiC whisker (diameter = 1.1 μm, length = 45 μm)	Hot-press (30 MPa)	2100	No	>99%	31.1	3.89	812	429
B_4C–SiC[174]	B_4C (0.24 μm), 30 vol% SiC whisker (diameter = 1.1 μm, length = 45 μm)	Hot-press (30 MPa)	2100	No	>99%	30.0	4.23	760	426

nano-carbon black, or microporous carbon can improve the mechanical properties of reaction-bonded B_4C–SiC ceramics, respectively. The addition of C can promote the sintering of B_4C–SiC ceramics; therefore, the increase in hardness and bending strength is attributed to the decrease in porosity of B_4C–SiC ceramics and a more uniform microstructure. The fracture mode of B_4C–SiC ceramics changes from a combination of intergranular and transgranular fracture to transgranular fracture only with the increase in C content from 0 to 10 vol%. However, excessive C (>10 vol% or >10 wt%) will lead to a decrease in mechanical properties for B_4C–SiC ceramics. The excessive C leads to the formation of larger-sized individual particles resulting from the aggregation of SiC and the formation of holes, which is attributed to the blockage of the channels from Si infiltration caused by the aggregation of SiC. Both the increase in grain size and the formation of holes deteriorate the mechanical properties of B_4C–SiC ceramics. Different from the research results mentioned above, Lee *et al.*[152] found that the hardness of SiC–30 wt% B_4C ceramics increases linearly with the increase in carbon black from 10 to 40 wt%. The increase in C content can increase the reactivity with Si, reducing the residual Si content in the final B_4C–SiC ceramics. Zhang *et al.*[101] introduced C in the form of a C layer deposited on B_4C particles into the preform. The mechanical properties of B_4C–SiC ceramics prepared from the C-coated B_4C particles are higher than those prepared from the mixture of uncoated B_4C and nano-carbon black. The C layer on B_4C particles can prevent the dissolution and reaction of B_4C grains in molten Si effectively; thus, the better mechanical properties of B_4C–SiC ceramics prepared from the C-coated B_4C particles are attributed to the higher relative density, higher B_4C content, the smaller grain size of B_4C, and the formation of many nano-SiC grains as well as a continuous ceramic skeleton of the nano-SiC grains-coated and -bonded B_4C grains, as mentioned in Section 3.5.2.3.

Furthermore, C can also be introduced in the form of fibers. On the one hand, carbon fibers can be used as a C source, and on the other hand, carbon fibers can also be used as a toughening phase. B_4C–SiC ceramics exhibit isotropic mechanical properties due to the homogeneous dispersion of the chopped carbon fibers. The main toughening mechanisms of carbon fibers in B_4C–SiC ceramics are considered to be fiber pullout and fiber debonding. Carbon fibers not only provide sufficient C for forming a ceramic skeleton structure but also control the distribution of residual Si. Song *et al.*[85] noted that the fracture toughness and bending strength of B_4C–SiC ceramics increase with an increase in carbon fibers content from 0 to 40 vol%. Carbon fibers can completely react with molten Si during Si infiltration, and there are no carbon fibers in the final B_4C–SiC ceramics. The residual Si content is decreased with the increase in carbon fibers content; also, the residual Si particles occupy the original positions of carbon fibers, forming fiber-like extensions, which is beneficial for lowering the defect sensitivity of the residual Si and controlling the size of the formed Si islands. However, the addition of an excess of carbon fibers (50 vol%) will generate too many β-SiC particles, causing a relatively high volume expansion, leading to the blockage of Si capillary channels and the formation of residual carbon fibers; thus, the mechanical properties are reduced. It is worth noting that if carbon fibers are only used as a C source, it is unnecessary to take measures to protect the carbon fibers. In contrast, if carbon fibers are used as a toughening material, the structure and mechanical properties of carbon fibers are inevitably degraded due to the interfacial reaction during the infiltration; adding carbon black in the preform can protect the carbon fibers from erosion to some extent since the molten Si will preferentially react with the carbon black due to its higher specific surface area.[176]

Moreover, the addition of SiC in the preform can form the core–rim structure of primary α-SiC surrounded by a secondary β-SiC rim (Section 3.5.2.1). Song *et al.*[60] mentioned that the mechanical properties of B_4C–SiC ceramics produced from the preform with the addition of SiC are higher than those of B_4C–SiC ceramics produced from the preform without the addition of SiC. This is because the formed SiC cannot nucleate and grow on the B_4C particles in the preform without the addition of SiC; thus, SiC formed and B_4C particles are distributed independently; a continuous ceramic skeleton is not formed. In contrast, in the preform with the addition of SiC, SiC formed can connect the original SiC particles to form a continuous ceramic skeleton, improving the mechanical properties.

Although better mechanical properties of reaction-bonded B_4C–SiC ceramics are achieved by generating the plate-like shaped SiC grains without adding free C in the preform, the addition of free C can improve the mechanical properties of B_4C–SiC ceramics by promoting the sintering performance and enhancing the microstructure. Therefore, the effect of free C on the mechanical properties of reaction-bonded B_4C–SiC ceramics is a competitive factor, which depends on the amount, form, *etc.* Some previous studies on the effect of C/SiC added in the preform on the mechanical properties of reaction-bonded B_4C–SiC ceramics are tabulated in Table 11.

4.4. Preparation process

In addition to optimizing raw material formulations, some efforts have been devoted to studying how to improve the mechanical properties of B_4C–SiC ceramics by adjusting process parameters. The preparation process affects the mechanical properties of B_4C–SiC ceramics mainly by changing the microstructure.

4.4.1. Preparation of the green body. Pores in the green body affect the mechanical properties of the obtained B_4C–SiC ceramics. Compaction pressure can control the porosity and pore size of the green body. Meanwhile, adjusting the porosity and pore size of the green body can help control the content and size of residual Si in the reaction-bonded B_4C–SiC ceramics. Zong *et al.*[177] investigated the effect of forming pressure on the mechanical properties of reaction-bonded B_4C–SiC ceramics. With the increase in forming pressure from 50 to 200 MPa, the porosity of the green body decreases, leading to the decreased porosity of the obtained reaction-bonded B_4C–SiC ceramics and the decreased content of free Si filled in the remaining pores, both of which are beneficial for improving the mechanical properties of B_4C–SiC ceramics. However, when the forming pressure exceeds 200 MPa, the pores in the

Table 11 Effect of C/SiC added in the preform on the mechanical properties of reaction-bonded B_4C–SiC ceramics

Ceramics	Raw material	Amount of C/SiC added	Sintering temperature (°C)	Residual Si content	Relative density (%)	Hardness (GPa)	Fracture toughness (MPa $m^{1/2}$)	Bending strength (MPa)	Young's modulus (GPa)
B_4C–SiC[144]	B_4C (5 μm), Si	0 vol% C	1650	—	99.7	17.1	2.70	268	—
B_4C–SiC[144]	B_4C (5 μm), carbon black, Si	5 vol% C	1650	—	99.6	18.9	3.96	305	—
B_4C–SiC[144]	B_4C (5 μm), carbon black, Si	10 vol% C	1650	—	99.8	19.6	3.83	358	—
B_4C–SiC[144]	B_4C (5 μm), carbon black, Si	20 vol% C	1650	—	99.2	15.3	3.10	226	—
B_4C–SiC[75]	B_4C (4.08 μm), Si	0 wt% C	1550	—	99.9	19.2	3.65	267	—
B_4C–SiC[75]	B_4C (4.08 μm), carbon black, Si	6 wt% C	1550	—	99.9	21.3	4.30	318	—
B_4C–SiC[75]	B_4C (4.08 μm), carbon black, Si	8 wt% C	1550	—	99.4	24.0	4.74	336	—
B_4C–SiC[75]	B_4C (4.08 μm), carbon black, Si	10 wt% C	1550	—	99.1	24.4	4.41	361	—
B_4C–SiC[75]	B_4C (4.08 μm), carbon black, Si	12 wt% C	1550	—	98.7	19.0	4.20	275	—
B_4C–SiC[175]	B_4C, microporous carbon, Si powder (200 mesh)	—	1600	—	98.4	22.6	4.74	286	332
SiC-30 wt% B_4C[152]	α-SiC (77 μm : 3 μm = 7 : 3), B_4C (15 μm), carbon black, Si powder (1 mm)	10 wt% C	1650	—	—	25.0	—	—	—
SiC-30 wt% B_4C[152]	α-SiC (77 μm : 3 μm = 7 : 3), B_4C (15 μm), carbon black, Si powder (1 mm)	20 wt% C	1650	—	—	27.6	—	—	—
SiC-30 wt% B_4C[152]	α-SiC (77 μm : 3 μm = 7 : 3), B_4C (15 μm), carbon black, Si powder (1 mm)	30 wt% C	1650	—	—	34.5	—	—	—
SiC-30 wt% B_4C[152]	α-SiC (77 μm : 3 μm = 7 : 3), B_4C (15 μm), carbon black, Si powder (1 mm)	40 wt% C	1650	—	—	37.3	—	—	—
B_4C–SiC[101]	C-coated B_4C particles prepared *via* the pyrolysis and carbonization of phenolic resin, Si lump (5–10 mm)	10 wt% C	1600	—	99.9	24.0	4.80	316	—
B_4C–SiC[101]	B_4C (2.14 μm), carbon black (22 nm), Si lump (5–10 mm)	10 wt% C	1600	—	99.7	19.0	3.50	457	—
SiC-15 wt% B_4C[85]	α-SiC (14 μm), B_4C (1.5 μm), Si	0 wt% C	1600	39.0 wt%	—	—	2.83	291	—
SiC-15 wt% B_4C[85]	α-SiC (14 μm), B_4C (1.5 μm), carbon fibers (diameter = 6 μm, length = 3 mm), Si	10 wt% C	1600	28.6 wt%	—	—	3.24	320	—
SiC-15 wt% B_4C[85]	α-SiC (14 μm), B_4C (1.5 μm), carbon fibers (diameter = 6 μm, length = 3 mm), Si	20 wt% C	1600	19.9 wt%	—	—	4.50	375	—
SiC-15 wt% B_4C[85]	α-SiC (14 μm), B_4C (1.5 μm), carbon fibers (diameter = 6 μm, length = 3 mm), Si	30 wt% C	1600	14.2 wt%	—	—	6.58	414	—
SiC-15 wt% B_4C[85]	α-SiC (14 μm), B_4C (1.5 μm), carbon fibers (diameter = 6 μm, length = 3 mm), Si	40 wt% C	1600	7.1 wt%	—	—	7.50	465	—
SiC-15 wt% B_4C[85]	α-SiC (14 μm), B_4C (1.5 μm), carbon fibers (diameter = 6 μm, length = 3 mm), Si	50 wt% C	1600	5.3 wt%	—	—	2.89	262	—
B_4C–SiC[60]	B_4C (14 μm), phenolic resin, Si	0 wt% SiC	1600	—	—	—	—	332	—
SiC-5 wt% B_4C[60]	B_4C (14 μm), α-SiC (14 μm), carbon black, phenolic resin, Si	68 wt% SiC	1600	15.6 vol%	—	—	4.06	325	—
SiC-15 wt% B_4C[60]	B_4C (14 μm), α-SiC (14 μm), carbon black, phenolic resin, Si	58 wt% SiC	1600	14.8 vol%	—	—	4.35	357	—
SiC-25 wt% B_4C[60]	B_4C (14 μm), α-SiC (14 μm), carbon black, phenolic resin, Si	48 wt% SiC	1600	13.2 vol%	—	—	4.58	407	—
SiC-35 wt% B_4C[60]	B_4C (14 μm), α-SiC (14 μm), carbon black, phenolic resin, Si	38 wt% SiC	1600	13.7 vol%	—	—	4.80	379	—
SiC-45 wt% B_4C[60]	B_4C (14 μm), α-SiC (14 μm), carbon black, phenolic resin, Si	28 wt% SiC	1600	14.9 vol%	—	—	5.12	367	—

green body become too narrow to be penetrated by molten Si because of the occupation of the newly formed SiC particles, increasing the porosity of the obtained reaction-bonded B_4C–SiC ceramics, thus decreasing the bending strength and fracture toughness. Besides the number of pores in the green body, the pore size in the green body can also affect the mechanical properties of reaction-bonded B_4C–SiC ceramics. Li *et al.*[76] stated that the porosity and pore size of the green body correspond to the volumetric fraction and size of the Si phase, respectively; the hardness of B_4C–SiC ceramics increases with the decrease in residual Si size. Therefore, decreasing the pore size in the green body can also increase the mechanical properties of reaction-bonded B_4C–SiC ceramics.

Moreover, preliminary sintering for preforms before infiltration with molten Si can increase the relative density of preforms;[142,156] an additional step, namely, the preliminary sintering of preforms, is added, and a product with decreased Si content is obtained. However, Dariel and Frage[99] found that the preliminary sintering of preforms has little effect on the mechanical properties of the obtained reaction-bonded B_4C–SiC ceramics, which is attributed to the rim structure connecting the original B_4C grains in both the preliminary sintered preforms and the green preforms. Hayun *et al.*[148] also noted that the preliminary sintering of preforms has no effect on the static mechanical properties and on the dynamic response of the resulting reaction-bonded B_4C–SiC ceramics, although preliminary sintering can lead to the formation of a continuous preform skeleton. This phenomenon is attributed to the similar final microstructures between the B_4C–SiC ceramics produced from the preforms with and without preliminary sintering, *i.e.*, the rim regions composed of $B_{12}(B, C, Si)_3$ connect the B_4C grains in both types of reaction-bonded B_4C–SiC ceramics.

In addition, the forming technique for the green body can affect the mechanical properties of the resulting B_4C–SiC ceramics. Xu *et al.*[100] used the conventional compression molding method and gel-casting method to produce preforms composed of B_4C and C, respectively, and found that the mechanical properties of the obtained reaction-bonded B_4C–SiC ceramics produced by the gel-casting method are higher than those of the reaction-bonded B_4C–SiC ceramics produced by the conventional compression molding method after the same liquid Si infiltration process. The higher mechanical properties are attributed to the microstructure of the obtained B_4C–SiC ceramics, *viz.*, the continuous SiC-bonded B_4C skeleton structure and decreased size of residual Si in the ceramics, resulting from the 3D-interconnected porous structure in the preform produced *via* the gel-casting route. Furthermore, residual Si inevitably exists in the reaction-bonded B_4C–SiC ceramics; however, it is possible to improve their mechanical properties as far as possible by controlling the size of residual Si. Non-uniform residual stress distributes throughout if the residual Si size is larger than 5 μm, leading to defect generation due to the presence of anomalous tensile stress in the interior of residual Si.[178] Ren *et al.*[103] observed that adjusting the content of the catalyst Na_2CO_3 in the resorcinol–formaldehyde gel system can help control the pore characteristics of the preform prepared by gel-casting, which can improve the mechanical properties of the reaction-bonded B_4C–SiC ceramics by controlling the content and size of residual Si. With an increase in catalyst content, on the one hand, the residual Si content is reduced; on the other hand, carbon particle size in the preform decreases, resulting in the decreased size of the SiC particles formed. However, as the size of carbon particles decreases to a nanometre size, nano-sized carbon particles undergo aggregation, leading to the formation of large-sized SiC particles and subsequent deterioration of mechanical properties due to the large residual stress during cooling. Also, the pore structure of the preform changes from a single macroporous or mesoporous structure to a hierarchical macroporous–mesoporous structure with the increase in catalyst content. The preform with a single mesoporous structure exhibits the best mechanical properties. Using the gel-casting method to produce the green body is a feasible and novel way to improve the mechanical properties of reaction-bonded B_4C–SiC ceramics.

Some previous studies on the effect of forming pressure and forming technique for the green body on the mechanical properties of reaction-bonded B_4C–SiC ceramics are tabulated in Table 12.

4.4.2. Parameters during sintering. Parameters during sintering mainly affect the mechanical properties of B_4C–SiC ceramics by changing their microstructure. Generally, fine grains are helpful in improving the mechanical properties of B_4C–SiC ceramics. Meanwhile, high relative density, which can be achieved by increasing sintering temperature, prolonging holding time, and enhancing sintering pressure (if any), allows B_4C–SiC ceramics to achieve better mechanical properties. It is worth noting that increasing the sintering temperature or prolonging the holding time can lead to grain coarsening, which is not conducive to improving the mechanical properties of B_4C–SiC ceramics.

4.4.2.1. Sintering temperature. For B_4C–SiC ceramics produced *via* pressureless sintering, Zhu *et al.*[107] reported that the hardness, bending strength, and fracture toughness of B_4C–15 wt% SiC ceramics first increase and then decrease with an increase in sintering temperature in the range of 2100 to 2200 °C. When the sintering temperature is 2150 °C, the mechanical properties of B_4C–SiC ceramics reach the maximum. With the increase in sintering temperature to 2150 °C, the improvement in mechanical properties of B_4C–SiC ceramics is attributed to the following aspects: (1) the porosity of the ceramics is reduced, and the pores are mostly round or regular polygons, the characteristics of which can reduce stress concentration and increase the bending strength; (2) clean phase boundaries between B_4C and SiC grains indicate that the bonding between B_4C and SiC is strong (Fig. 8b), which has an vital influence on the mechanical properties of B_4C–SiC ceramics; (3) graphite formed due to the crystallisation of the sintering aid of carbon black can hinder the movement of grain boundaries at the high temperature stage, improving the mechanical properties; (4) the phase boundary between B_4C and graphite is clean and narrow, and such a semi-coherent interface with low stress results in a high bending strength; (5) the existence of SiC particles can cause crack deflection (Fig. 13a)

Table 12 Effect of forming pressure and forming technique for the green body on the mechanical properties of reaction-bonded B_4C–SiC ceramics

Ceramics	Raw material	Forming technique of preform	Forming pressure (MPa)	Open porosity of the green body (%)	Sintering temperature (°C)	Open porosity (%)	Residual Si content (vol%)	Hardness (GPa)	Fracture toughness (MPa $m^{1/2}$)	Bending strength (MPa)	Young's modulus (GPa)
B_4C–SiC^{177}	B_4C, carbon black, Si lump	Compression molding	50	49.4	1550	0.95	38.5	16.8	3.80	246	—
B_4C–SiC^{177}	B_4C, carbon black, Si lump	Compression molding	100	46.3	1550	0.40	32.8	18.2	4.05	263	—
B_4C–SiC^{177}	B_4C, carbon black, Si lump	Compression molding	150	44.3	1550	0.23	30.6	21.9	4.28	283	—
B_4C–SiC^{177}	B_4C, carbon black, Si lump	Compression molding	200	42.3	1550	0.19	28.8	24.0	4.90	319	—
B_4C–SiC^{177}	B_4C, carbon black, Si lump	Compression molding	250	41.7	1550	0.30	26.8	24.6	4.59	310	—
B_4C–SiC^{100}	B_4C (2.41 μm), carbon black, Si lump	Compression molding	200	39.1	1480	—	—	17.4	3.61	330	—
B_4C–SiC^{100}	B_4C (2.41 μm), carbon black, Si lump	Gel-casting	—	37.7	1480	—	—	19.4	4.37	389	—

that may occur because of the layered structure within SiC grains, crack branching (Fig. 13b), and crack bridging (Fig. 13c), prolonging the crack-propagation, inhibiting crack-tip propagation, and increasing the energy consumption; thus, the fracture toughness of the B_4C–SiC ceramics is increased. However, a higher sintering temperature will lead to abnormal grain growth and increased porosity caused by the rapid movement of grain boundaries, which can deteriorate the mechanical properties of B_4C–SiC ceramics.

For B_4C–SiC ceramics prepared by hot-press sintering, Shi *et al.*[83] found that the hardness and bending strength of B_4C–20 vol% SiC ceramics increase with an increase in sintering temperature from 1900 to 2100 °C, which is attributed to the reduced porosity with an increase in sintering temperature. The bending strength of B_4C–SiC ceramics strongly depends on porosity, and the relationship between porosity (θ) and bending strength (σ_w) of B_4C–20 vol% SiC ceramics can be expressed as $\sigma_w = 257\exp(-2.18\theta)$. Compared with pure B_4C ceramics, the B_4C–20 vol% SiC ceramics exhibit higher hardness after different sintering temperatures; however, the bending strength of B_4C–20 vol% SiC ceramics is higher than that of pure B_4C ceramics only after sintering at 1900 °C, and the bending strength of B_4C–20 vol% SiC ceramics is slightly lower than that of pure B_4C ceramics after sintering at 2000 and 2100 °C. Zhang *et al.*[98] stated that the hardness and bending strength of B_4C–50 wt% SiC ceramics increase linearly with the increase in sintering temperature in the range of 1800–1950 °C, which is attributed to the gradually increased densification; however, the fracture roughness of the ceramics first increases and then decreases. When the sintering temperature is 1850 °C, the fracture toughness reaches the maximum because there are a number of pores inside the ceramics sintered at that temperature and these pores can consume fracture energy when cracks pass through them. Chen *et al.*[110] reported that the mechanical properties of B_4C–20 wt% SiC ceramics increase with the increase in sintering temperature from 1800 to 1900 °C, which is attributed to the smaller grains and denser microstructure at higher sintering temperatures. The B_4C–20 wt% SiC ceramics exhibit better mechanical properties than the pure B_4C ceramics. The fracture mode of the B_4C–20 wt% SiC ceramics is mainly transgranular fracture at any temperature; however, partial crack deflection and grain pullout are enhanced with an increase in sintering temperature (Fig. 14).

For spark plasma sintered B_4C–SiC ceramics, Wu *et al.*[111] observed that the hardness and fracture toughness of B_4C–20 vol% SiC ceramics increase with the increase in sintering temperature from 1900 to 2000 °C. The improved mechanical properties are attributed to the increased relative density with the increase in sintering temperature, independent of the phase change because no new phases are formed during sintering. When the sintering temperature is higher than 2000 °C, the change in mechanical properties of B_4C–20 vol% SiC ceramics is not obvious. The increased sintering temperature does not change the mode of crack propagation, that is, the fracture mechanism of the ceramics sintered at different sintering temperatures is the transgranular fracture. However, the number of

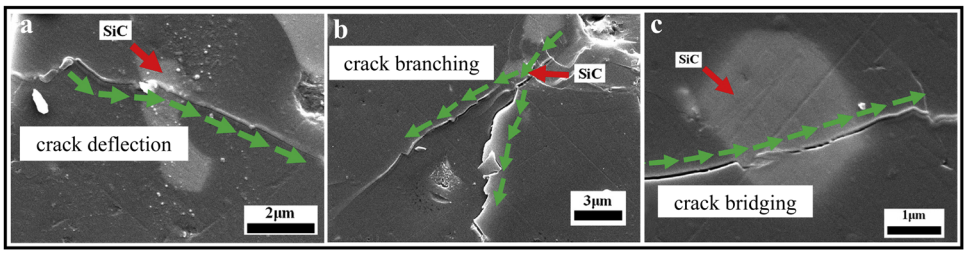

Fig. 13 Crack propagation on the surface of pressureless sintered B_4C–15 wt% SiC ceramics: (a) crack deflection, (b) crack branching, and (c) crack bridging[107] (reprinted with permission, Copyright 2019, Elsevier).

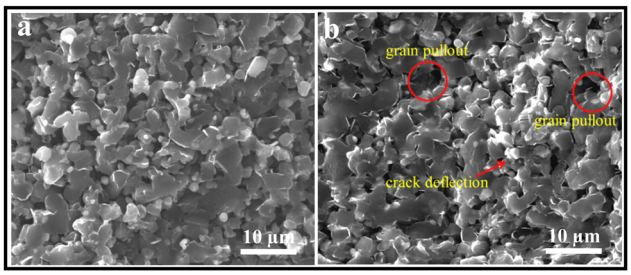

Fig. 14 Fracture surfaces of hot-press sintered B_4C–20 wt% SiC ceramics at different sintering temperatures: (a) 1800 °C and (b) 1900 °C.[110]

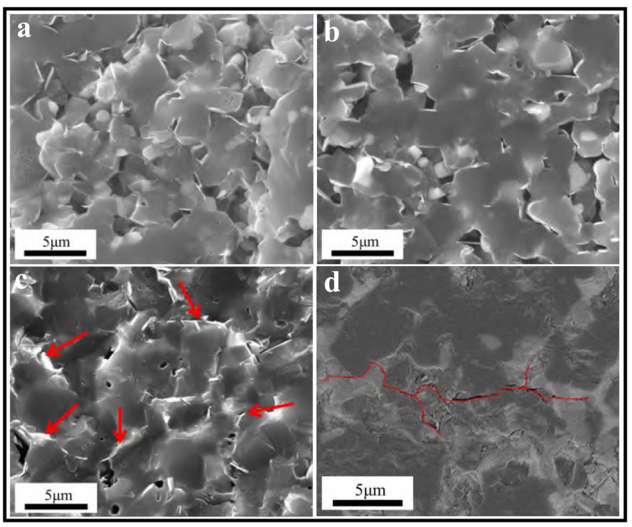

Fig. 15 Fracture surfaces of hot-press sintered B_4C–20 wt% SiC ceramics produced at different sintering pressures: (a) 30 MPa, (b) 35 MPa, and (c) 40 MPa.[122] (d) Indentation crack deflection in hot-press sintered B_4C–20 wt% SiC ceramics produced at a sintering pressure of 40 MPa.[122]

pores in the ceramics gradually decreases with the increase in sintering temperature; thus, the crack propagation is more hindered. Also, the reduction of porosity can increase the probability of cracks passing through the SiC grains, resulting in a significant increase in fracture toughness.

For B_4C–SiC ceramics fabricated by reaction-bonded sintering, sintering temperature can alter phase volume fractions. Zhang *et al.*[117] found that the hardness, fracture toughness, and bending strength of B_4C–SiC ceramics increase with the increase in infiltration temperature from 1450 to 1600 °C. The improved hardness and bending strength are attributed to the gradually decreased porosity, and the increased fracture toughness is caused by the increased *in situ* formed SiC with a layered structure. When the infiltration temperature is more than 1600 °C, the fracture toughness increases continuously; however, the hardness and bending strength decrease, resulting from the increased porosity and the larger flaws due to the increased grain size of B_4C particles and the presence of large SiC zones.

4.4.2.2. Holding time. Tomohiro *et al.*[78] reported that the bending strength and fracture toughness of the hot-press sintered B_4C–15 vol% SiC ceramics decrease with the increase in holding time from 0.5 to 2 h when the sintering temperature is 2200 °C, which is attributed to the increased grain size and the increased flaw size in the ceramics with the increase in holding time.

4.4.2.3. Sintering pressure. Chen *et al.*[122] noted that the mechanical properties of hot-press sintered B_4C–20 wt% SiC ceramics increase with the increase in sintering pressure from 30 to 40 MPa, which is attributed to the increased relative density and decreased grain size of the B_4C–SiC ceramics with the increase in sintering pressure. The fracture mode of the B_4C–SiC ceramics is mainly transgranular fracture at different sintering pressures (Fig. 15a–c); however, cracks tend to deflect with the increase in sintering pressure. The residual stress is caused due to different thermal expansion coefficients between B_4C and SiC during hot-press sintering, forming the microcracks at the weak interface between B_4C and SiC because the hot-press sintered B_4C–20 wt% SiC ceramics are produced by liquid-phase sintering with Al_2O_3 and Y_2O_3 as sintering aids. When the sintering pressure is low, the microstructure is loose; thus, it is difficult to generate a crack deflection effect, leading to lower fracture toughness. However, under high sintering pressure, when the fracture crack extends to the microcrack, it will preferentially orient in the direction of the microcrack (Fig. 15d), so that the fracture crack will deflect and bifurcate, improving the fracture toughness.

Some previous studies on the effect of parameters during sintering on the mechanical properties of B_4C–SiC ceramics are tabulated in Table 13.

4.5. Sintering aids

The addition of sintering aids can promote the sintering of B_4C–SiC ceramics *via* solid-state sintering or liquid-phase sintering

Table 13 Effect of parameters during sintering on the mechanical properties of B_4C–SiC ceramics

Ceramics	Raw material	Sintering method	Sintering temperature (°C)	Holding time	Sintering pressure (MPa)	Sintering aid	Relative density (%)	Hardness (GPa)	Fracture toughness (MPa $m^{1/2}$)	Bending strength (MPa)	Young's modulus (GPa)
B_4C-15 wt% SiC[107]	B_4C (0.8 μm), SiC (0.5 μm)	Pressureless	2100	1 h	No	2 wt% carbon black	91.6	16.2	2.20	145	—
B_4C-15 wt% SiC[107]	B_4C (0.8 μm), SiC (0.5 μm)	Pressureless	2125	1 h	No	2 wt% carbon black	93.6	22.1	2.60	231	—
B_4C-15 wt% SiC[107]	B_4C (0.8 μm), SiC (0.5 μm)	Pressureless	2150	1 h	No	2 wt% carbon black	95.3	25.5	2.81	296	—
B_4C-15 wt% SiC[107]	B_4C (0.8 μm), SiC (0.5 μm)	Pressureless	2175	1 h	No	2 wt% carbon black	93.1	22.0	2.40	193	—
B_4C[83]	B_4C (10.22 μm)	Hot-press	1900	1 h	20	No	71.9	3.2	—	134	—
B_4C-20 vol% SiC[83]	B_4C (10.22 μm), β-SiC (1.07 μm)	Hot-press	1900	1 h	20	No	73.7	3.7	—	150	—
B_4C[83]	B_4C (10.22 μm)	Hot-press	2000	1 h	20	No	77.0	5.0	—	164	—
B_4C-20 vol% SiC[83]	B_4C (10.22 μm), β-SiC (1.07 μm)	Hot-press	2000	1 h	20	No	77.8	6.1	—	153	—
B_4C[83]	B_4C (10.22 μm)	Hot-press	2100	1 h	20	No	87.9	11.5	—	196	—
B_4C-20 vol% SiC[83]	B_4C (10.22 μm), β-SiC (1.07 μm)	Hot-press	2100	1 h	20	No	87.0	12.8	—	194	—
B_4C-50 wt% SiC[98]	B_4C, SiC, mean particle size of 0.7 μm	Hot-press	1800	0.5 h	30	No	74.0	6.0	3.20	214	—
B_4C-50 wt% SiC[98]	B_4C, SiC, mean particle size of 0.7 μm	Hot-press	1850	0.5 h	30	No	79.2	8.0	5.20	263	—
B_4C-50 wt% SiC[98]	B_4C, SiC, mean particle size of 0.7 μm	Hot-press	1900	0.5 h	30	No	89.2	18.0	4.90	366	—
B_4C-50 wt% SiC[98]	B_4C, SiC, mean particle size of 0.7 μm	Hot-press	1950	0.5 h	30	No	96.4	24.0	4.60	430	—
B_4C[110]	B_4C (0.8 μm)	Hot-press	1800	0.5 h	30	10 wt% (Al_2O_3 + Y_2O_3)	97.2	8.2	2.58	257	—
B_4C-20 wt% SiC[110]	B_4C (0.8 μm), SiC (0.45 μm)	Hot-press	1800	0.5 h	30	10 wt% (Al_2O_3 + Y_2O_3)	94.0	12.0	3.28	237	—
B_4C[110]	B_4C (0.8 μm)	Hot-press	1900	0.5 h	30	10 wt% (Al_2O_3 + Y_2O_3)	98.6	20.0	4.01	264	—
B_4C-20 wt% SiC[110]	B_4C (0.8 μm), SiC (0.45 μm)	Hot-press	1900	0.5 h	30	10 wt% (Al_2O_3 + Y_2O_3)	98.5	17.0	4.79	313	—
B_4C-20 vol% SiC[111]	B_4C (3.5 μm), SiC (0.5 μm)	Spark plasma	1900	10 min	40	No	90.1	16.7	3.93	—	—
B_4C-20 vol% SiC[111]	B_4C (3.5 μm), SiC (0.5 μm)	Spark plasma	1950	10 min	40	No	91.0	17.2	4.12	—	—
B_4C-20 vol% SiC[111]	B_4C (3.5 μm), SiC (0.5 μm)	Spark plasma	2000	10 min	40	No	96.3	32.4	4.78	—	—
B_4C-20 vol% SiC[111]	B_4C (3.5 μm), SiC (0.5 μm)	Spark plasma	2050	10 min	40	No	96.6	32.9	4.74	—	—
B_4C-20 vol% SiC[111]	B_4C (3.5 μm), SiC (0.5 μm)	Spark plasma	2100	10 min	40	No	96.8	33.4	4.68	—	—
B_4C–SiC[117]	B_4C (4.08 μm), carbon black, Si lump	Reaction	1450	1 h	No	No	99.8	15.0	3.33	312	—
B_4C–SiC[117]	B_4C (4.08 μm), carbon black, Si lump	Reaction	1500	1 h	No	No	99.8	16.9	3.63	315	—
B_4C–SiC[117]	B_4C (4.08 μm), carbon black, Si lump	Reaction	1550	1 h	No	No	99.9	17.0	3.66	319	—
B_4C–SiC[117]	B_4C (4.08 μm), carbon black, Si lump	Reaction	1600	1 h	No	No	99.9	19.0	3.80	344	—
B_4C–SiC[117]	B_4C (4.08 μm), carbon black, Si lump	Reaction	1650	1 h	No	No	99.8	13.7	3.97	290	—
B_4C-15 vol% SiC[78]	B_4C (0.72 μm), β-SiC (0.3 μm)	Hot-press	2200	0.5 h	30	No	99.7	—	4.73	680	—
B_4C-15 vol% SiC[78]	B_4C (0.72 μm), β-SiC (0.3 μm)	Hot-press	2200	1 h	30	No	99.7	—	4.70	553	—
B_4C-15 vol% SiC[78]	B_4C (0.72 μm), β-SiC (0.3 μm)	Hot-press	2200	2 h	30	No	99.7	—	4.20	396	—
B_4C-20 wt% SiC[122]	B_4C (0.8 μm), SiC (0.45 μm)	Hot-press	1900	0.5 h	30	10 wt% (Al_2O_3 + Y_2O_3)	98.5	17.0	4.79	313	—
B_4C-20 wt% SiC[122]	B_4C (0.8 μm), SiC (0.45 μm)	Hot-press	1900	0.5 h	35	10 wt% (Al_2O_3 + Y_2O_3)	98.6	25.7	6.94	366	—
B_4C-20 wt% SiC[122]	B_4C (0.8 μm), SiC (0.45 μm)	Hot-press	1900	0.5 h	40	10 wt% (Al_2O_3 + Y_2O_3)	99.0	32.6	7.21	448	—

(Section 3.4). In general, under the liquid-phase sintering mechanism, amorphous secondary phases remain at the phase boundary of the composite ceramics. Accordingly, numerous processes, such as creep, diffusion, crack growth, oxidation, and corrosion will occur during the applications depending on the amount and the composition of boundary phases, which can affect the performance, especially at high temperatures, and even shorten the service life of ceramics.[179] Compared with liquid-phase sintering, the ceramics can achieve better high-temperature performance under the solid-state sintering mechanism. Different sintering aids have different effects on the mechanical properties of B_4C–SiC ceramics. Some types of sintering aids benefit only the densification of B_4C–SiC ceramics, not their mechanical properties.

4.5.1. C. Moshtaghioun *et al.*[112] reported that the graphite sintering aid can promote the densification of the spark plasma sintered B_4C–15 wt% SiC ceramics; however, the addition of graphite increases the sizes of both B_4C and SiC grains, thus decreasing the hardness and fracture toughness of the ceramics. Meanwhile, the residual graphite softens the B_4C–SiC ceramics and weakens the interface between the B_4C and SiC grains.

In addition, the graphite sintering aid also has an effect on the creep resistance of B_4C–SiC ceramics at high temperatures.[126] The total deformation of B_4C–SiC ceramics with 2 wt% graphite and without graphite is 25% and 30%, respectively. In the case of B_4C–SiC ceramics with graphite after deformation, the cavitation that is created during deformation occurs in the ceramics; however, the complicated networks of dislocations, twinning, and trapped dislocations in twins are the main characteristics in the B_4C–SiC ceramics without graphite. In the absence of graphite, the B_4C–SiC ceramics show a similar plastic behavior as pure B_4C polycrystalline ceramics. In the presence of graphite, the deformation of B_4C–SiC ceramics is controlled by either solution–precipitation or grain sliding controlled by the viscosity of the glassy phase. The creep resistance of B_4C–SiC ceramics is strongly dependent on the presence of a graphite layer along the grain boundary. For the B_4C–SiC ceramics with graphite, grain boundary sliding is a more favorable process under creep, permitting ductility to be increased to a greater strain value. Therefore, due to an enhanced creep resistance, B_4C–SiC ceramics with graphite opens up new perspectives of structural materials with complex shapes for high-temperature applications.

4.5.2. Oxide. Jamale and Kumar[127] studied the effect of Al_2O_3 addition on the mechanical properties of spark plasma sintered B_4C–10 wt% SiC ceramics. With an increase in the amount of relatively softer Al_2O_3 from 3 to 6 wt%, the hardness of B_4C–10 wt% SiC ceramics slightly decreases, but the fracture toughness increases. Transgranular fracture is still the dominant fracture mode in the B_4C–10 wt% SiC ceramics after the addition of Al_2O_3, resulting from the minor difference in thermal expansion coefficients between B_4C and SiC. Sahin *et al.*[96] observed that the addition of 5 wt% Y_2O_3 can slightly enhance the hardness of spark plasma sintered B_4C–SiC ceramics, which is attributed to the improved relative density resulting from the formation of glassy phases. Rocha and Melo[88] found that the pressureless sintered B_4C–10 wt% SiC ceramics with the addition of sintering aids of AlN–Y_2O_3 can achieve higher hardness than that with the addition of sintering aids of Al_2O_3–Y_2O_3, which is attributed to the higher relative density of B_4C–10 wt% SiC ceramics after the addition of AlN–Y_2O_3. Zhu *et al.*[129] reported that an appropriate amount of sintering aid CeO_2 can improve the mechanical properties of pressureless sintered B_4C–15 wt% SiC ceramics. On the one hand, CeB_6 grains formed *in situ via* the reaction between B_4C and CeO_2 disperse on the B_4C grain boundaries; these CeB_6 grains can inhibit the movement of grain boundary, which is beneficial for inhibiting grain growth and refining grains. On the other hand, a residual stress field is formed around the CeB_6 grains during the cooling process due to the higher thermal expansion coefficient of CeB_6 than that of SiC and B_4C,[180] contributing to improved fracture toughness for B_4C–SiC ceramics. The toughening mechanisms are crack deflection owing to the thermal expansion mismatch between CeB_6 and B_4C and crack bridging at the crack tip by the CeB_6 grain (Fig. 16). However, the addition of excessive CeO_2 will increase the porosity of B_4C–SiC ceramics, leading to the reduction in mechanical properties.

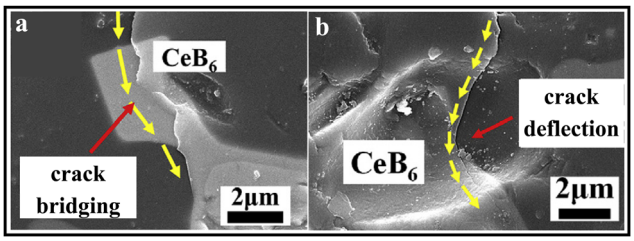

Fig. 16 Crack propagating on the surface of pressureless sintered B_4C–15 wt% SiC ceramics with the sintering aid of 5 wt% CeO_2: (a) crack bridging and (b) crack deflection[129] (reproduced with permission, Copyright 2013, Elsevier).

4.5.3. Si. Du *et al.*[132] stated that the addition of sintering aid Si can improve the mechanical properties of hot-press sintered B_4C–15 wt% SiC ceramics, in which SiC is obtained from PCS after pyrolyzing. On the one hand, Si forms a liquid phase at high temperatures, promoting densification and decreasing residual porosity; on the other hand, Si can react with residual C generated from the pyrolysis of PCS to form SiC, removing the soft C-rich phase that can reduce the hardness of B_4C–SiC ceramics. However, Sahani and Chaira[131] found that the addition of sintering aid Si in the range of 2–20 wt% cannot enhance the hardness of B_4C–60 wt% SiC ceramics produced by pressureless sintering or spark plasma sintering, although the relative density of the B_4C-60 wt% SiC ceramics is increased after the addition of Si. The hardness of B_4C–60 wt% SiC ceramics containing 10 wt% Si is close to that of B_4C–60 wt% SiC ceramics without Si, which is attributed to the reduced pore size and refined microstructure resulting from the sufficient Si addition. The addition of excessive Si will produce a large amount of residual Si in the matrix, reducing the hardness of the B_4C–60 wt% SiC ceramics.

Some previous studies on the effect of sintering aids on the mechanical properties of B_4C–SiC ceramics are tabulated in Table 14.

Table 14 Effect of sintering aids on the mechanical properties of B_4C–SiC ceramics

Ceramics	Raw material	Sintering aid	Sintering method	Sintering temperature (°C)	Relative density (%)	Hardness (GPa)	Fracture toughness (MPa $m^{1/2}$)	Bending strength (MPa)	Young's modulus (GPa)
B_4C-15 wt% SiC[112]	B_4C (0.5 μm), β-SiC (0.5 μm)	No	Spark plasma (75 MPa)	1650 (×3 min)	96.6	30.3	6.0	—	—
B_4C-15 wt% SiC[112]	B_4C (0.5 μm), β-SiC (0.5 μm)	2 wt% graphite	Spark plasma (75 MPa)	1650 (×3 min)	98.8	25.7	5.5	—	—
B_4C-15 wt% SiC[112]	B_4C (0.5 μm), β-SiC (0.5 μm)	No	Spark plasma (75 MPa)	1700 (×3 min)	99.4	36.2	5.7	—	—
B_4C-15 wt% SiC[112]	B_4C (0.5 μm), β-SiC (0.5 μm)	2 wt% graphite	Spark plasma (75 MPa)	1700 (×3 min)	100.0	29.3	5.3	—	—
B_4C-10 wt% SiC[127]	B_4C, SiC	3 wt% Al_2O_3	Spark plasma (40 MPa)	1800 (×10 min)	99.5	35.1	5.9	—	—
B_4C-10 wt% SiC[127]	B_4C, SiC	6 wt% Al_2O_3	Spark plasma (40 MPa)	1800 (×10 min)	99.1	33.7	6.5	—	—
B_4C-5 vol% SiC[96]	B_4C, α-SiC	No	Spark plasma (40 MPa)	1750 (×5 min)	98.0	34.4	—	—	—
B_4C-5 vol% SiC[96]	B_4C, α-SiC	5 wt% Y_2O_3	Spark plasma (40 MPa)	1750 (×5 min)	98.3	35.3	—	—	—
B_4C-10 vol% SiC[96]	B_4C, α-SiC	No	Spark plasma (40 MPa)	1750 (×5 min)	98.0	33.4	—	—	—
B_4C-10 vol% SiC[96]	B_4C, α-SiC	5 wt% Y_2O_3	Spark plasma (40 MPa)	1750 (×5 min)	98.8	34.4	—	—	—
B_4C-15 vol% SiC[96]	B_4C, α-SiC	No	Spark plasma (40 MPa)	1750 (×5 min)	97.8	31.1	—	—	—
B_4C-15 vol% SiC[96]	B_4C, α-SiC	5 wt% Y_2O_3	Spark plasma (40 MPa)	1750 (×5 min)	98.2	33.0	—	—	—
B_4C-10 wt% SiC[88]	B_4C, β-SiC	10 vol% (Al_2O_3 : Y_2O_3 = 5 : 3, molar ratio)	Pressureless	2000	91.5	29.5	—	—	—
B_4C-10 wt% SiC[88]	B_4C, β-SiC	10 vol% (AlN : Y_2O_3 = 3 : 2, molar ratio)	Pressureless	2000	93.4	30.3	—	—	—
B_4C-15 wt% SiC[129]	B_4C (0.8 μm), SiC (0.5 μm)	No	Pressureless	2150	85.8	19.8	2.40	194	—
B_4C-15 wt% SiC[129]	B_4C (0.8 μm), SiC (0.5 μm)	1 wt% CeO_2	Pressureless	2150	91.2	26.0	3.25	270	—
B_4C-15 wt% SiC[129]	B_4C (0.8 μm), SiC (0.5 μm)	3 wt% CeO_2	Pressureless	2150	92.6	29.4	3.59	330	—
B_4C-15 wt% SiC[129]	B_4C (0.8 μm), SiC (0.5 μm)	5 wt% CeO_2	Pressureless	2150	96.4	32.2	4.32	380	—
B_4C-15 wt% SiC[129]	B_4C (0.8 μm), SiC (0.5 μm)	7 wt% CeO_2	Pressureless	2150	94.6	29.0	4.19	350	—
B_4C-15 wt% SiC[129]	B_4C (0.8 μm), SiC (0.5 μm)	9 wt% CeO_2	Pressureless	2150	93.4	27.0	4.00	330	—
B_4C-15 wt% SiC[132]	B_4C (3.5 μm), PCS	No	Hot-press (30 MPa)	1950	95.4	24.0	4.96	265	—
B_4C-15 wt% SiC[132]	B_4C (3.5 μm), PCS	4 wt% Si	Hot-press (30 MPa)	1950	95.8	26.4	5.06	260	—
B_4C-15 wt% SiC[132]	B_4C (3.5 μm), PCS	8 wt% Si	Hot-press (30 MPa)	1950	97.8	29.8	5.34	324	—
B_4C-15 wt% SiC[132]	B_4C (3.5 μm), PCS	11.4 wt% Si	Hot-press (30 MPa)	1950	99.2	33.2	5.64	389	—
B_4C-15 wt% SiC[132]	B_4C (3.5 μm), PCS	15 wt% Si	Hot-press (30 MPa)	1950	98.3	31.0	5.40	350	—
B_4C-60 wt% SiC[131]	B_4C, SiC	No	Pressureless	1950	89.0	20.0	—	—	—
B_4C-60 wt% SiC[131]	B_4C, SiC	2 wt% Si	Pressureless	1950	88.0	14.0	—	—	—
B_4C-60 wt% SiC[131]	B_4C, SiC	5 wt% Si	Pressureless	1950	89.0	16.2	—	—	—
B_4C-60 wt% SiC[131]	B_4C, SiC	10 wt% Si	Pressureless	1950	92.0	18.1	—	—	—
B_4C-60 wt% SiC[131]	B_4C, SiC	20 wt% Si	Pressureless	1950	90.0	15.0	—	—	—
B_4C-60 wt% SiC[131]	B_4C, SiC	No	Spark plasma (50 MPa)	1600 (×5 min)	94.0	28.0	—	—	—
B_4C-60 wt% SiC[131]	B_4C, SiC	2 wt% Si	Spark plasma (50 MPa)	1350 (×5 min)	94.6	22.0	—	—	—
B_4C-60 wt% SiC[131]	B_4C, SiC	5 wt% Si	Spark plasma (50 MPa)	1350 (×5 min)	96.3	24.4	—	—	—
B_4C-60 wt% SiC[131]	B_4C, SiC	10 wt% Si	Spark plasma (50 MPa)	1350 (×5 min)	98.0	27.8	—	—	—
B_4C-60 wt% SiC[131]	B_4C, SiC	20 wt% Si	Spark plasma (50 MPa)	1350 (×5 min)	97.0	24.0	—	—	—

5. Future development trend

B_4C–SiC composite ceramics have emerged as a novel structural ceramic material for engineering applications. Looking forward, several aspects need to be further researched to enhance the understanding and fulfill their wide applications.

5.1. Investigation of high-temperature performance and other properties

B_4C–SiC ceramics are dimensionally and structurally stable against a wide range of temperature variations due to chemical inertness and high-temperature resistance. High-temperature-resistant ceramics have the potential to have a significant impact on improving energy efficiency. The application of lightweight ceramics can lead to energy saving in various fields like the chemical industry, environment, automobile, aircraft engine parts, and power. As a potential high-temperature structural component, the mechanical properties of B_4C–SiC ceramics at high temperatures need to be further investigated.

Currently, the investigation for B_4C–SiC ceramics is mostly focused on conventional mechanical properties evaluation, and other mechanical properties are seldom reported. For example, as bulletproof materials, B_4C–SiC ceramics are used against high-speed armor-piercing projectiles and hard steel-core bullets; thus, the compressive strength and impact strength of B_4C–SiC ceramics also need to be investigated deeply. Although the bending strength and hardness of the SiC–B_4C ceramics increase with the increase in B_4C content from 0 to 15 wt%, their impact strength exhibits the highest value as the B_4C content is 5 wt%.[151] Therefore, all the mechanical property parameters need to be considered comprehensively. In addition, B_4C–SiC ceramics have received considerable scientific attention for direct conversion between thermal and electric energy applications.[181,182] Accordingly, the thermal properties and electrical properties of B_4C–SiC ceramics need to be evaluated.

5.2. Development of new sintering aids

To date, the sintering performance of B_4C–SiC ceramics can be enhanced by using sintering aids. However, some sintering aids only benefit densification or fracture toughness, not strength or hardness, and even deteriorate mechanical properties. To mitigate or overcome this disadvantage, new sintering aids should be developed to increase the fracture toughness while maintaining a high hardness for B_4C–SiC ceramics. Moreover, the use of current sintering aids may cause a reduction in the high-temperature mechanical properties of B_4C–SiC ceramics. Therefore, the development of new sintering aids for high-performance applications of B_4C–SiC ceramics at low and high temperatures is still a severe challenge.

5.3. Research on B_4C–SiC nanocomposite ceramics

Due to the nanometer size effect, B_4C–SiC nanocomposite ceramics exhibit better performance and have wider application prospects. However, one of the problems is that it is difficult and costly to produce B_4C–SiC nanocomposite ceramics by directly mixing commercial nano-sized B_4C and SiC powders and subsequent sintering. New ways and technologies should be explored to fabricate B_4C–SiC nanocomposite ceramics, enabling us to further broaden the application fields of B_4C–SiC ceramics. From the point of view of special properties and potential applications, the research on B_4C–SiC nanocomposite ceramics is meaningful.

5.4. Preparation of new forms of ceramics composed of B_4C–SiC

In addition to the traditional dense B_4C–SiC block ceramics with uniform composition, the B_4C–SiC component can also be used to prepare other forms of ceramic materials, such as gradient ceramics, laminated ceramics, porous ceramics, and ceramic hollow microspheres. Furthermore, due to the excellent performance of the B_4C–SiC binary system, it is estimated that more and more new forms of ceramics composed of B_4C–SiC will gradually appear.

5.4.1. Gradient ceramics/laminated ceramics. Gradient ceramics are a kind of inhomogeneous composite ceramics with at least two phases. One of the important characteristics of gradient ceramics is that the microstructure and performance present gradual gradient change along the thickness direction due to the continuous change of the component.[183] As a result, the specific performance in a specific direction of the gradient ceramics is superior to homogeneous counterparts composed of similar components.[184] Therefore, gradient ceramics are a potential material that can be applied in a wide range of engineering fields, such as nuclear reactions, aerospace, and internal combustion engines.[185] B_4C and SiC are the preferred materials for producing gradient ceramics owing to their excellent properties. Zhang *et al.*[186] successfully prepared B_4C–SiC gradient ceramics with six layers structure. The composition of the prepared B_4C–SiC gradient ceramics exhibits obvious gradient characteristics, the interface between adjacent layers is well combined and there are no cracks at the interface, resulting from the good physical and chemical compatibility between B_4C and SiC as well as their little difference in thermal expansion coefficients. Meanwhile, the mechanical properties of B_4C–SiC gradient ceramics show the characteristics of gradient transition along the thickness direction of gradient layers. Especially, the B_4C–SiC gradient ceramics have excellent thermal shock resistance, which is ascribed to the tight bonding between different layers and the unique multi-layer gradient structure. Microcracks can be generated at the interface layer under the action of the shear stress between the gradient layers, which is caused by the different thermal expansion coefficients between layers due to the different composition ratios of each layer. When the main cracks formed during the thermal shock pass through the interface layer, these cracks can be passivated by the microcracks at the interface. The B_4C–SiC gradient ceramics can decrease the damage by enhancing thermal conductivity, thermal shock resistance, and brittleness under the condition of temperature gradients. Therefore, the B_4C–SiC ceramics in the form of composition gradient distribution have better effects on some properties than homogeneous B_4C–SiC block ceramics.

In order to improve the fracture toughness of ceramics, a laminated bionic design can be applied. Generally, there are two toughening mechanisms of laminated ceramics based on the bonding strength of the interface between the layers. One is the residual compressive stress owing to the thermal mismatch at the strong interface, and the other is the delamination and deflection of cracks at the weak interface. Sun *et al.*[141] prepared a kind of laminated B_4C–SiC ceramics by tape casting. Compared with the fracture toughness of the block B_4C–SiC ceramics, the laminated B_4C–SiC ceramics possess higher fracture toughness, which is attributed to the strong interface bond between the layers resulting from the residual compressive stress in the laminated ceramics; also, the laminated B_4C–SiC ceramics have bending strength than the block B_4C–SiC ceramics. Therefore, the layered structure design can improve the mechanical properties of B_4C–SiC ceramics.

5.4.2. Porous ceramics. Porous ceramics are a kind of material with open pores and high open porosity. It is suitable for precise filtration and separation of various media; thus, it is often prepared as ceramic membranes. Compared with traditional porous ceramic membrane supports, membrane supports composed of SiC–B_4C porous ceramics can exhibit better corrosion resistance in hot acidic and alkaline solutions.[187] Also, SiC–B_4C porous ceramics have higher flexural strength than pure SiC porous ceramics, which is attributed to the microstructure of interpenetrated networks formed by large plate-like SiC grains interpenetrating with equiaxed SiC grains in the SiC–B_4C porous ceramics.[187] Compared with dense SiC–B_4C block ceramics, SiC–B_4C porous ceramics are a new form of SiC–B_4C composites.

5.4.3. Ceramic hollow microspheres. The ceramic hollow microspheres are an important engineering material, which can be applied as fillers in composites, ignition targets for inertial confinement fusion, and catalyst supports.[188] In particular, inertial confinement fusion is a sustainable, clean energy and is considered as an effective solution to energy crisis. The ignition target, a vital component for inertial confinement fusion, needs to meet many strict requirements in term of material, surface roughness, and sphericity.[189,190] Due to their high melting point, high thermal conductivity, and excellent thermal stability, B_4C and SiC are estimated as the ignition target materials for inertial confinement fusion.[191] Yan *et al.*[192] used a combination of slurry-coating and precursor conversion methods to prepare B_4C–SiC hollow microspheres with a smooth surface and high crush load. The obtained B_4C–SiC hollow microspheres possess a diameter of 1.6–1.9 mm and a wall thickness of 10–60 μm; the B_4C–SiC hollow microspheres have a high sphericity of 99.6%. Compared with pure B_4C hollow microspheres prepared by the CVD method, whose wall thickness can hardly reach 20 μm, the B_4C–SiC hollow microspheres obtained through a combination of slurry-coating and precursor conversion method exhibit higher wall thickness. B_4C–SiC ceramics with other complex shapes can also be produced by this method.

5.5. Exploration of new material of ternary systems or quaternary systems based on B_4C–SiC binary ceramics

B_4C–SiC binary ceramics exhibit better sinterability and mechanical properties than pure B_4C and SiC ceramics. Recently, the performance of ternary or quaternary systems based on B_4C–SiC binary ceramics has attracted much attention, such as B_4C–SiC–TiB_2,[193–205] B_4C–SiC–CrB_2,[206] B_4C–SiC–NbB_2,[207] B_4C–SiC–MoB_2,[208] B_4C–SiC–HfB_2,[209,210] B_4C–SiC–ZrB_2,[211,212] B_4C–SiC–WC,[213] B_4C–SiC–Al_2O_3,[214] B_4C–SiC–rGO,[215] B_4C–SiC–carbon nanotubes,[216] B_4C–SiC–carbon fiber,[217] B_4C–SiC–Si,[218,219] B_4C–SiC–Mo,[220] B_4C–SiC–Al,[221–223] B_4C–SiC–Al_2O_3–MgB_2,[224] and B_4C–SiC–Si–TiB_2.[225] The demand for B_4C–SiC with good performance promotes further exploration of new materials of ternary or quaternary systems with improved properties based on B_4C–SiC binary ceramics.

5.6. Study on the combination of mechanical properties and tribological properties

As a novel ceramic material with low friction and low wear, B_4C–SiC ceramics exhibit satisfactory tribological properties under both unlubricated and water-lubricated sliding conditions.[226–232] However, the tribological properties of the solid-state sintered B_4C–SiC ceramics under high load need to be further improved due to the relatively low fracture toughness.[233] Therefore, how to improve the tribological properties of B_4C–SiC ceramics under harsh conditions by controlling their mechanical properties remains to be further studied.

6. Conclusions

B_4C–SiC composite ceramics are a very promising alternative to pure B_4C ceramics and pure SiC ceramics. B_4C–SiC ceramics exhibit a combination of the desirable performance of B_4C and SiC. The mechanical properties of B_4C–SiC ceramics are determined by a number of factors, as mentioned in this review. Some values of mechanical properties of B_4C–SiC ceramics reported in the literature vary considerably, and some research conclusions are not uniform so far. The measurement of mechanical properties is strongly dependent on the measuring method, instrument, and operator. The comparison of mechanical properties reported in different literature studies can only be regarded as a reference, even for the B_4C–SiC ceramics prepared by the same preparation process. Design and exploration of novel advanced ceramic materials for high-performance applications are important to accelerate the development of modern material engineering. B_4C–SiC ceramics are a potentially promising material for a variety of applications. This review is of practical significance for the promotion and application of B_4C–SiC ceramics.

Conflicts of interest

There are no conflicts to declare.

Acknowledgements

The author would like to express his gratitude to his grandfather and grandmother. The author was brought up by his grandfather and grandmother from birth. The author's grandfather passed away 13 years ago, and the author's grandmother

died 5 years ago. The author would like to use this article as a way to commemorate his grandfather and grandmother and express his yearning.

References

1 W. Zhang, S. Yamashita, T. Kumazawa, F. Ozeki, H. Hyuga and H. Kita, Tribological properties of B_4C ceramics prepared by pressureless sintering and annealed at different temperatures, *Tribol. Trans.*, 2020, **63**(4), 672–682.
2 A. Zare, M. R. He, M. Straker, M. V. S. Chandrashekhare, M. Spencer, K. J. Hemker, J. W. McCauley and K. T. Ramesh, Mechanical characterization of boron carbide single crystals, *J. Am. Ceram. Soc.*, 2022, **105**(5), 3030–3042.
3 W. Zhang, S. Yamashita and H. Kita, Self lubrication of pressureless sintered SiC ceramics, *J. Mater. Res. Technol.*, 2020, **9**(6), 12880–12888.
4 X. M. Ren, B. Y. Ma, F. Qian, W. G. Yang, G. Q. Liu, J. K. Yu, Y. R. Zhang and Q. Zhu, Green synthesis of porous SiC ceramics using silicon kerf waste in different sintering atmospheres and optimization of pore structure, *Ceram. Int.*, 2021, **47**(18), 26366–26374.
5 C. Ojalvo, V. Zamora, R. Moreno, F. Guiberteau and A. L. Ortiz, Transient liquid-phase assisted spark-plasma sintering and dry sliding wear of B_4C ceramics fabricated from B_4C nanopowders, *J. Eur. Ceram. Soc.*, 2021, **41**(3), 1869–1877.
6 M. N. Mirzayev, B. A. Abdurakhimov, S. H. Jabarov, M. Y. Tashmetov, E. Demir, N. V. Tiep, N. A. Ismayilova, Y. I. Aliyev, E. Popov, D. M. Mirzayeva, S. I. Karaaslan and G. I. Georgiev, Effect of high intense electron beam irradiation on structural and Raman properties of boron carbide micro powder, *Int. J. Mod. Phys. B*, 2020, **34**(4), 2050008.
7 L. Vargas-Gonzalez and R. F. Speyer, Flexural strength, fracture toughness, and hardness of silicon carbide and boron carbide armor ceramics, *Int. J. Appl. Ceram. Technol.*, 2010, **7**(5), 643–651.
8 W. C. Guo, A. Y. Wang, Q. L. He, T. Tian, C. Liu, L. X. Hu, Y. W. Shi, L. S. Liu, W. M. Wang and Z. Y. Fu, Microstructure and mechanical properties of B_4C–TiB_2 ceramic composites prepared via a two-step method, *J. Eur. Ceram. Soc.*, 2021, **41**(14), 6952–6961.
9 W. Zhang, X. Y. Chen, S. Yamashita, M. Kubota and H. Kita, B_4C–SiC ceramics with interfacial nanorelief morphologies and low underwater friction and wear, *ACS Appl. Nano Mater.*, 2021, **4**(3), 3159–3166.
10 M. M. Balakrishnarajan, P. D. Pancharatna and R. Hoffmann, Structure and bonding in boron carbide: the invincibility of imperfections, *New J. Chem.*, 2007, **31**(4), 473–485.
11 D. Gosset and M. Colin, Boron carbides of various compositions: An improved method for X-rays characterisation, *J. Nucl. Mater.*, 1991, **183**(3), 161–173.
12 S. Mondal, Charge transfer and fractional bonds in stoichiometric boron carbide, *Chem. Mater.*, 2017, **29**(15), 6191–6194.
13 S. Mondal, E. Bykova, S. Dey, S. I. Ali, N. Dubrovinskaia, L. Dubrovinsky, G. Parakhonskiy and S. van Smaalen, Disorder and defects are not intrinsic to boron carbide, *Sci. Rep.*, 2016, **6**, 19330.
14 C. M. Xu, Y. B. Cai, K. Flodström, Z. S. Li, S. Esmaeilzadeh and G. J. Zhang, Spark plasma sintering of B_4C ceramics: the effects of milling medium and TiB_2 addition, *Int. J. Refract. Met. Hard Mater.*, 2012, **30**(1), 139–144.
15 W. Zhang, S. Yamashita and H. Kita, Progress in pressureless sintering of boron carbide ceramics-A review, *Adv. Appl. Ceram.*, 2019, **118**(4), 222–239.
16 H. T. Laker, L. Hermasson and J. Adlerborn, Hot isostatic pressing and its applicability to silicon carbide and boron carbide, *High Tech Ceramics Proceeding of 6th CIMTEC*, 1987, 795–803.
17 D. R. Secrist, Phase equilibria in the system boron carbide-silicon carbide, *J. Am. Ceram. Soc.*, 1964, **47**(3), 127–130.
18 E. Gugel, R. Kieffer, G. Leimer and P. Ettmayer, *Solid State Chemistry*, NBS Special Publication 364, Washington DC, 1972, p. 505.
19 J. D. Hong, K. E. Spear and V. S. Stubican, Directional solidification of SiC–B_4C eutectic: growth and some properties, *Mater. Res. Bull.*, 1979, **14**(6), 775–783.
20 F. Thévenot, Sintering of boron carbide and boron carbide-silicon carbide two-phase materials and their properties, *J. Nucl. Mater.*, 1988, **152**(2–3), 154–162.
21 M. Bougoin and F. Thévenot, Pressureless sintering of boron carbide with an addition of polycarbosilane, *J. Mater. Sci.*, 1987, **22**(1), 109–114.
22 J. E. Zorzi, C. A. Perottoni and J. A. H. da Jornada, Hardness and wear resistance of B_4C ceramics prepared with several additives, *Mater. Lett.*, 2005, **59**(23), 2932–2935.
23 S. Prochazka and R. M. Scanlan, Effect of boron and carbon on sintering of SiC, *J. Am. Ceram. Soc.*, 1975, **58**(1–2), 72.
24 Z. A. Yaşar, V. A. DeLucca and R. A. Haber, Effect of boron carbide additive and sintering temperature – Dwelling time on silicon carbide properties, *Ceram. Int.*, 2021, **47**(5), 7177–7182.
25 R. M. Williams, B. N. Juterbock, C. R. Peters and T. J. Whalen, Forming and sintering behavior of B- and C-doped α- and β-SiC, *J. Am. Ceram. Soc.*, 1984, **67**(4), 62–64.
26 L. Stobierski and A. Gubernat, Sintering of silicon carbide II. Effect of boron, *Ceram. Int.*, 2003, **29**(4), 355–361.
27 H. N. Yoshimura, A. C. Da Curz, Y. Zhou and H. Tanaka, Sintering of 6H(α)-SiC and 3C(β)-SiC powders with B_4C and C additives, *J. Mater. Sci.*, 2002, **37**(8), 1541–1546.
28 M. S. Datta, A. K. Bandyopadhyay and B. Chaudhuri, Sintering of nano crystalline α silicon carbide by doping with boron carbide, *Bull. Mater. Sci.*, 2002, **25**(3), 181–189.
29 C. Greskovich and J. H. Rosolowski, Sintering of covalent solids, *J. Am. Ceram. Soc.*, 1976, **59**(7–8), 336–343.
30 G. H. Wroblewska, E. Nold and F. ThLimmler, The role of boron and carbon additions on the microstructural development of pressureless sintered silicon carbide, *Ceram. Int.*, 1990, **16**, 201–209.
31 A. Maître, A. V. Put, J. P. Laval, S. Valette and G. Trolliard, Role of boron on the spark plasma sintering of an α-SiC powder, *J. Eur. Ceram. Soc.*, 2008, **28**(9), 1881–1890.

32 W. J. Clegg, Role of carbon in the sintering of boron-doped silicon carbide, *J. Am. Ceram. Soc.*, 2000, **83**(5), 1039–1043.
33 L. Stobierski and A. Gubernat, Sintering of silicon carbide I. Effect of carbon, *Ceram. Int.*, 2003, **29**(3), 287–292.
34 J. M. Bind and J. V. Biggers, Hot-pressing of silicon carbide with 1% boron carbide addition, *J. Am. Ceram. Soc.*, 1975, **58**(7–8), 304–306.
35 C. R. Li, S. Li, D. An and Z. P. Xie, Microstructure and mechanical properties of spark plasma sintered SiC ceramics aided by B_4C, *Ceram. Int.*, 2020, **46**(8), 10142–10146.
36 S. Yamada, K. Hirao, Y. Yamauchi and S. Kanzaki, B_4C-CrB_2 composites with improved mechanical properties, *J. Eur. Ceram. Soc.*, 2003, **23**(3), 561–565.
37 S. Gupta, S. K. Sharma, B. V. M. Kumar and Y. W. Kim, Tribological characteristics of SiC ceramics sintered with a small amount of yttria, *Ceram. Int.*, 2015, **41**(10), 14780–14789.
38 P. H. Li, M. D. Ma, Y. J. Wu, X. Zhang, Y. K. Chang, Z. W. Zhuge, L. Sun, W. T. Hu, D. L. Yu, B. Xu, Z. S. Zhao, J. Y. Chen, J. L. He and Y. J. Tian, Preparation of dense B_4C ceramics by spark plasma sintering of high-purity nanoparticles, *J. Eur. Ceram. Soc.*, 2021, **41**(7), 3929–3936.
39 R. Q. Ma, J. H. Shi, W. X. Lin and J. J. Chen, Synthesis and sintering of nanocrystalline SiC ceramic powders, *Mater. Chem. Phys.*, 2020, **253**, 123445.
40 X. X. Lyu, Z. Y. Zhao, H. L. Sun, X. S. Jiang, C. F. Hu, T. F. Song and Z. P. Luo, Influence of Y_2O_3 contents on sintering and mechanical properties of B_4C-Al_2O_3 multiphase ceramic composites, *J. Mater. Res. Technol.*, 2020, **9**(5), 11687–11701.
41 H. R. Baharvandi, A. M. Hadian, A. Abdizadeh and N. Ehsani, Investigation on addition of ZrO_2-3 mol% Y_2O_3 powder on sintering behavior and mechanical properties of B_4C, *J. Mater. Sci.*, 2006, **41**(16), 5269–5272.
42 W. Zhang, X. Y. Chen, S. Yamashita, M. Kubota and H. Kita, Frictional characteristics of carbide ceramics in water, *J. Tribol.*, 2022, **144**(1), 011702.
43 W. Zhang, S. Yamashita, T. Kumazawa, F. Ozeki, H. Hyuga and H. Kita, Influence of surface roughness parameters and surface morphology on friction performance of ceramics, *J. Ceram. Soc. Jpn.*, 2019, **127**(11), 837–842.
44 V. Lankau, H. P. Martin, R. Hempel-Weber, N. Oeschler and A. Michaelis, Preparation and thermoelectric characterization of SiC–B_4C composites, *J. Electron. Mater.*, 2010, **39**(9), 1809–1813.
45 M. Uehara, R. Shiraishi, A. Nogami, N. Enomoto and J. Hojo, SiC–B_4C composites for synergistic enhancement of thermoelectric property, *J. Eur. Ceram. Soc.*, 2004, **24**(2), 409–412.
46 F. Thévenot, Boron carbide-A comprehensive review, *J. Eur. Ceram. Soc.*, 1990, **6**(4), 205–225.
47 A. K. Suri, C. Subramanian, J. K. Sonber and T. S. R. C. Murthy, Synthesis and consolidation of boron carbide: a review, *Int. Mater. Rev.*, 2010, **55**(1), 4–40.
48 V. Domnich, S. Reynaud, R. A. Haber and M. Chhowalla, Boron carbide: structure, properties, and stability under stress, *J. Am. Ceram. Soc.*, 2011, **94**(11), 3605–3628.
49 W. Zhang, A review of tribological properties for boron carbide ceramics, *Prog. Mater. Sci.*, 2021, **116**, 100718.
50 W. Zhang, S. Yamashita and H. Kita, Progress in tribological research of SiC ceramics in unlubricated sliding-A review, *Mater. Des.*, 2020, **190**, 108528.
51 W. Zhang, Tribology of SiC ceramics under lubrication: Features, developments, and perspectives, *Curr. Opin. Solid State Mater. Sci.*, 2022, **26**(4), 101000.
52 W. Zhang, An overview of the synthesis of silicon carbide-boron carbide composite powders, *Nanotechnol. Rev.*, 2023, **12**(1), DOI: **10.1515/ntrev-2022-0571**.
53 W. Zhang, A novel ceramic with low friction and wear toward tribological applications: Boron carbide-silicon carbide, *Adv. Colloid Interface Sci.*, 2022, **301**, 102604.
54 K. M. Taylor and R. J. Pallick, *Dense carbide composite for armor and abrasives*, *U. S. Patent*, US3765300, 1973.
55 Z. Zhang, Y. J. Zhang, H. Y. Gong, X. Guo, Y. B. Zhang, X. L. Wang and J. C. Yu, Influence of carbon content on ceramic injection molding of reaction-bonded silicon carbide, *Int. J. Appl. Ceram. Technol.*, 2016, **13**(5), 838–843.
56 P. S. Grinchuk, M. V. Kiyashko, H. M. Abuhimd, M. S. Alshahrani, D. V. Solovei, M. O. Stepkin, A. V. Akulich, M. D. Shashkov, T. A. Kuznetsova, S. M. Danilova-Tretiak, L. E. Evseeva and K. V. Nikolaeva, Advanced technology for fabrication of reaction-bonded SiC with controlled composition and properties, *J. Eur. Ceram. Soc.*, 2021, **41**(12), 5813–5824.
57 S. Hayun, A. Weizmann, H. Dilman, M. P. Dariel and N. Frage, Rim region growth and its composition in reaction bonded boron carbide composites with core-rim structure, *J. Phys.: Conf. Ser.*, 2009, **176**, 012009.
58 R. J. Li, *Ceramic-metal composites*, Metallurgical Industry Press, Beijing, second edn, 2004 (in Chinese).
59 A. L. Yurkov, B. S. Skidan and A. B. Ponomarev, Reaction between boron carbide and silicon, *Ogneupory*, 1987, **2**, 31–33.
60 S. C. Song, C. G. Bao and K. K. Wang, Studies of microstructure and mechanical properties of SiC/B_4C composites based on reaction sintering, *China Sciencepaper*, 2017, **12**(4), 425–429. (in Chinese).
61 R. Z. Liu, Q. W. Duan, W. W. Gu, H. Y. Jin, S. C. Xu and J. F. Yang, A study on reaction bonded ceramics fabricated by silicon infiltration to B_4C preforms, *Mater. Sci. Forum*, 2012, **724**, 343–346.
62 A. L. Yurkov, A. M. Starchenko and B. S. Skidan, Reaction sintering of boron carbide, *Refract. Ind. Ceram.*, 1989, **30**(11–12), 731–736.
63 A. Thuault, S. Marinel, E. Savary, R. Heuguet, S. Saunier, D. Goeuriot and D. Agrawal, Processing of reaction-bonded B_4C–SiC composites in a single-mode microwave cavity, *Ceram. Int.*, 2013, **39**(2), 1215–1219.
64 B. Matović, J. Maletaškić, T. Prikhna, V. Urbanovich, V. Girman, M. Lisnichuk, B. Todorović, K. Yoshida and I. C. Alagić, Characterization of B_4C–SiC ceramic composites prepared by ultra-high pressure sintering, *J. Eur. Ceram. Soc.*, 2021, **41**(9), 4755–4760.

65 S. Ilić, S. Zec, M. Rosić, V. Maksimović, J. Ružić, V. Urbanovich and B. Matović, High pressure densification of nanocrystalline mullite powder, *Ceram. Int.*, 2016, **42**(4), 5319–5325.
66 Z. A. Munir, U. Anselmi-Tamburini and M. Ohyanagi, The effect of electric field and pressure on the synthesis and consolidation of materials: a review of the spark plasma sintering method, *J. Mater. Sci.*, 2006, **41**(3), 763–777.
67 D. Mallick, T. K. Kayal, J. Ghosh, O. P. Chakrabarti, S. Biswas and H. S. Maiti, Development of multi-phase B–Si–C ceramic composite by reaction sintering, *Ceram. Int.*, 2009, **35**(4), 1667–1669.
68 G. Magnani, G. Beltrami, G. L. Minoccari and L. Pilotti, Pressureless sintering and properties of αSiC–B_4C composite, *J. Eur. Ceram. Soc.*, 2001, **21**(5), 633–638.
69 J. Y. Cho, T. An, S. Ji, Y. Kim, H. Shin, S. W. Kim, S. H. Bae, M. Kim and C. Park, The effects of B_4C addition on the microstructure and mechanical properties of SiC prepared using powders recovered from kerf loss sludge, *Ceram. Int.*, 2017, **43**(17), 15332–15338.
70 W. Zhang, S. Yamashita and H. Kita, Tribological properties of SiC–B_4C ceramics under dry sliding condition, *J. Eur. Ceram. Soc.*, 2020, **40**(8), 2855–2861.
71 Z. A. Yaşar and R. A. Haber, Evaluating the role of uniformity on the properties of B_4C–SiC composites, *Ceram. Int.*, 2021, **47**(4), 4838–4844.
72 S. M. So, W. H. Choi, K. H. Kim, J. S. Park, M. S. Kim, J. Park, Y. S. Lim and H. S. Kim, Mechanical properties of B_4C–SiC composites fabricated by hot-press sintering, *Ceram. Int.*, 2020, **46**(7), 9575–9581.
73 Y. Murata and R. H. Smoak, Densification of silicon carbide by the addition of BN, BP, and B_4C, and correlation to their solid solubilities, *Proceedings of the International Symposium of Factors in Densification and Sintering of Oxide and Non-oxide Ceramics*, Hakone, Japan, 1978, pp. 382–399.
74 Y. L. Zhang, Y. M. Zhang, M. Hu and X. G. Song, Effect of B_4C content on densification behavior of SiC–B_4C ceramics, *Adv. Mater. Res.*, 2014, **997**, 454–456.
75 C. P. Zhang, H. Q. Ru, X. Y. Yue and W. Wang, Studies on the SiC/B_4C composite fabricated by reaction bonded SiC, *Rare Met. Mater. Eng.*, 2011, **40**(s1), 536–539. (in Chinese).
76 X. G. Li, D. L. Jiang, J. X. Zhang, Y. Z. Zhu, Z. M. Chen and Z. R. Huang, Reaction-bonded B_4C with high hardness, *Int. J. Appl. Ceram. Technol.*, 2016, **13**(3), 584–592.
77 S. Hayun, H. Dilman, M. P. Dariel and N. Frage, in *Advances in Sintering Science and Technology: Ceramic Transactions*, ed. R. K. Bordia and E. A. Olevsky, American Ceramic Society, Hoboken, NJ, 2010, 209, pp. 29–41.
78 Y. Tomohiro, N. Atsushi, S. Katsuaki and N. Koichi, Preparation and properties of B_4C–SiC composite, *J. Jpn. Soc. Powder Powder Metall.*, 1990, **37**(4), 571–574. (in Japanese).
79 W. Chen, W. H. Hao, Z. Q. Zhao, N. R. He, X. Q. Li and H. Q. Li, Mechanical properties and tribological characteristics of B_4C–SiC ceramic composite in artificial seawater, *J. Asian Ceram. Soc.*, 2021, **9**(4), 1495–1505.
80 A. Moradkhani and H. Baharvandi, Mechanical properties and fracture behavior of B_4C-nano/micro SiC composites produced by pressureless sintering, *Int. J. Refract. Met. Hard Mater.*, 2018, **70**, 107–115.
81 R. Caram and S. Milenkovic, Microstructure of Ni–Ni_3Si eutectic alloy produced by directional solidification, *J. Cryst. Grow.*, 1999, **198–199**, 844–849.
82 I. Gunjishima, T. Akashi and T. Goto, Characterization of directionally solidified B_4C–SiC composites prepared by a floating zone method, *Mater. Trans.*, 2002, **43**(9), 2309–2315.
83 X. L. Shi, C. Zhang, Y. Tan, F. M. Xu, Y. L. Dong and L. Wang, Preparation and properties of B_4C–SiC composite ceramics, *Mater. Mech. Eng.*, 2009, **33**(12), 77–80. (in Chinese).
84 S. Hayun, A. Weizmann, M. P. Dariel and N. Frage, The effect of particle size distribution on the microstructure and the mechanical properties of boron carbide-based reaction-bonded composites, *Int. J. Appl. Ceram. Technol.*, 2009, **6**(4), 492–500.
85 S. C. Song, C. G. Bao and B. Wang, Effect of the addition of carbon fibres on the microstructure and mechanical properties of reaction bonded B_4C/SiC composites, *J. Eur. Ceram. Soc.*, 2016, **36**(8), 1905–1913.
86 Z. A. Yaşar and R. Haber, Effect of acid etching time and concentration on oxygen content of powder on the microstructure and elastic properties of silicon carbide densified by SPS, *Int. J. Mater. Sci. Appl.*, 2020, **9**(1), 7–13.
87 C. Hwang, Q. Yang, S. Xiang, V. Domnich, A. U. Khan, K. Y. Xie, K. J. Hemker and R. A. Haber, Fabrication of dense B_4C-preceramic polymer derived SiC composite, *J. Eur. Ceram. Soc.*, 2019, **39**(4), 718–725.
88 R. M. D. Rocha and F. C. L. D. Melo, Pressureless sintering of B_4C–SiC composites for armor applications, *Ceram. Eng. Sci. Proc.*, 2010, **30**(5), 113–119.
89 R. M. D. Rocha and F. C. L. D. Melo, Sintering of B_4C–SiC composites with AlN–Y_2O_3 addition, *Mater. Sci. Forum*, 2012, **727–728**, 850–855.
90 S. C. Zunjarrao, A. Rahman and R. P. Singh, Characterization of the evolution and properties of silicon carbide derived from a preceramic polymer precursor, *J. Am. Ceram. Soc.*, 2013, **96**(6), 1869–1876.
91 X. W. Du, Z. X. Zhang, W. M. Wang, H. Wang and Z. Y. Fu, Microstructure and properties of B_4C–SiC composites prepared by polycarbosilane-coating/B_4C powder route, *J. Eur. Ceram. Soc.*, 2014, **34**(5), 1123–1129.
92 W. S. Lin and L. He, SiC/B_4C multiphase ceramics using polycarbosilane-coating B_4C as raw materials prepared insuit by warm pressing and sintering, *Mater. Mech. Eng.*, 2011, **35**(5), 11–18. (in Chinese).
93 R. Lörcher, K. Strecker, R. Riedel and R. Telle, Microstructure and oxidation behaviour of boron carbide based ceramics doped with polysilane derived silicon carbide, *Solid State Phenom.*, 1990, **8–9**, 479–492.
94 Z. X. Zhang, X. W. Du, Z. L. Li, W. M. Wang, J. Y. Zhang and Z. Y. Fu, Microstructures and mechanical properties of B_4C–SiC intergranular/intragranular nanocomposite ceramics fabricated from B_4C, Si, and graphite powders, *J. Eur. Ceram. Soc.*, 2014, **34**(10), 2153–2161.
95 X. R. Zhang, Z. X. Zhang, W. M. Wang, H. W. Che, X. L. Zhang, Y. M. Bai, L. N. Zhang and Z. Y. Fu, Densification

behaviour and mechanical properties of B_4C–SiC intergranular/intragranular nanocomposites fabricated through spark plasma sintering assisted by mechanochemistry, *Ceram. Int.*, 2017, **43**(2), 1904–1910.

96 F. C. Sahin, B. Apak, I. Akin, H. E. Kanbur, D. H. Genckan, A. Turan, G. Goller and O. Yucel, Spark plasma sintering of B_4C–SiC composites, *Solid State Sci.*, 2012, **14**(11–12), 1660–1663.

97 Z. Pánek, The synthesis of SiC–B_4C ceramics by combustion during hot-pressing, *J. Eur. Ceram. Soc.*, 1993, **11**(3), 231–236.

98 Z. X. Zhang, X. W. Du, W. M. Wang, Z. Y. Fu and H. Wang, Preparation of B_4C–SiC composite ceramics through hot pressing assisted by mechanical alloying, *Int. J. Refract. Met. Hard Mater.*, 2013, **41**, 270–275.

99 M. P. Dariel and N. Frage, Reaction bonded boron carbide: recent developments, *Adv. Appl. Ceram.*, 2012, **111**(5–6), 301–310.

100 Y. F. Xu, H. Q. Ru, H. B. Long, J. Zhao and W. Wang, Gel-casting process-derived 3D-interconnected porous carbon/B_4C preform for reaction-bonded boron carbide composites, *Int. J. Appl. Ceram. Technol.*, 2018, **15**(2), 409–417.

101 C. P. Zhang, Q. Xia, L. F. Han, Y. L. Zhao, N. Huang, Q. X. Ren, X. Zhang and H. Q. Ru, Fabrication of carbon-coated boron carbide particle and its role in the reaction bonding of boron carbide by silicon infiltration, *J. Eur. Ceram. Soc.*, 2022, **42**(3), 860–868.

102 Y. F. Xu, H. Q. Ru, H. B. Long, J. Zhao, W. Wang and X. Y. Yue, Gel-cast hierarchical porous B_4C/C preform and its role in fabricating reaction bonded boron carbide composites, *Ceram. Int.*, 2017, **43**(5), 4062–4067.

103 Q. X. Ren, D. Feng, H. Q. Ru, Y. Jiang, C. C. Ye, Y. Zhang, W. Wang and C. P. Zhang, Controllability of the pore characteristics of B_4C/C preform prepared by gel-casting and the properties of RBBC composites, *Ceram. Int.*, 2019, **45**(17), 22682–22687.

104 S. Kimura and K. Terashima, A review of measurement of thermophysical properties of silicon melt, *J. Cryst. Grow.*, 1997, **180**(3–4), 323–333.

105 R. Pampuch, E. Walasek and J. Bialoskórski, Reaction mechanism in carbon-liquid silicon systems at elevated temperatures, *Ceram. Int.*, 1986, **12**(2), 99–106.

106 M. H. Hon and R. F. Davis, Self-diffusion of ^{30}Si in polycrystalline β-SiC, *J. Mater. Sci.*, 1980, **15**(8), 2073–2080.

107 Y. Zhu, D. J. Luo, Z. J. Li, Y. W. Wang, H. W. Cheng, F. C. Wang and T. Chen, Effect of sintering temperature on the mechanical properties and microstructures of pressureless-sintered B_4C/SiC ceramic composite with carbon additive, *J. Alloys Compd.*, 2020, **820**, 153153.

108 L. J. Vandeperre and J. H. Teo, Pressureless sintering of SiC–B_4C composites, *Adv. Ceram. Armor IX*, 2014, 101–108.

109 Y. L. Zhang, Y. M. Zhang, C. H. Li and J. P. Li, Influence of reaction temperature on the densification behavior of the SiC/B_4C composites, *Appl. Mech. Mater.*, 2015, **727–728**, 11–14.

110 W. Chen, W. H. Hao, D. Q. Gao, Z. X. Wang and Z. Q. Zhao, Effect of sintering temperature on microstructure and physical and mechanical properties of B_4C matrix composite ceramic, *Superhard Mater. Eng.*, 2020, **32**(6), 35–40. (in Chinese).

111 Y. C. Wu, J. W. Cao, X. J. Gao, Z. P. Li and C. Wang, Effect of temperature on mechanical properties of B_4C–SiC prepared by SPS sintering, *Ordnance Mater. Sci. Eng.*, 2019, **42**(2), 21–24. (in Chinese).

112 B. M. Moshtaghioun, A. L. Ortiz, D. G. García and A. D. Rodríguez, Toughening of super-hard ultra-fine grained B_4C densified by spark-plasma sintering via SiC addition, *J. Eur. Ceram. Soc.*, 2013, **33**(8), 1395–1401.

113 Z. F. Chen, Y. C. Su and Y. B. Cheng, Formation and sintering mechanisms of reaction bonded silicon carbide-boron carbide composites, *Key Eng. Mater.*, 2007, **352**, 207–212.

114 S. S. Ordan'yan, D. D. Nesmelov and A. I. Ovsienko, Phase formation during reactive sintering of the B_4C–SiC-Si(Al) composite (Review), *Refract. Ind. Ceram.*, 2018, **58**(6), 666–672.

115 D. D. Nesmelov and S. N. Perevislov, Reaction sintered materials based on boron carbide and silicon carbide, *Glass Ceram.*, 2015, **71**(9–10), 313–319.

116 H. B. Sun, Y. J. Zhang and Q. S. Li, Preparation and characterization of reaction sintering B_4C/SiC composite ceramic, *Key Eng. Mater.*, 2014, **602–603**, 536–539.

117 C. P. Zhang, H. Q. Ru, W. Wang, X. Y. Yue and J. Zhao, The role of infiltration temperature in the reaction bonding of boron carbide by silicon infiltration, *J. Am. Ceram. Soc.*, 2014, **97**(10), 3286–3293.

118 C. P. Zhang, H. Q. Ru, H. Zong, W. K. Sun, J. H. Zhu, W. Wang and X. Y. Yue, Coarsening of boron carbide grains during the infiltration of porous boron carbide preforms by molten silicon, *Ceram. Int.*, 2016, **42**(16), 18681–18691.

119 F. C. Frank, On the kinematic theory of crystal growth and dissolution processes, II, *Zeitschrift für Physikalische Chemie*, 1972, **77**(1–6), 84–92.

120 P. G. Karandikar, S. Wong, G. Evans and M. K. Aghajanian, Microstructural development and phase changes in reaction bonded boron carbide, *Adv. Ceram. Armor VI*, 2010, **31**, 251–259.

121 M. N. Rahaman, *Ceramic processing and sintering*, New York, 2nd edn, 2003.

122 W. Chen, W. H. Hao, D. Q. Gao and X. Q. Li, Study on the preparation of B_4C–SiC composite ceramics and their physical-mechanical properties, *Mater. China*, 2022, **41**(5), 407–412.

123 S. L. Dole, S. Prochazka and R. H. Doremus, Microstructural coarsening during sintering of boron carbide, *J. Am. Ceram. Soc.*, 1989, **72**(6), 958–966.

124 H. Lee and R. F. Speyer, Pressureless sintering of boron carbide, *J. Am. Ceram. Soc.*, 2003, **86**(9), 1468–1473.

125 C. A. Galán, A. L. Ortiz, F. Guiberteau and L. L. Shaw, High-energy ball-milling of ZrB_2 in the presence of graphite, *J. Am. Ceram. Soc.*, 2010, **93**(10), 3072–3075.

126 B. M. Moshtaghioun, D. G. García and A. D. Rodríguez, High-temperature plastic deformation of spark plasma

sintered boron carbide-based composites: the case study of B_4C–SiC with/without graphite (g), *J. Eur. Ceram. Soc.*, 2016, **36**(5), 1127–1134.

127 S. Jamale and B. V. M. Kumar, Sintering and sliding wear studies of B_4C–SiC composites, *Int. J. Refract. Met. Hard Mater.*, 2020, **87**, 105124.

128 Y. Zhou, H. Tanaka, S. Otani and Y. Bando, Low-temperature pressureless sintering of α-SiC with Al_4C_3–B_4C–C additions, *J. Am. Ceram. Soc.*, 1999, **82**(8), 1959–1964.

129 Y. Zhu, F. C. Wang, Y. W. Wang, H. W. Cheng, D. J. Luo and Y. Z. Zhao, Mechanical properties and microstructure evolution of pressureless-sintered B_4C–SiC ceramic composite with CeO_2 additive, *Ceram. Int.*, 2019, **45**(12), 15108–15115.

130 B. Y. Yin and L. S. Wang, Study on physical properties of hot-pressing sintered B_4C ceramic, *At. Energy Sci. Technol.*, 2004, **38**(5), 429–431.

131 P. Sahani and D. Chaira, Nonlubricated sliding wear behavior study of SiC–B_4C–Si cermet against a diamond indenter, *J. Tribol.*, 2017, **139**(5), 051601.

132 X. W. Du, Y. Wang, Z. X. Zhang, F. Zhang, W. M. Wang and Z. Y. Fu, Effects of silicon addition on the microstructure and properties of B_4C–SiC composite prepared with polycarbosilane-coated B_4C powder, *Mater. Sci. Eng., A*, 2015, **636**, 133–137.

133 S. J. Cho, C. D. Um and S. S. Kim, Wear and wear transition in silicon carbide ceramics during sliding, *J. Am. Ceram. Soc.*, 1996, **79**(5), 1247–1251.

134 S. G. Lee, Y. W. Kim and M. Mitomo, Relationship between microstructure and fracture toughness of toughened silicon carbide ceramics, *J. Am. Ceram. Soc.*, 2004, **84**(6), 1347–1353.

135 B. V. M. Kumar, Y. W. Kim, D. S. Lim and W. S. Seo, Influence of small amount of sintering additives on unlubricated sliding wear properties of SiC ceramics, *Ceram. Int.*, 2011, **37**(8), 3599–3608.

136 W. Zhang, S. Yamashita, T. Kumazawa, F. Ozeki, H. Hyuga, W. Norimatsu and H. Kita, A study on formation mechanisms of relief structure formed in situ on the surface of ceramics, *Ceram. Int.*, 2019, **45**(17), 23143–23148.

137 S. Hayun, A. Weizmann, M. P. Dariel and N. Frage, Microstructural evolution during the infiltration of boron carbide with molten silicon, *J. Eur. Ceram. Soc.*, 2010, **30**(4), 1007–1014.

138 S. Hayun, H. Dilman, M. P. Dariel, N. Frage and S. Dub, The effect of carbon source on the microstructure and the mechanical properties of reaction bonded boron carbide, in *Advances in Sintering Science and Technology: Ceramic Transactions*, ed. R. K. Bordia and E. A. Olevsky, American Ceramic Society, Baltimore, MD USA, 2010, pp. 29–39.

139 P. Jannotti, G. Subhash, J. Q. Zheng, V. Halls, P. G. Karandikar, S. Salamone and M. K. Aghajanian, Raman spectroscopic characterization of the core-rim structure in reaction bonded boron carbide ceramics, *Appl. Phys. Lett.*, 2015, **106**, 041903.

140 T. S. Wang, C. Y. Ni and P. Karandikar, Microstructural characteristics of reaction-bonded B_4C/SiC composite, *Charact. Miner., Met., Mater.*, 2016, 279–286.

141 M. Y. Sun, Y. H. Bai, M. X. Li, S. W. Fan and L. F. Cheng, In situ toughened two-phase B_{12}(C, Si, B)$_3$–SiC ceramics fabricated via liquid silicon infiltration, *J. Am. Ceram. Soc.*, 2019, **102**(4), 2094–2103.

142 S. Hayun, N. Frage and M. P. Dariel, The morphology of ceramic phases in B_xC–SiC–Si infiltrated composites, *J. Solid State Chem.*, 2006, **179**(9), 2875–2879.

143 S. Aroati, M. Cafri, H. Dilman, M. P. Dariel and N. Frage, Preparation of reaction bonded silicon carbide (RBSC) using boron carbide as an alternative source of carbon, *J. Eur. Ceram. Soc.*, 2011, **31**(5), 841–845.

144 X. J. Gao, J. W. Cao, L. F. Cheng, D. M. Yan, C. Zhang and P. Man, Effect of carbon content on mechanical properties of SiC/B_4C prepared by reaction sintering, *J. Inorg. Mater.*, 2015, **30**(1), 102–106.

145 M. W. Barsoum, *Fundamentals of Ceramics*, The Mc Graw-Hill Companies, Inc., New York, 1997.

146 M. Flinders, D. Ray, A. Anderson and R. A. Cutler, High-toughness silicon carbide as armor, *J. Am. Ceram. Soc.*, 2005, **88**(8), 2217–2226.

147 Y. A. Kalandaragh, A. S. Namini, Z. Ahmadi and M. S. Asl, Reinforcing effects of SiC whiskers and carbon nanoparticles in spark plasma sintered ZrB_2 matrix composites, *Ceram. Int.*, 2018, **44**(16), 19932–19938.

148 S. Hayun, M. P. Dariel, N. Frage and E. Zaretsky, The high-strain-rate dynamic response of boron carbide-based composites: The effect of microstructure, *Acta Mater.*, 2010, **58**(5), 1721–1731.

149 W. Zhang, J. Zhang, C. L. Duan, H. Geng and Y. Han, Research progress in Al_2O_3 thermal shock resistant ceramics, *J. Shenyang Univ. Technol.*, 2020, **42**(6), 624–647. (in Chinese).

150 K. J. McClellan, F. Chu, J. M. Roper and I. Shindo, Room temperature single crystal elastic constants of boron carbide, *J. Mater. Sci.*, 2001, **36**(14), 3403–3407.

151 Z. Keçeli, H. Ögünç, T. Boyraz, H. Gökçe, O. Addemir and M. L. Öveçoğlu, Effects of B_4C addition on the microstructural and thermal properties of hot pressed SiC ceramic matrix composites, *J. Achiev. Mater. Manuf. Eng.*, 2009, **37**(2), 428–433.

152 K. S. Lee, I. S. Han, Y. H. Chung, S. K. Woo and S. W. Lee, Hardness and wear resistance of reaction bonded SiC–B_4C composite, *Mater. Sci. Forum*, 2005, **486–487**, 245–248.

153 I. S. Han, K. S. Lee, D. W. Seo and S. K. Woo, Improvement of mechanical properties in RBSC by boron carbide addition, *J. Mater. Sci. Lett.*, 2002, **21**, 703–706.

154 W. S. Lin and N. X. Fang, Mechanical properties and microstructure of reaction sintering B_4C/SiC ceramics, *Appl. Mech. Mater.*, 2011, **66–68**, 510–515.

155 Z. H. Luo, D. L. Jiang, J. X. Zhang, Q. L. Lin, Z. M. Chen and Z. R. Huang, Influence of phenolic resin impregnation on the properties of reaction-bonded silicon carbide, *Int. J. Appl. Ceram. Technol.*, 2013, **10**(3), 519–526.

156 S. Hayun, D. Rittel, N. Frage and M. P. Dariel, Static and dynamic mechanical properties of infiltrated B_4C–Si composites, *Mater. Sci. Eng., A*, 2008, **487**(1–2), 405–409.

157 P. Chhillar, M. K. Aghajanian, D. D. Marchant, R. A. Haber and M. Sennett, The effect of Si content on the properties of B_4C–SiC–Si composites, *Adv. Ceram. Armor III*, 2009, 161–167.

158 M. Patel, V. V. B. Prasad and J. Subrahmanyam, Compressive property of liquid silicon (infiltrated) boron carbide, *Trans. Indian Inst. Met.*, 2010, **63**(6), 863–866.

159 B. Paliwal and K. T. Ramesh, Effect of crack growth dynamics on the rate-sensitive behavior of hot-pressed boron carbide, *Scr. Mater.*, 2007, **57**(6), 481–484.

160 R. P. Messner and Y. M. Chiang, Processing of reaction-bonded silicon carbide without residual silicon phase, *Ceram. Eng. Sci. Proc.*, 1988, **9**(7–8), 1053–1059.

161 L. Sigl, H. Thaler and K. A. Schwetz, *Composite materials based on boron carbide, titanium diboride and elemental carbon and processes for the preparation of same*, *U. S. Patent*, US5543370, 1994.

162 L. S. Sigl, Processing and mechanical properties of boron carbide sintered with TiC, *J. Eur. Ceram. Soc.*, 1998, **18**(11), 1521–1529.

163 S. Hayun, N. Frage, H. Dilman, V. Tourbabin and M. P. Dariel, Synthesis of dense B_4C–SiC–TiB_2 composites, *Ceram. Trans.*, 2006, **178**, 37–44.

164 T. Ellert and N. Frage, On the effects of particle size and preform porosity on the mechanical properties of reaction-bonded boron carbide infiltrated with Al–Si alloy at 950 °C, *Ceram. Int.*, 2020, **46**(11), 18994–18999.

165 Y. X. Zhai, Z. M. Li, H. B. Sun and Y. J. Zhang, Preparation and process research of reaction sintering B_4C/SiC composite ceramic, *J. Ceram.*, 2017, **38**(4), 481–485. (in Chinese).

166 P. Barick, D. C. Jana and N. Thiyagarajan, Effect of particle size on the mechanical properties of reaction bonded boron carbide ceramics, *Ceram. Int.*, 2013, **39**(1), 763–770.

167 O. P. Chakrabarti, S. Ghosh and J. Mukerji, Influence of grain size, free silicon content and temperature on the strength and toughness of reaction-bonded silicon carbide, *Ceram. Int.*, 1994, **20**(5), 283–286.

168 V. Raghavan, *Materials Science & Engineering*, Prentice-Hall of India, New Delhi, India, 2000.

169 G. D. Quinn and R. C. Bradt, On the vickers indentation fracture test, *J. Am. Ceram. Soc.*, 2007, **90**(3), 673–680.

170 Y. C. Zhou, D. W. Ni, Y. M. Kan, P. He, S. M. Dong and X. Y. Zhang, Microstructure and mechanical properties of reaction bonded B_4C–SiC composites: the effect of polycarbosilane addition, *Ceram. Int.*, 2017, **43**(8), 5887–5895.

171 H. K. Wei, Y. J. Zhang and X. Y. Deng, Effect of silicon additions on the hot pressing of B_4C, *J. Ceram. Proc. Res.*, 2011, **12**(5), 599–601.

172 H. K. Wei, Y. J. Zhang and H. Y. Gong, SiC/B_4C composites prepared by hot pressing, *Bull. Chin. Ceram. Soc.*, 2009, **28**(2), 249–252.

173 J. L. Wang, W. S. Lin, Z. W. Jiang, L. H. Duan and G. L. Yang, The preparation and properties of SiC_w/B_4C composites infiltrated with molten silicon, *Ceram. Int.*, 2014, **40**(5), 6793–6798.

174 N. Tamari, H. Kobayashi, T. Tanaka, I. Kondoh and S. Kose, Mechanical properties of B_4C–SiC whisker composite ceramics, *J. Ceram. Soc. Jpn.*, 1990, **98**(10), 1159–1163.

175 Q. Q. Lin, S. M. Dong, P. He, H. J. Zhou and J. B. Hu, Microstructure and property of TiB_2 reinforced reaction-bonded B_4C composites, *J. Inorg. Mater.*, 2015, **30**(6), 667–672.

176 Y. M. Zhang, S. Li, J. C. Han and Y. F. Zhou, Fabrication and characterization of random chopped fiber reinforced reaction bonded silicon carbide composite, *Ceram. Int.*, 2012, **38**(2), 1261–1266.

177 H. Zong, C. P. Zhang, H. Q. Ru, H. Huang, J. H. Zhu, H. B. Xu and Q. Xia, Effect of forming pressure on microstructure and mechanical properties of B_4C–SiC–Si ceramic composites, *Key Eng. Mater.*, 2017, **768**, 152–158.

178 P. Jannotti, G. Subhash, J. Zheng and V. Halls, Measurement of microscale residual stresses in multi-phase ceramic composites using Raman spectroscopy, *Acta Mater.*, 2017, **129**, 482–491.

179 G. Magnani, G. L. Minoccari and L. Pilotti, Flexural strength and toughness of liquid phase sintered silicon carbide, *Ceram. Int.*, 2000, **26**(5), 495–500.

180 K. W. Peng, H. L. Ma, R. Chen, W. Y. Wu and G. F. Tu, Toughening B_4C/Al ceramics by in situ CeB_6 particles in B_4C, *Chin. J. Rare Met.*, 2009, **33**(6), 850–854. (in Chinese).

181 S. Q. Ding, S. M. Zhu, Y. P. Zeng and D. L. Jiang, Fabrication of mullite-bonded porous silicon carbide ceramics by in situ reaction bonding, *J. Eur. Ceram. Soc.*, 2007, **27**(4), 2095–2102.

182 S. F. Liu, Y. P. Zeng and D. L. Jiang, Fabrication and characterization of cordierite-bonded porous SiC ceramics, *Ceram. Int.*, 2009, **35**(2), 597–602.

183 F. Gong, J. Zhao, G. L. Liu and X. Y. Ni, Design and fabrication of TiB_2–TiC–Al_2O_3 gradient composite ceramic tool materials reinforced by VC/Cr_3C_2 additives, *Ceram. Int.*, 2021, **47**(14), 20341–20351.

184 D. K. Jha, T. Kant and R. K. Singh, A critical review of recent research on functionally graded plates, *Compos. Struct.*, 2013, **96**, 833–849.

185 K. M. Cho, I. D. Choi and I. M. Park, Thermal properties and fracture behavior of compositionally graded Al–SiC_p composites, *Mater. Sci. Forum*, 2004, **449–452**, 621–624.

186 L. Zhang, X. P. Ren, J. K. Li and C. C. Dong, Microstructure and mechanical properties of spark plasma sintered SiC–B_4C gradient ceramics with Al additive, *Ceram. Int.*, 2021, **47**(21), 30844–30851.

187 W. M. Guo, H. N. Xiao, J. X. Liu, J. J. Liang, P. Z. Gao and G. M. Zeng, Effects of B_4C on the microstructure and phase transformation of porous SiC ceramics, *Ceram. Int.*, 2015, **41**(9), 11117–11124.

188 J. K. Cochran, Ceramic hollow spheres and their applications, *Curr. Opin. Solid State Mater. Sci.*, 1998, **3**(5), 474–479.

189 R. S. Craxton, K. S. Anderson, T. R. Boehly, V. N. Goncharov, D. R. Harding, J. P. Knauer, R. L. Mccrory, P. W. Mckenty, D. D. Meyerhofer, J. F. Myatt, A. J. Schmitt, J. D. Sethian, R. W. Short, S. Skupsky, W. Theobald,

W. L. Kruer, K. Tanaka, R. Betti, T. J. B. Collins, J. A. Delettrez, S. X. Hu, J. A. Marozas, A. V. Maximov, D. T. Michel, P. B. Radha, S. P. Regan, T. C. Sangster, W. Seka, A. A. Solodov, J. M. Soures, C. Stoeckl and J. D. Zuegel, Direct-drive inertial confinement fusion: a review, *Phys. Plasmas*, 2015, **22**, 110501.

190 J. L. Kline, S. H. Batha, L. R. Benedetti, D. Bennett, S. Bhandarkar, L. F. B. Hopkins, J. Biener, M. M. Biener, R. Bionta, E. Bond, D. Bradley, T. Braun, D. A. Callahan, J. Caggiano, C. Cerjan, B. Cagadas, D. Clark, C. Castro, E. L. Dewald, T. Döppner, L. Divol, R. D. Spears, M. Eckart, D. Edgell, M. Farrell, J. Field, D. N. Fittinghoff, M. G. Johnson, G. Grim, S. Haan, B. M. Haines, A. V. Hamza, E. P. Hartouni, R. Hatarik, K. Henderson, H. W. Herrmann, D. Hinkel, D. Ho, M. Hohenberger, D. Hoover, H. Huang, M. L. Hoppe, O. A. Hurricane, N. Izumi, S. Johnson, O. S. Jones, S. Khan, B. J. Kozioziemski, C. Kong, J. Kroll, G. A. Kyrala, S. LePape, T. Ma, A. J. Mackinnon, A. G. MacPhee, S. MacLaren, L. Masse, J. McNaney, N. B. Meezan, J. F. Merrill, J. L. Milovich, J. Moody, A. Nikroo, A. Pak, P. Patel, L. Peterson, E. Piceno, L. Pickworth, J. E. Ralph, N. Rice, H. F. Robey, J. S. Ross, J. R. Rygg, M. R. Sacks, J. Salmonson, D. Sayre, J. D. Sater, M. Schneider, M. Schoff, S. Sepke, R. Seugling, V. Smalyuk, B. Spears, M. Stadermann, W. Stoeffl, D. J. Strozzi, R. Tipton, C. Thomas, R. P. J. Town, P. L. Volegov, C. Walters, M. Wang, C. Wilde, E. Woerner, C. Yeamans, S. A. Yi, B. Yoxall, A. B. Zylstra, J. Kilkenny, O. L. Landen, W. Hsing and M. J. Edwards, Progress of indirect drive inertial confinement fusion in the United States, *Nuclear Fusion*, 2019, **59**, 112018.

191 C. Tang, Z. B. He, X. S. He, J. L. Huang, Y. Yi, H. B. Wang and T. Wang, Preparation and characterization of SiC hollow microspheres, *Mater. Lett.*, 2017, **207**, 104–108.

192 D. X. Yan, J. H. Chen, Y. Zhang and Y. Z. Gou, B_4C/SiC ceramic hollow microspheres prepared by slurry-coating and precursor conversion method, *J. Eur. Ceram. Soc.*, 2022, **42**(2), 392–401.

193 A. J. Li, Y. H. Zhen, Q. Yin, L. P. Ma and Y. S. Yin, Microstructure and properties of (SiC, TiB_2)/B_4C composites by reaction hot pressing, *Ceram. Int.*, 2006, **32**(8), 849–856.

194 L. Yu, H. Q. Ru, J. D. Cai and L. Zuo, Microstructure and properties of C-SiC–B_4C composites prepared by hot pressing sintering(I), *J. Northeast. Univ.*, 2007, **28**(11), 1571–1574. (in Chinese).

195 L. Yu, H. Q. Ru, J. D. Cai, C. Yang, L. Zuo and X. X. Xue, Microstructure and mechanical properties of hot pressed C-SiC–B_4C–TiB_2 composites, *Chin. J. Nonferrous Met.*, 2008, **18**(2), 271–277. (in Chinese).

196 L. Yu, H. Q. Ru, J. D. Cai and L. Zuo, Effect of hot pressing temperature on the microstructure and properties of C–SiC–B_4C composite, *Chin. J. Mater. Res.*, 2008, **22**(1), 107–112. (in Chinese).

197 L. Yu, H. Q. Ru, L. Zuo and X. X. Xue, Microstructure and properties of C–SiC–B_4C composites prepared by coating processing, *J. Mater. Metall.*, 2009, **8**(4), 272–277. (in Chinese).

198 C. Wu, S. H. Xie and Y. K. Li, Microstructure evolution and phase transformation of TiB_2/SiC/B_4C composites synthesized from Ti–SiC–B_4C ternary system, *Int. J. Appl. Ceram. Technol.*, 2017, **14**(6), 1055–1061.

199 X. R. Zhang, Z. X. Zhang, W. M. Wang, X. L. Zhang, J. B. Mu, G. S. Wang and Z. Y. Fu, Preparation of B_4C composites toughened by TiB_2–SiC agglomerates, *J. Eur. Ceram. Soc.*, 2017, **37**(2), 865–869.

200 X. R. Zhang, Z. X. Zhang, W. M. Wang, J. H. Shan, H. W. Che, J. B. Mu and G. S. Wang, Microstructure and mechanical properties of B_4C–TiB_2–SiC composites toughened by composite structural toughening phases, *J. Am. Ceram. Soc.*, 2017, **100**(7), 3099–3107.

201 Q. L. He, A. Y. Wang, C. Liu, W. M. Wang, H. Wang and Z. Y. Fu, Microstructures and mechanical properties of B_4C–TiB_2–SiC composites fabricated by ball milling and hot pressing, *J. Eur. Ceram. Soc.*, 2018, **38**(7), 2832–2840.

202 S. P. Yin, Z. H. Zhang, X. W. Cheng, T. J. Su, Z. Y. Hu, Q. Song and H. Wang, Spark plasma sintering of B_4C–TiB_2–SiC composite ceramics using B_4C, Ti_3SiC_2 and Si as starting materials, *Ceram. Int.*, 2018, **44**(17), 21626–21632.

203 X. R. Zhang, Z. X. Zhang, Y. M. Liu, A. Y. Wang, S. Tian, W. M. Wang and J. Wang, High-performance B_4C–TiB_2–SiC composites with tuneable properties fabricated by reactive hot pressing, *J. Eur. Ceram. Soc.*, 2019, **39**(10), 2995–3002.

204 S. Wang, L. M. Li, S. Yan, Y. Y. Deng, S. B. Gao and P. F. Xing, Preparing B_4C–SiC–TiB_2 composites via reactive pressureless sintering with B_4C and $TiSi_2$ as raw materials, *J. Mater. Res. Technol.*, 2020, **9**(4), 8685–8696.

205 Y. Y. Liu, X. S. Wu, M. Liu, Y. H. Huang and Z. R. Huang, Microstructure and mechanical properties of B_4C–TiB_2–SiC composites fabricated by spark plasma sintering, *Ceram. Int.*, 2020, **46**(3), 3793–3800.

206 S. Wang, Y. Y. Deng, M. S. Yang, L. Y. Wang, H. Q. Li and P. F. Xing, Microstructure and mechanical property of B_4C–SiC–CrB_2 composites fabricated via reactive hot pressing, *Ceram. Int.*, 2020, **46**(18), 29261–29270.

207 M. Upatov, J. Vleugels, Y. Koval, V. Bolbut and I. Bogomol, Microstructure and mechanical properties of B_4C–NbB_2–SiC ternary eutectic composites by a crucible-free zone melting method, *J. Eur. Ceram. Soc.*, 2021, **41**(2), 1189–1196.

208 V. Zamora, C. Ojalvo, F. Guiberteau, O. B. López and A. L. Ortiz, Ultra-low wear B_4C–SiC–MoB_2 composites fabricated at lower temperature from B_4C with $MoSi_2$ additives, *J. Eur. Ceram. Soc.*, 2021, **41**(16), 68–75.

209 R. Tu, N. Li, Q. Z. Li, S. Zhang, L. M. Zhang and T. Goto, Microstructure and mechanical properties of B_4C–HfB_2–SiC ternary eutectic composites prepared by arc melting, *J. Eur. Ceram. Soc.*, 2016, **36**(4), 959–966.

210 K. Kasraee, S. A. Tayebifard, H. Roghani and M. S. Asl, Preparation of B_4C–SiC–HfB_2 nanocomposite by mechanically activated combustion synthesis, *Ceram. Int.*, 2020, **46**(8), 12288–12295.

211 M. D. Alvari, M. G. Kakroudi, B. Salahimehr, R. Alaghmandfard, M. S. Asl and M. Mohammadi, Microstructure, mechanical properties, and oxidation behavior of hot-pressed ZrB_2–SiC–B_4C composites, *Ceram. Int.*, 2021, **47**(7), 9627–9634.

212 Z. L. Qu, R. J. He, X. M. Cheng and D. N. Fang, Fabrication and characterization of B_4C–ZrB_2–SiC ceramics with simultaneously improved high temperature strength and oxidation resistance up to 1600 °C, *Ceram. Int.*, 2016, **42**(7), 8000–8004.

213 N. Hosseini, A. Fazili, M. R. Derakhshandeh, L. Nikzad, M. Bahamirian and M. Razavi, Effect of Co addition on microstructural and mechanical properties of WC–B_4C–SiC composites, *Ceram. Int.*, 2021, **47**(11), 15771–15782.

214 H. R. Baharvandi and A. M. Hadian, Investigation on addition of kaolinite on sintering behavior and mechanical properties of B_4C, *J. Mater. Eng. Perf.*, 2009, **18**(4), 433–437.

215 L. X. Hu, A. Y. Wang, T. Tian, C. Liu, W. C. Guo, Q. L. He, H. Wang, J. J. Xie, W. M. Wang and Z. Y. Fu, Effects of SiC on the microstructures and mechanical properties of B_4C–SiC–rGO composites prepared using spark plasma sintering, *J. Eur. Ceram. Soc.*, 2022, **42**(4), 1282–1291.

216 W. S. Lin, N. X. Fang and L. He, Wear properties of reaction sintered B_4C composites, *Adv. Mater. Res.*, 2011, **152–153**, 883–886.

217 W. H. Zhang, L. F. Cheng, Y. S. Liu, L. T. Zhang, W. B. Yang and S. T. Zhou, Fracture behaviors and mechanism of 2D C/SiC–BC_x composite under tensile load, *Mater. Sci. Eng., A*, 2011, **530**, 297–303.

218 P. Sahani, S. K. Karak, B. Mishra, D. Chakravarty and D. Chaira, A comparative study on SiC–B_4C–Si cermet prepared by pressureless sintering and spark plasma sintering methods, *Metall. Mater. Trans. A*, 2016, **47**(6), 3065–3076.

219 M. Zhang, W. K. Zhang, Y. J. Zhang and L. Z. Gao, Fabrication, microstructure and mechanical behavior of SiC_w–B_4C–Si composite, *Mater. Sci. Eng., A*, 2012, **552**, 410–414.

220 H. Y. Wu, M. X. Gao, D. Zhu, S. C. Zhang, Y. Pan, H. G. Pan, Y. F. Liu, F. J. Oliveira and J. M. Vieira, SiC whisker reinforced multi-carbides composites prepared from B_4C and pyrolyzed rice husks via reactive infiltration, *Ceram. Int.*, 2012, **38**(5), 3519–3527.

221 S. Hayun, H. Dilman, M. P. Dariel and N. Frage, The effect of aluminum on the microstructure and phase composition of boron carbide infiltrated with silicon, *Mater. Chem. Phys.*, 2009, **118**(2–3), 490–495.

222 P. Sahani, S. K. Karak, B. Mishra, D. Chakravarty and D. Chaira, Effect of Al addition on SiC–B_4C cermet prepared by pressureless sintering and spark plasma sintering methods, *Int. J. Refract. Met. Hard Mater.*, 2016, **57**, 31–41.

223 A. Kisasoz, K. A. Guler and A. Karaaslan, Infiltration of A6063 aluminium alloy into SiC—B_4C hybrid preforms using vacuum assisted block mould investment casting technique, *Trans. Nonferrous Met. Soc. China*, 2012, **22**(7), 1563–1567.

224 H. R. Baharvandi, A. M. Hadian, H. Abdizade and N. Ehsani, Investigation on addition of talc on sintering behavior and mechanical properties of B_4C, *J. Mater. Eng. Perform.*, 2006, **15**(3), 280–283.

225 M. Patel, J. Subrahmanyam, V. V. B. Prasad and R. Goyal, Processing and characterization of B_4C–SiC–Si–TiB_2 composites, *Mater. Sci. Eng., A*, 2010, **527**, 4109–4112.

226 W. Zhang, S. Yamashita, T. Kumazawa, F. Ozeki, H. Hyuga and H. Kita, Effect of nanorelief structure formed in situ on tribological properties of ceramics in dry sliding, *Ceram. Int.*, 2019, **45**(11), 13818–13824.

227 W. Zhang, S. Yamashita, T. Kumazawa, F. Ozeki, H. Hyuga and H. Kita, Study on friction behavior of SiC–B_4C composite ceramics after annealing, *Ind. Lubr. Tribol.*, 2020, **72**(5), 673–679.

228 W. Zhang, S. Yamashita and H. Kita, Effect of counterbody on tribological properties of B_4C–SiC composite ceramics, *Wear*, 2020, **458–459**, 203418.

229 W. Zhang, S. Yamashita and H. Kita, A study of B_4C–SiC composite for self-lubrication, *J. Am. Ceram. Soc.*, 2021, **104**(5), 2325–2336.

230 W. Zhang, X. Y. Chen, S. Yamashita, M. Kubota and H. Kita, Effect of water temperature on tribological performance of B_4C–SiC ceramics under water lubrication, *Tribol. Lett.*, 2021, **69**(2), 34.

231 W. Zhang, X. Y. Chen, S. Yamashita, M. Kubota and H. Kita, Tribological behavior of B_4C–SiC composite ceramics under water lubrication: influence of counterpart, *Mater. Sci. Technol.*, 2021, **37**(9), 863–876.

232 W. Chen, X. T. Liu, W. H. Hao, C. L. Zhu and X. Q. Li, Tribological behaviors of B_4C–SiC composites self-mated pairs in seawater and pure water, *Int. J. Appl. Ceram. Technol.*, 2023, **20**(2), 1298–1308.

233 W. Zhang, S. Yamashita and H. Kita, Effects of load on tribological properties of B_4C and B_4C–SiC ceramics sliding against SiC balls, *J. Asian Ceram. Soc.*, 2020, **8**(3), 586–596.